การสังเคราะห์พอลิไอโซพรีนและไอโซพรีนโคพอลิเมอร์ขนาดนาโนด้วยไมโครอิมัลชันพอลิเมอไรเซชัน และไดอีมีดไฮโดรจิเนชัน

นางสาวบัณฑิตา ทรัพย์ไพบูลย์สุข

วิทยานิพนธ์นี้เป็นส่วนหนึ่งของการศึกษาตามหลักสูตรปริญญาวิทยาศาสตรดุษฎีบัณฑิต
สาขาวิชาเคมีเทคนิค ภาควิชาเคมีเทคนิค
คณะวิทยาศาสตร์ จุฬาลงกรณ์มหาวิทยาลัย
ปีการศึกษา 2553

SYNTHESIS OF NANOSIZE POLYISOPRENE AND ISOPRENE COPOLYMER BY MICROEMULSION POLYMERIZATION AND THEIR DIIMIDE HYDROGENATION

Miss Bunthita Suppaibulsuk

A Dissertation Submitted in Partial Fulfillment of the Requirements

for the Degree of Doctor of Philosophy Program in Chemical Technology

Department of Chemical Technology

Faculty of Science

Chulalongkorn University

Academic year 2010

Thesis Title	SYNTHESIS OF NANOSIZE POLYISOPRENE AND ISOPRENE COPOLYMER BY MICROEMULSION POLYMERIZATION AND THEIR DIIMIDE HYDROGENATION
By	Miss Bunthita Suppaibulsuk
Field of Study	Chemical Technology
Thesis Advisor	Professor Pattarapan Prasassarakich, Ph. D.
Thesis Co-Advisors	Professor Garry L. Rempel, Ph. D.

Accepted by the Faculty of Science, Chulalongkorn University in Partial Fulfillment of the Requirements for the Doctoral Degree

…….. Dean of the Faculty of Science

(Professor Supot Hannongbua, Dr. rer. nat.)

THESIS COMMITTEE

…….. Chairman

(Associate Professor Tharapong Vitidsant, Doctorat de l'INPT)

…….……. Thesis Advisor

(Professor Pattarapan Prasassarakich, Ph. D.)

…….. Thesis Co-Advisor

(Professor Garry L. Rempel, Ph. D.)

…….. Examiner

(Assistant Professor Napida Hinchiranan, Ph.D.)

…….. Examiner

(Assistant Professor Sirilux Poompradub, Ph.D.)

…….. External Examiner

(Suwadee Kongparakul, Ph.D.)

บัณฑิตา ทรัพย์ไพบูลย์สุข : การสังเคราะห์พอลิไอโซพรีนและไอโซพรีนโคพอลิเมอร์ขนาดนาโนด้วยไมโครอิมัลชันพอลิเมอไรเซชัน และไดอีมีดไฮโดรจิเนชัน. (SYNTHESIS OF NANOSIZE POLYISOPRENE AND ISOPRENE COPOLYMER BY MICROEMULSION POLYMERIZATION AND THEIR DIIMIDE HYDROGENATION) อ. ที่ปรึกษาวิทยานิพนธ์หลัก : ศ.ดร.ภัทรพรรณ ประศาสน์สารกิจ, อ. ที่ปรึกษาวิทยานิพนธ์ร่วม : Prof. Gary L. Rempel, **170** หน้า.

งานวิจัยนี้เป็นการศึกษาการสังเคราะห์อนุภาคนาโนของพอลิไอโซพรีนด้วยวิธีดิฟเฟอเรนเชียลไมโครอิมัลชันพอลิเมอไรเซชันซึ่งใช้ 2,2-เอโซบิวทีโรไนไทรล์เป็นตัวริเริ่ม ตัวแปรที่มีผลอย่างมีนัยสำคัญต่อขนาดอนุภาคนาโนของพอลิไอโซพรีนคือความเข้มข้นของตัวริเริ่ม อุณหภูมิของปฏิกิริยา และ ความเร็วของการปั่นกวน ภาวะเหมาะสมให้ค่าการเปลี่ยนของมอนอเมอร์สูงสุดร้อยละ 90 และมีขนาดอนุภาคพอลิไอโซพรีนเฉลี่ย 27 นาโนเมตร การดัดแปรทางเคมีของโครงสร้างไม่อิ่มตัวพอลิไอโซพรีนเป็นกระบวนการที่น่าสนใจในการเตรียมหรือปรับปรุงวัสดุพอลิเมอร์ งานวิจัยนี้ยังศึกษากราฟต์โคพอลิเมอไรเซชันของเมทิลเมทาคริเลทหรือสไตรีนบนพอลิไอโซพรีนขนาดอนุภาคนาโนใช้คิวมีนไฮโดรเปอร์ออกไซด์เป็นตัวริเริ่มแบบรีดอกซ์ ซึ่งที่ภาวะเหมาะสมของการกราฟต์เมทิลเมทาคริเลทบนพอลิไอโซพรีนได้ค่าประสิทธิภาพการกราฟต์ร้อยละ 77 และขนาดอนุภาคกราฟต์เมทิลเมทาคริเลทบนพอลิไอโซพรีนเฉลี่ย 49 นาโนเมตร สำหรับกราฟต์สไตรีนกบนพอลิไอโซพรีนที่ภาวะเหมาะสมได้ค่าประสิทธิภาพสูงสุดร้อยละ 75.9 และการเปลี่ยนของมอนอเมอร์ร้อยละ 90 สำหรับการศึกษาไฮโดรจิเนชันของอนุภาคนาโนพอลิไอโซพรีนด้วยไดอีมีดรีดักชันใช้ไฮดราซีนไฮเดรทกับไฮโดรเจนเปอร์ออกไซด์ และมีคอปเปอร์ไอออนเป็นตัวเร่งปฏิกิริยา ผลคือได้ไฮโดรจิเนชันร้อยละ 75 อนุภาคนาโนพอลิไอโซพรีนขนาดเล็กมีค่าคงที่อัตราการเกิดปฏิกิริยามากกว่าอนุภาคขนาดใหญ่ นอกจากนี้อนุภาคนาโนของพอลิไอโซพรีน และพอลิไอโซพรีนดัดแปรสามารถใช้เป็นตัวเพิ่มเสถียรภาพคอลลอยด์สำหรับน้ำยางธรรมชาติพรีวัลคาไนซ์ ค่าความต้านทานแรงดึง ระยะยืด และความแข็งของยางผสมลดลงเมื่อเติมอนุภาคนาโนของพอลิไอโซพรีน และพอลิไอโซพรีนดัดแปร สำหรับการทดสอบการบ่มด้วยความร้อนพบว่ารีเทนชันของความต้านทานแรงดึง ระยะยืด และความแข็งหลังการบ่มมีค่าสูงขึ้นเมื่อเทียบกับยางธรรมชาติ จากการศึกษาสันฐานวิทยาของยางผสมเมื่อมีการเติมอนุภาคนาโนของพอลิไอโซพรีน และพอลิไอโซพรีนดัดแปรผสมในยางธรรมชาติแสดงรอยแตกบนพื้นผิวเปลี่ยนจากสภาพยืดหยุ่นไปเป็นสภาพเปราะ

ภาควิชา เคมีเทคนิค ลายมือชื่อนิสิต .....

สาขาวิชา เคมีเทคนิค ลายมือชื่อ อ.ที่ปรึกษาวิทยานิพนธ์หลัก .....

ปีการศึกษา 2553 ลายมือชื่อ อ.ที่ปรึกษาวิทยานิพนธ์ร่วม .....

4973868423 : MAJOR CHEMICAL TECHNOLOGY
KEYWORDS: NANOPARTICLES / POLYISOPRENE / DIFFERENTIAL MICROEMULSION POLYMERIZATION / GRAFT COPOLYMERIZATION / HYDROGENATION / DIIMIDE REDUCTION

BUNTHITA SUPPAIBULSUK : SYNTHESIS OF NANOSIZE POLYISOPRENE AND ISOPRENE COPOLYMER BY MICROEMULSION POLYMERIZATION AND THEIR DIIMIDE HYDROGENATION. THESIS ADVISOR : PROF. PATTARAPAN PRASASSARAKICH, PH.D., THESIS CO-ADVISOR : PROF. GARRY L. REMPEL, PH.D., 170 pp.

The synthesis of nanosized polyisoprene (PIP) latex was carried out by differential microemulsion polymerization using 2, 2'-Azoisobutyronitrile (AIBN) as initiator. The main effects on PIP particle size were the amount of initiator, reaction temperature and stirring speed. The optimum conditions gave highest monomer conversion of 90% and average particle size of PIP of 27 nm. Chemical modification of unsaturated PIP has been an attractive process for preparation or improvement of polymeric materials. The graft copolymerization of methyl methacrylate (MMA) or styrene (ST) onto nanosized PIP was carried out by using cumene hydroperoxide (CHPO) and tetraethylene pentamine (TEPA) as redox initiators. The optimum conditions of methyl methacrylate graft on polyisoprene (MMA-g-PIP) synthesis gave high grafting efficiency (GE = 77%) and average particle size of MMA-g-PIP of 49 nm. For styrene graft on polyisoprene (ST-g-PIP) synthesis, the optimum condition gave high GE (75.9%) and monomer conversion (90%). While hydrogenation of nanosized PIP latex via diimide reduction was accomplished by using hydrazine hydrate/hydrogen peroxide and Cu^{2+} as catalyst and 75% hydrogenation was achieved. The nanosized PIP with smaller particle size gave higher rate constant than that of large particle size. Moreover, nanosized PIP and ST-g-PIP could be used as colloid stabilizer for pre-vulcanized natural rubber (NR) latex. Tensile strength, elongation at break and hardness of rubber blends were reduced by addition of nanosized PIP and ST-g-PIP. From ageing test, the retentions of tensile strength and elongation of compounds was high compared with NR. Morphology studies of the compounds showed that the addition of nanosized PIP and ST-g-PIP has changed the fracture surface behavior from ductile behavior to brittle type.

Department : Chemical Technology Student's Signature .....
Field of Study : Chemical Technology Advisor's Signature .....
Academic Year : 2010 Co-Advisor's Signature .....

ACKNOWLEDGEMENTS

The author would like to express her gratitude to her supervisors, Prof. Dr. Pattarapan Prasassarakich, and Prof. Dr. Garry L. Rempel for their encouraging guidance, supervision and helpful suggestion throughout this research. The author also would like to acknowledge Assoc. Prof. Dr. Tharapong Vitidsant, Asst. Prof. Dr. Napida Hinchiranan, Asst. Prof. Dr. Sirilux Poompradub, and Dr. Suwadee Kongparakul for their participation on the dissertation chairman and members of thesis committee, respectively.

The author wishes to express her thankfulness to all people in the associated institutions and companies for their kind assistance and collaboration: Dr. Jialong Wu for his encouragement and helpful suggestion during this research at University of Waterloo, Canada.

Many thanks are going to technicians of the Department of Chemical Engineering, University of Waterloo for helping in maintaining the equipment, technicians of the Department of Chemical Technology, Chulalongkorn University, and Rubber Research Institute for assisting in polymer characterization.

Thanks go towards Golden Jubilee Scholarship (Thailand Research Fund, Grant No. PHD/0159/2548) and Natural Science and Engineering Research Council of Canada (NSERC) for financial support of this research.

Finally, the author wishes to express her deep gratitude to her family for their love, support, and encouragement throughout the tenure of her Ph.D. program.

CONTENTS

PAGE

CONTENTS (Continued)

PAGE

CONTENTS (Continued)

PAGE

CONTENTS (Continued)

PAGE

CONTENTS (Continued)

PAGE

CONTENTS (Continued)

PAGE

LIST OF TABLES

PAGE

LIST OF TABLES (continued)

PAGE

LIST OF TABLES (continued)

PAGE

LIST OF FIGURES

PAGE

LIST OF FIGURES (continued)

PAGE

LIST OF FIGURES (continued)

PAGE

LIST OF FIGURES (continued)

PAGE

LIST OF FIGURES (continued)

PAGE

LIST OF FIGURES (continued)

PAGE

NOMENCLATURES

AIBN	:	2,2’ - Azoisobutyronitrile
APS	:	Ammonium Persulfate
ASTM	:	American Standard of Testing Material
CHPO	:	Cumene Hydroperoxide
DRC	:	Dry Rubber Content
DMA	:	Dynamic Mechanical Analysis
D_n	:	Number-Average Diameter
DSC	:	Differential Scanning Calorimetry
E’	:	Storage or Elastic Modulus
E”	:	Loss or viscous Modulus
EPDM	:	Ethylene – Propylene Copolymer
FTIR	:	Fourier Transform Infrared Spectroscopy
GE	:	Grafting Efficiency
GPC	:	Gel Permeation Chromatography
HNR	:	Hydrogenated Natural Rubber
HPIP	:	Hydrogenated synthesis Polyisoprene
HSBR	:	Hydrogenated Styrene – Butadiene Rubber
HYD	:	Hydrogenation Degree
INT	:	Initiator
IP	:	Isoprene Monomer
Ir	:	Iridium
k’	:	Pseudo-First-Order Rate Constant
KOH	:	Potassium Hydroxide
MEK	:	Methyl Ethyl Ketone
M_w	:	Weight-Average Molecular Weight
M_n	:	Number-Average Molecular Weight
MMA	:	Methyl Methacrylate
MW	:	Molecular Weight
n-DM	:	*n*-Dodecyl Mercaptan
NaOH	:	Sodium hydroxide
NMR	:	Nuclear Magnetic Resonance Spectroscopy

NOMENCLATURES (continued)

NR	:	Natural Rubber
NRL	:	Natural Rubber Latex
Os	:	Osmium
PCy_3	:	Tricyclohexylphosphine
Pd	:	Palladium
phr	:	Part per Hundred
PDI	:	Polydispersity Index
PIP	:	Synthetic Polyisoprene
PMMA	:	Poly(methyl methacrylate)
PS	:	Polystyrene
Rh	:	Rhodium
Ru	:	Ruthenium
S	:	Sulfur
SBR	:	Styrene – Butadiene Rubber
SDS	:	Sodium dodecyl sulfate
SEM	:	Scanning Electron Microscopy
SHC	:	Sodium bicarbonate
SS	:	Stirring Speed
ST	:	Styrene
T_g	:	Glass Transition Temperature
T_{id}	:	Initial Decomposition Temperature
T_{max}	:	Maximum Decomposition Temperature
tan δ	:	Loss angle or ratio of E" to E'
TEM	:	Transmission Electron Microscopy
TEMP	:	Reaction Temperature
TEPA	:	Tetraethylene Pentamine
TGA	:	Thermogravimetric Analysis
ZDEC	:	Zinc Diethyl Dithiocarbamate
ZnO	:	Zinc Oxide

CHAPTER I

INTRODUCTION

1.1 Motivation

Nanoscale science and technology have attracted much more attention in recent years. Nanotechnology deals with materials with size of less than 100 nm and will play an important role in the next industrial revolution. Not only can nanotechnology provide new materials for industrial and personal use, but it also can be utilized to improve the properties of products. Nanomaterials are expected to be used in various applications such as pharmaceuticals, catalysis, paints, coatings and textiles. Polymer nanomaterials are within one of the many branches of nanotechnology. An interesting topic involving polymer materials is the synthesis of nanosized rubber particles by microemulsion polymerization. Rubber is a diene polymer that has important roles in industry. Rubber emulsions with nanosized particles could be used for many applications such as film, coating, membrane and friction materials with excellent physical properties such as resilience, tear strength and high abrasion resistance [1].

1.2 Polymer Nanomaterials

Polymer nanomaterials have gained much attention because of the enhanced properties of nanosized polymers and various attractive applications such as in textiles, paints, coatings, polishing, packaging and pharmaceuticals [2-4]. Miniemulsion [5, 6] and microemulsion polymerization [7, 8] are the common methods used to synthesize polymer nanoparticles.

1.2.1 Miniemulsion Polymerization

Miniemulsion is an emulsion polymerization which has some similarity to conventional emulsion polymerization comprising two immiscible liquid phases.

The reaction approximates an emulsion or miniemulsion polymerization depening on the monomer droplet size [9]. Then, miniemulsion polymerization has droplet sizes of less than 500 nm, large droplet surface area, and most of the surfactant is adsorbed at the droplet surface. Miniemulsion polymerization is a technique that uses highly water-insoluble monomers to make very small particles. This method is useful for producing high solid content latexes. Both water-soluble and oil-soluble initiators have been used in miniemulsion polymerization. Miniemulsion polymerization uses an equal or even a lower amount of surfactant than that employed in conventional emulsion polymerization. The particle sizes from miniemulsion are smaller than those obtained by emulsion polymerization but larger than those obtained by microemulsion polymerization.

The miniemulsion polymerization is introduced for nanoparticle synthesis [5]. The particle sizes of miniemulsion are usually within a range of 50-500 nm relating with the monomer droplet size. Then, the monomer droplet can be prepared by shearing a system containing oil, water, a surfactant, and an osmotic pressure agent. The process of miniemulsion polymerization is illustrated in Figure 1.1. In the first stage, the stirrer employed in conventional emulsion polymerization is used to make the monomer emulsion with larger droplets. After that, high shear equipment is used to make the smaller droplets. Subsequently, initiator is added and polymerization starts to produce fine polymer particles.

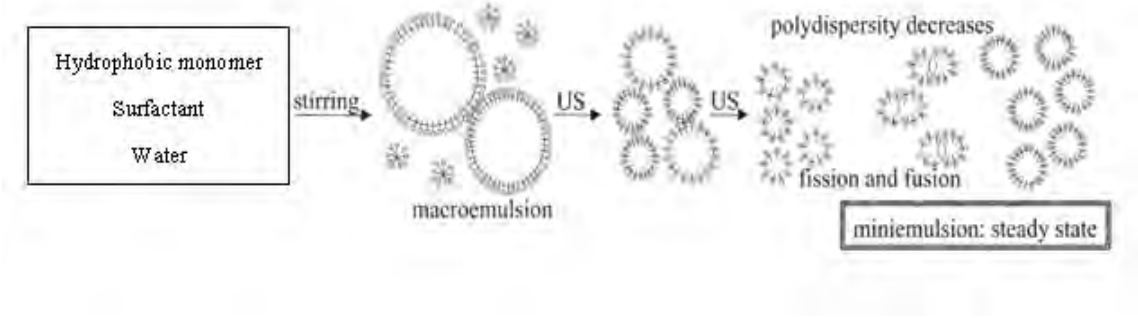

Figure 1.1 Illustration for the formation of a miniemulsion polymerization induced by ultrasound (US) [5].

1.2.2 Microemulsion Polymerization

The microemulsion polymerization method which is an emulsion polymerization for preparing polymer nanosized particles is different from the conventional emulsion polymerization method. Although in both methods, the initiation takes place in the water phase or the monomer-swollen micelles, the microemulsion polymerization is thermodynamically stable and particle sizes of 10 to 100 nm can be achieved [9].

Microemulsion polymerization, which firstly came into being in the early 1980s, can produce transparent or translucent polymer microlatexes [10, 11]. The particle size from microemulsion polymerization is considerably smaller, usually 10-50 nm, as opposed to conventional emulsion polymerization where the particle size is in the range of 100 to 1000 nm. In microemulsion polymerization, the initial surface area of micelles is larger by several orders of magnitude than the total surface area of the final polymer particle. The small fraction of micelles is nucleated or used to stabilize the polymer particles. A comparison of micelle size in heterophase polymerization processes is presented in Figure 1.2.

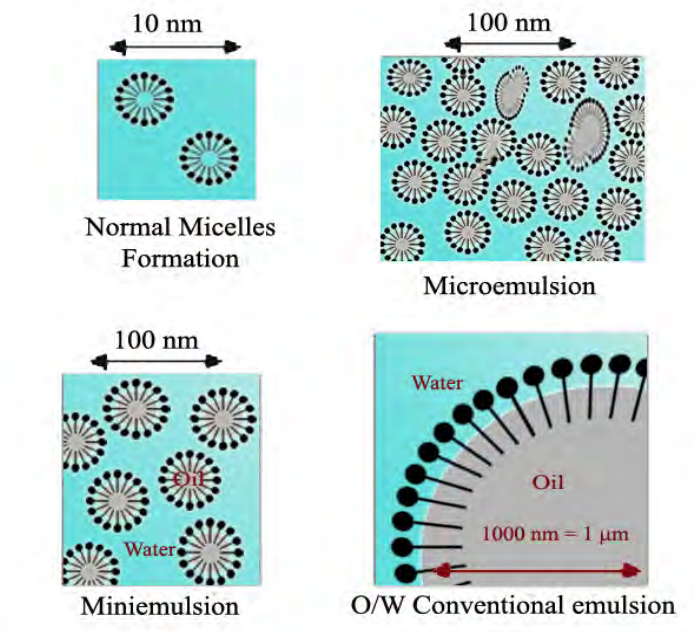

Figure 1.2 Scheme representation of micelles size in heterophase polymerization processes.

The microemulsion droplet is the locus of initiation in the microemulsion polymerization of a hydrophobic monomer initiated by a water or oil soluble initiator. In the oil-soluble case, the initiation has two main approaches for the production of radicals. In the monomer swollen polymer particles, formed radicals are desorbed to the aqueous phase; and in the aqueous phase, formed radicals are produced from the fraction of the oil-soluble initiator dissolved in water which initiates the growth of the polymer chains in both the aqueous phase and the monomer-swollen micelles or polymer particles [12-14].

For early investigation of microemulsion polymerization, methyl methacrylate (MMA) and styrene (ST) were the major monomer for preparation of polymer nanoparticles. Many investigators have reported the influences of various process parameters on nanoparticle size. Atik and Thomas [10] studied microemulsion polymerization of ST which was carried out in a solution containing cetytrimethlammonium bromide (CTAB) as surfactant, water and hexanol. The polystyrene particle size was obtained at 20-40 nm in diameter at a CTAB/ST weight ratio equal to 1.

Yildiz and Capek [13] reported the microemulsion polymerization of ST in the presence of macroinimer. The effects of ionic and non-ionic emulsifier were also investigated to find the kinetics of electrostatically and sterically-stabilized microemulsion polymerization of ST with and without macromonomeric azoinitiator (MIM). The microemulsion polymerization stabilized by ionic emulsifier, sodium dodecyl sulfate (SDS) or non-ionic emulsifier Tween 20 (Tw 20) was initiated by a ammonium peroxodisulfate (APS)/sodium thiosulfate (STS) redox system. The Tw 20-stabilized microemulsion polymerization was much faster than that of the SDS-stabilized microemulsion polymerization. This was attributed to the higher Tw 20 concentration and increased solubilization of MIM and comonomer concentration in the polymer particles. The smallest polystyrene particle size achieved was around 25 nm.

Capek and Chudej [15] also studied the fine emulsion polymerization of styrene with non-ionic emulsifier. When using the microemulsion method to prepare nanosized polymer particles, much more surfactant together with some co-surfactant was used compared with conventional emulsion polymerization. The co-surfactant was used to help in further reducing the interfacial tension. The amount of surfactant used was generally very high, with a surfactant/monomer weight ratio equal to or often larger than 1. This method could produce a particle size as small as 10 nm.

For the influence of using cationic surfactant, the polymerizations of ST and MMA at room temperature in ternary Winsor I-like systems were investigated. Gan et al. [16] studied the polymerization of ST in a Winsor I-like system. The higher ST/dodecyltrimethylammonium bromide (DTAB) weight ratio (15:1) was used and the particle size was in range of 46-95.5 nm, with a polystyrene content of 15 %weight. While Loh et al. [17] explored the polymerization of MMA in winsor i-like system, the method produced high molecular weight poly(methyl methacrylate) (PMMA) with a relatively high weight ratio of polymer to surfactant (around 8:1). The PMMA latex particles of nanosizes were around 30-60 nm in diameter.

From literature reviews, many investigators focused on the relation between particle size and the monomer to surfactant ratio. Then, two major drawbacks have limited the applications of microemulsion polymerization: (1) low monomer/surfactant weight ratios were required to get small particles; (2) the microlatexes could only be made at low concentrations with the polymer content being usually less than 10 %weight [18, 19]. Thus, another approach in the study of microemulsion polymerization is an attempt to increase the solid content and also to decrease the amount of surfactant while producing nanosized particles.

To solve these two drawbacks, Ming et al. [20, 21] studied the modification of microemulsion polymerization method by method of adding monomer to system. Thus, a small amount of monomer was added into the reaction flask at the beginning of this polymerization. After that, the remaining monomer was added drop-wise into microemulsion polymerization at the design condition. For

synthesis of PMMA nanoparticles via modified microemulsion polymerization using redox initiator, the number average diameter (D_n) of the PMMA particles obtained was larger than 13 nm with a MMA/SDS ratio being about 10:1 [20]. While using this monomer addition method to prepare polystyrene nanoparticles using redox intiator, polystyrene average particle size was 16.7 nm with a solid content of 15% [21]. In addition to monomer feeding as mentioned above, a semi-continuous addition of monomer was another method that was widely used in modified microemulsion polymerization.

Rabelero et al. [22] reported the production of highsolids content polystyrene latex by microemulsion polymerization using semi-continuous feeding of the monomer. The average particle size of the polystyrene nanoparticles was 27.4 nm with a high solid content of 38.0% when the ST/DTAB weight ratio was about 4:1. Roy et al. [23] also investigated the semi-continuous microemulsion copolymerization of MMA and butylacrylate. A high solid content of 45.2% with an average particle size of 30 nm could be obtained through microemulsion polymerization using Dowfax 1A-1 as surfactant (an anionic surfactant).

Recently, Dan et al. [24] studied the synthesis and structure of PMMA microlatex. The experiment was carried out by microemulsion polymerization using semi-continuous feeding of monomer induced by potassium persulfate initiator. The results showed that the polymer content was 30-40 wt% and D_n was 17-33 nm with lower weight ratio of emulsifier to water (SDS/water, 0.01-0.03) and emulsifier to monomer (SDS/MMA $\leq$ 0.05).

1.2.3 Differential Microemulsion Polymerization

In the previous section, a few microemulsion polymerization methods have been described for the preparation of nanosized polymers. Conventional or the modified microemulsion polymerization has many advantages such as small particle size and no need for solvent in the system, however, the major disadvantage of these polymerization methods is the necessity of a high amount of surfactant. Surfactants are not only expensive but they also have a significantly negative impact on the

properties of the synthesized polymer. Thus, the differential microemulsion polymerization method has been developed by the research group of G. L. Rempel at the University of Waterloo. This method is expected to be a practical technical route in that the amount of surfactant required can be decreased while still maintaining the nanoparticle size. Diferential microemulsion polymerization, similar to emulsion polymerization, is performed with water, surfactant, water-insoluble monomer and water or oil soluble initiator. In addition, it still requires a certain temperature to initiate polymerization and agitation to form an emulsion. For the differential method, the monomer is continuously and slowly added to the polymerization system with mild agitation [25]. Smaller monomer-swollen micelles were formed by this monomer addition method. In addition, the continuous feeding of monomer will cause the monomer amount in the reaction system to be much lower and hence there are no monomer droplets during polymerization because the monomer added to the reaction system is quickly consumed by the growing chains in the polymer particle. In this case, there usually exist monomer droplets which act like a monomer reservoir. The free radical in the micelles will propagate with enough monomer transfered quickly from the monomer reservoir. The process of differential microemulsion polymerization is shown in Figure 1.3.

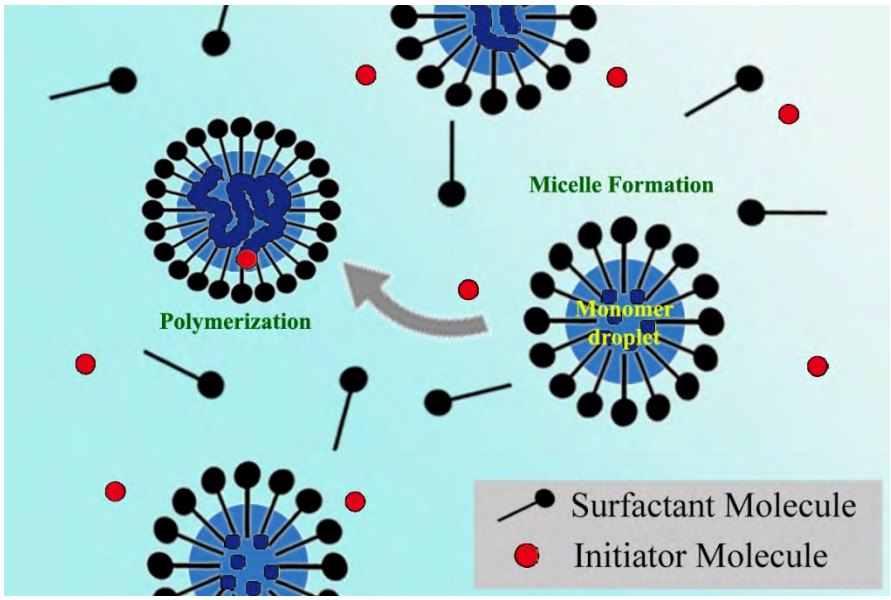

Figure 1.3 Scheme of differential microemulsion polymerization of a hydrophobic monomer.

He et al. [25, 26] studied the synthesis of PMMA nanosized particles by differential microemulsion polymerization. SDS as surfactant and ammonium persulfate (APS) as water-soluble initiator, were used in this system. The particle size of PMMA was less than 20 nm in diameter with low weight ratios of SDS/MMA and SDS/water weight ratios of 1:18 and 1:120, respectively. These results showed that the amount of the surfactant required was indeed much lower when compared with other methods. Moreover, a nanosized acrylonitrile-butadiene copolymer latex (NBR) and nanosized styrene-butadiene copolymer latex (SBR) were also successfully produced by using differential microemulsion polymerization initiated by APS [25]. For synthesis of nanosized NBR latex, the particle size could be reduced to less than 20 nm in diameter at a SDS/monomer and SDS/water weight ratio of 1:9 and 1:80, respectively. Whereas for the preparation of nanosized particles of SBR by the differential microemulsion method, the nanoparticle size of SBR was larger than that of NBR. However, the nanoparticle size of SBR could be made smaller when a core-shell method with some PMMA as seed or a higher reaction temperature was employed.

Norakankorn et al. [27, 28] investigated the synthesis of PMMA nanoparticles initiated by 2,2'-Azoisobutyronitrile (AIBN) via differential microemulsion polymerization. The particle size of PMMA was about 20 nm with a high molecular weight around 1×10^6 and a polydispersity index of about 1–2 was observed in this oil-soluble initiated system. The surfactant amount required could be as low as 1:130 of the MMA amount by weight (SDS/MMA) and the SDS/water ratio could be as low as 1:600, which was much less than the corresponding amounts reported in the literature. In addition, a maximum conversion of 98.6% could be achieved in 1 h.

From these results, it is important to note that the differential microemulsion polymerization initiated by oil-soluble initiator could generate the maximum conversion within a short reaction time in the presence of less surfactant without the need of a co-surfactant and with a high monomer-to-water ratio.

1.3 Chemical Modifications

Chemical modification of unsaturated polymers has been an attractive process for preparation or improvement of novel polymeric materials, which are often inaccessible by conventional polymerization. The modification of polymer materials can be achieved either by the synthesis of new polymers, by new polymerization process, or by the blending of existing polymers having various properties. The chemical functionalization or structural modifications of unsaturated polymer such as cross-linking (vulcanization and curing), grafting, degradation, oxidation, isomerization, cyclization and hydrogenation have been studied for altering and optimizing the physical and mechanical properties of polymers [29-33]. Diene-based polymers which are the most important commercial polymers such as polyisoprene (PIP), polybutadiene (PBD), nitrile butadiene rubber (NBR), styrene butadiene rubber (SBR) and natural rubber (NR) have the presence of unsaturated carbon–carbon double bonds in their backbone structure. The residual carbon–carbon double bonds which were present in the polymer structure are susceptible to thermal and oxidative degradation when exposed to harsh operating systems, resulting in a break down of the structural properties of the polymers. In many research works, graft copolymerization, hydrogenation and vulcanization are interesting areas and will be subsequently described.

1.3.1 Graft Copolymerization

The modification of particle surface by grafting of a monomer on polymer chain is of interest for both academic and industrial sectors. The advantages of graft copolymerization are the increase in colloid stability and improvement of the inferior properties without sacrificing the superior properties. Graft copolymers contain a long sequence of one monomer (often referred to as the backbone polymer) with one or more branches (grafts) with a long sequence of a second monomer [34]. Graft copolymerization is a process in which a backbone polymer chain has attached to it polymeric side chains (grafts) of a different chemical nature [35]. Thus, a graft copolymer is a branched copolymer in which the side chains are structurally distinct from the main chain with random distribution. Figure 1.4 shows an illustration of a

graft copolymer which describes the main chain and side chains as being composed of distinct homopolymers. However, the individual chains of a graft copolymer may be homopolymers or copolymers.

The synthesis of graft copolymers is a sequential process requiring second or multiple step polymerization schemes. Synthesis of graft copolymers mostly involve radical polymerization [34]. The essential requirements for the preparation of graft copolymers are (1) chain transfer to a saturated or unsaturated polymer, (2) activation by photochemical or radiative methods, and (3) introduction and subsequent activation of peroxide and hydroperoxide groups.

The numerous ways for the synthesis of graft copolymers can be divided into three categories. The first pathway to prepare graft copolymers is termed “grafting onto”. The growing chain B attacks the polymer backbone A with formation of a long branch. The second method is called “grafting from”. This means that active sites are generated at the polymer backbone A which initiate the polymerization of monomer B. Another possibility which is called “grafting through” involves the homo and copolymerization of macromonomers, usually a vinyl macromonomer. For this purpose, macromolecules with only one polymerizable end group are needed.

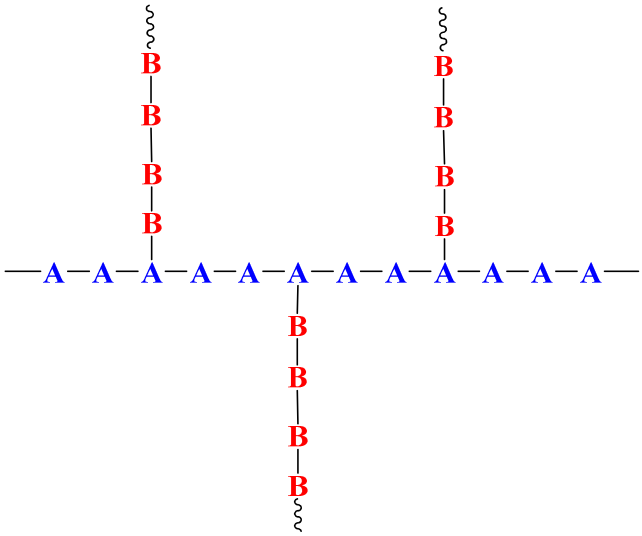

Figure 1.4 Illustration of graft copolymers when chains of a polymer made from monomer B are graft onto a polymer chain of monomer A.

For the final product of a graft copolymerization of monomer B onto the backbone of polymer A, it usually will contain three species [36]:

1. Homopolymer of B which results from homopolymerization of monomer B.
2. Homopolymer of A which is the original backbone polymer A. Then, this backbone is not attacked by free radicals. Thus this is not involved in the graft copolymerization.
3. Graft copolymers which has graft of polymer B branching out from the backbone polymer A.

While the grafting efficiency depends on the competition of the reaction between monomer and backbone for initiator radicals, growing polymer radicals and termination processes. For rubber modification, the polymer backbone can be NR, PB, SBR and NBR due to the presence of C=C bonds grafting monomers such as MMA, ST, acrylonitrile, ethyl methacrylate, maleic anhydride, 2-hydroxyethyl methacrylate.

NR comprised mainly of (*cis*-1,4-polyisoprene) is one example of a backbone polymer with an isoprene repeating unit. NR is well known to be superior among elastic materials with outstanding mechanical properties while it is inferior in oil, ozone and weather resistances. The chemical modification of NR by grafting with vinyl monomers combines the desirable properties of both NR and the polymer of the monomer.

Graft polymerization onto NR has been carried out in solution, dry solid rubber, and latex phases. The graft copolymerization of vinyl monomers such as methyl methacrylate (MMA) [37, 38], styrene (ST) [38, 39], ST-co-MMA [40-42] have been reported. Graft NR-based composite latex particles have some properties better than those of inherent ones and can be used as impact modifiers in thermoplastics [43-45]. For graft copolymerization onto NR, MMA and ST are the most suitable monomers [46]. Many investigators have reported on the influences of

various process parameters on the modification of NR by grafting reactions in both latex and solution.

Generally, the graft copolymerization onto NR can be initiated by water-soluble, oil-soluble initiators and redox initiator systems; Gosh et al. [47] reported the graft copolymerization of MMA onto NR by using benzyl peroxide (BPO) or azo-bis-isobutyronitrile (AIBN) as initiator. The grafting efficiency increased with increasing initiator concentration, monomer concentration. The grafting efficiency of the AIBN system was lower than that of the BPO system. However, this result was opposite to some reports which claimed that AIBN was not an effective initiator for graft copolymerization of MMA onto NR. Thiraphattaraphun et al. [48] studied the grafting of the MMA monomer onto natural rubber using potassium persulfate as an water-soluble initiator. The grafting efficiency increased with increasing initiator concentrationand monomer concentration but decreased with increasing amount of rubber and temperature.

Besides utilization of water-soluble and oil-soluble initiators, graft copolymerization can be carried out using a redox initiator. Redox initiation usually results in grafting with a minimum homopolymerization since only the polymer radical is formed. Mishara et al. [49] studied graft copolymerization of MMA onto rubber initiated by hydrogen peroxide-sodium thiosulphate redox system in aqueous medium. The results showed that the graft yield and percentage of grafting increased with increasing monomer amount and initiator concentration and decreased with increasing reaction temperature.

Oliveira et al. [46, 50] investigated the graft copolymerization of dimethylaminoethyl methacrylate (DMAEMA) or MMA onto NR initiated by a redox couple. The tetraethylene pentamine (TEPA, hydrophilic) and cumene hydroperoxide (CHPO, hydrophobic) redox couple could promote grafting at the interface between hydrophobic NR particles and hydrophilic DMAEMA or MMA. The formation of graft copolymers of modified NR with core-shell morphology as well as satisfactory efficiency of grafting occurred at high concentrations of both monomers. At lower concentrations, the grafting was not significant.

Kangwansupamonkon et al. [51] studied the modification of NR by grafting with hydrophilic vinyl monomers. The CHPO/TEPA, t-BHP/TEPA or $K_2S_2O_8/K_2S_2O_5$ initiation system for grafting of DMAEMA on NR latex gave different grafting efficiencies and CHPO/TEPA was most effective followed by t-BHP/TEPA and $K_2S_2O_8/K_2S_2O_5$.

Kochthongrasamee et al. [52] also studied the effects of redox initiator on graft copolymerization of MMA onto NR. For the grafting of MMA onto NR using CHPO/TEPA, t-BHPO/TEPA and potassium persulfate/sodium thiosulfate ($K_2S_2O_8/Na_2S_2O_3$) redox initiator, it was found that CHPO dissolved very well in the oil phase and TBHPO dissolved moderately in the oil phase, while $K_2S_2O_8/Na_2S_2O_3$ initiation performed in the water-phase and the CHPO/TEPA redox system was found to improve the grafting efficiency.

George et al. [53] investigated the graft copolymerization of MMA onto NR using CHPO/TEPA as redox initiators. The percent grafting increased with increasing MMA content while the grafting efficiency decreased. Secondary nucleation of PMMA was observed when oleic acid was used as a surfactant, while SDS and nonionic nonyl phenol poly(ethylene oxide) used as surfactants gave core-shell morphology with heavily coated PMMA onto particles of smaller size while the larger particles were coated only at higher MMA content.

Manaresi et al. [54] presented the kinetics of graft copolymerization of ST on cis-1,4-polybutadiene. The results showed that the polymerization rate and the polystyrene molecular weights decreased with the rubber content of the solution. The grafting efficiency was found to be substantially independent of the peroxide concentration, but to increase with rubber content. Sundberg et al. [55] also investigated the grafting of ST onto polybutadiene lattices in batch and semi-continuous reactiors. The results showed that the grafting efficiency increased with increasing temperature but it decreased with increasing concentration of a chain-transfer agent.

Xu et al. [56] reported the grafting of ST onto poly(ethyl acrylate) in polyethyl acrylate (PEA) as a seed emulsion process. The grafting efficiency was found to decrease with increasing reaction time, initiator concentration, surfactant concentration and monomer-to-polymer ratio. These results gave rise to the same conclusion as those for grafting of ST onto poly(butyl acrylate) in emulsion initiated with potassium persulfate [57]. This work reported that the grafting reactions occurred between two components on the composite latex particles. Moreover, the highest grafting efficiency in the initial period of seeded emulsion polymerization supported the fact that the surfaces of PEA particles were the sites for the polymerization of styrene.

1.3.2 Hydrogenation Using Diimide Reduction

The modification, particularly the hydrogenation of polydienes, has been studied for many years. The hydrogenation is a very useful method for chemical modification involving reduction of unsaturated hydrocarbon bonds in diene rubber [58]. It improves the physical, chemical and thermal properties of diene-based elastomers. The hydrogenation of polydienes, such as polyacrylonitrile-*co*-butadiene (NBR) [58, 59], polystyrene-*co*-butadiene (SBR) [60] and natural rubber (NR) [61, 62], can be performed with elemental hydrogen in the presence of transition metal catalysts such as $OsHCl(CO)(O_2)(PCy_3)_2$, $RuCl_2(PPh_3)_3$ and $RhCl(PPh_3)_3$. The hydrogenation of NBR [63-70], SBR [71, 72] and NR [73] can also be conducted by using noncatalytic methods, using an organic reagent such as diimide (N_2H_2). The catalytic hydrogenation normally requires special equipment because the reaction is carried out at high temperature and high pressure. Furthermore, severe conditions of catalytic hydrogenation may cause degradation. Therefore, other mild reducing agents which perform under milder conditions have been explored and are preferred. Diimide hydrogenation of the unsaturated rubbers can be prepared at atmospheric pressure with relatively simple apparatus and procedures. As a potential alternative of the conventional hydrogenation technology, the diimide hydrogenation has received increasing attention in the area of hydrogenation of polydienes rubber in latex form.

The hydrogenation process using diimide, which is generated from the redox reaction between hydrogen peroxide and hydrazine hydrate, is energetically favorable. The diimide reduction technique could directly convert elastomers in latex form to its saturated latex form when the elastomer was treated with hydrazine hydrate, an oxidant, and a metal ion catalyst without using a high pressure vessel, organic solvent, or hydrogen gas.

Wideman and Lawson [63] introduced the use of the diimide method to hydrogenate NBR latex. The hydrazine hydrate/hydrogen peroxide (or oxygen) redox system was used to produce diimide in situ, and copper ion (or ferric sulfonate) was used as a catalyst and 80% hydrogenation was achieved. However, it was also found that for natural rubber latex, only 25 % hydrogenation was achieved at 100 $^{\circ}$C in 3 h. Based on this patent [63], Parker et al. [64, 65] provided more refined results and a detailed process for the preparation of highly saturated nitrile rubber latex. For the diimide reduction mechanism, the diimide system occurred at the surface of the particles [64]. Carboxylated surfactants which were adsorbed at the latex particle surface played an important role by forming hydrazinium carboxylates with hydrazine and copper ions. Then, the generated diimide intermediates were stabilized by Cu^{2+} and effectively reduced the carbon–carbon double bonds [65]. The mechanism of diimide hydrogenation was proposed as shown in Figure 1.5 according to the reactions given by the following equations:

$$N_2H_4 + H_2O_2 \xrightarrow{CuSO_4} N_2H_2 + 2H_2O \quad (1.1)$$

$$N_2H_4 + 2\,H_2O_2 \rightarrow N_2 + 4H_2O \quad (1.2)$$

$$NH{=}NH \xrightarrow{CuSO_4} N_2 + H_2 \quad (1.3)$$

$$2NH{=}NH \xrightarrow{CuSO_4} NH_2\text{-}NH_2 + N_2 \quad (1.4)$$

$$NH{=}NH + \text{-}[CH{=}CH]\text{-} \rightarrow N_2 + \text{-}[CH_2\text{-}CH_2]\text{-} \quad (1.5)$$

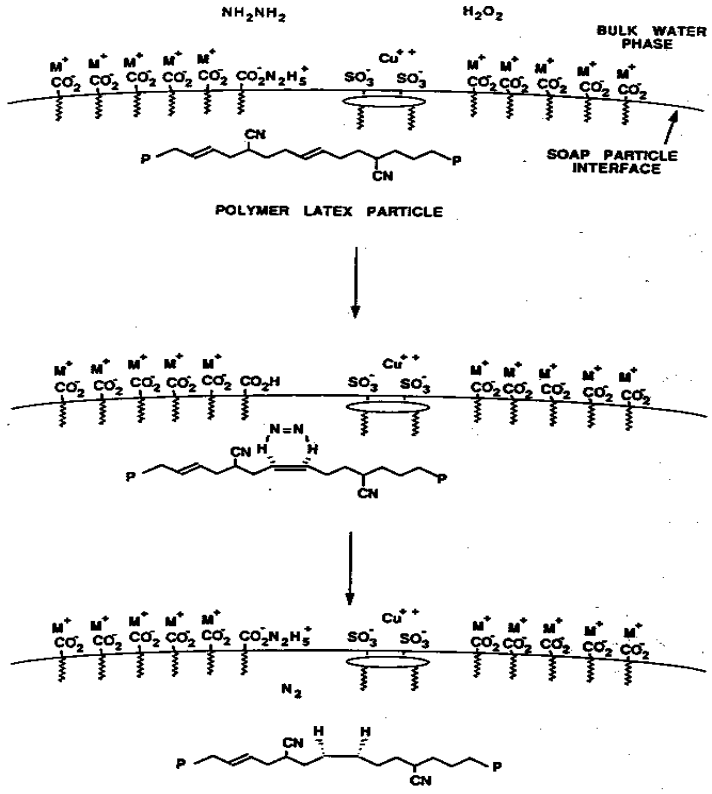

Figure 1.5 Proposed mechanism for hydrogenation [64].

Xie et al. [66] investigated the hydrogenation of NBR latex by hydrogen peroxide and hydrazine with copper sulfate as catalyst. A hydrogenation degree of 87% was achieved after 6 h at 40 °C for a mole ratio of hydrazine to carbon–carbon double bonds of 2.5:1. However, a problem for this process was gel formation. When p-tert-butylprocatchecol was used as an inhibitor for the gel formation, it reduced the percent gel from 94.3 to 21.7%.

Zhou et al. [67] also studied the hydrogenation of NBR latex by hydrogen peroxide and hydrazine with boric acid as catalyst promoter and hydroquinone as inhibitor. A hydrogenation degree of 81.3% was achieved with a low gel fraction of 3% in 6 h at 60 °C. However, this work also showed that the dropwise addition of hydrogen peroxide to reaction system gave higher hydrogenation efficiency.

Lin et al. [68-70] investigated the hydrogenation process of NBR by examining the hydrogenation efficiency and hydrogenation degree. The diimide hydrogenation of NBR latex using boric acid as a promoter could increase the hydrogenation efficiency to a level of nearly 100% when the degree of hydrogenation was below 60% [68]. During the diimide hydrogenation, it was noted that hydrogen peroxide decomposition, and some reactions related to oxygen, and the redox reaction between hydrogen peroxide and hydrazine were capable of generating radicals [69]. The comprehensive simulation of the diimide hydrogenation process was carried out by taking into account the diimide generation reaction, the hydrogenation reaction, the side reaction between hydrogen peroxide and diimide, the disproportionation of diimide and the diimide diffusion process. It was found that the diimide diffusion interfered with the diimide hydrogenation of the NBR latex, even though the particle diameter was as small as 72 nm [70].

He et al. [71] studied the diimide hydrogenation of styrene-butadiene rubber (SBR) latex as a function of different particle sizes. It was found that the hydrogenation of carbon–carbon double bonds depended on the latex particle size and the extent of crosslinking in the particles. The SBR latex with a diameter of 50 nm could be hydrogenated to 91% using 1 mol of hydrazine/hydrogen peroxide per mole carbon double bond. For the SBR latex with a diameter of 230 nm, the hydrogenation degree was only 42%. The effect of particle size on %hydrogenation could be explained according to a “Layer model”. The copper ion catalyst was postulated as staying at the surface of the latex particles. By modulating the concentration of copper ions at the particle surface, higher degrees of hydrogenation could be attained. Moreover, the gel fraction of SBR latex was increased after the hydrogenation.

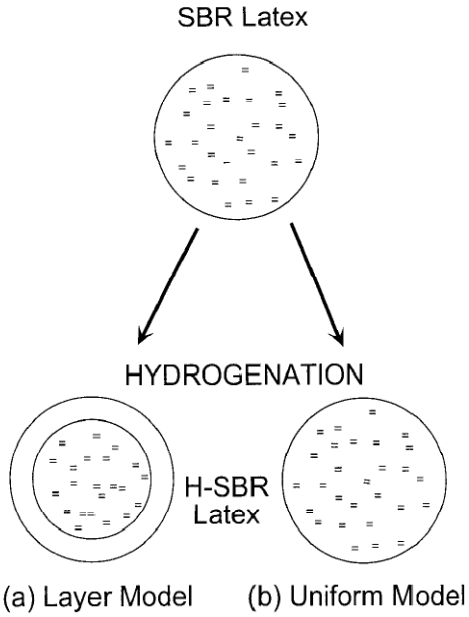

Figure 1.6 Two models for the distribution of double bonds in hydrogenated SBR latex particle: (a) layer model and (b) uniform model [71].

Sarker et al. [72] also investigated the effects of various reaction conditions on the hydrogenation of SBR latex such as reaction time and temperature, pH of latex, and concentration of the hydrogen peroxide, hydrazine, and nature of the catalyst on the hydrogenation degree, calculated from NMR spectroscopy. From this investigation, the degree of hydrogenation increased with increasing reaction time, temperature, the concentration of reactants and catalyst. A maximum of 94% hydrogenation was obtained in this work. The diimide reduction of SBR was first-order with respect to the olefinic substrate, and the apparent activation energy was 9.5 kJ/mol. Moreover, the glass transition temperature increased with increasing hydrogenation degree due to development of crystalline segments.

Mahittikul et al. [73] studied the diimide hydrogenation of natural rubber latex (NR) with diimide using copper sulfate as catalyst. It was found that 67.8% hydrogenation was achieved within 6 h at 55 °C and a low rubber concentration and a high hydrazine concentration provided the optimum condition. Cupric acetate was a highly active catalyst for the reaction and the addition of a

controlled amount of gelatin demonstrated a beneficial effect on the degree of hydrogenation, whereas, the use of the stabilizer, sodium dodecyl sulfate (SDS), in the latex particle in the reaction system reduced the degree of hydrogenation. In the presence of SDS, a longer reaction time and a higher amount of hydrazine hydrate were required for NR latex hydrogenation. For gel formation during hydrogenation, it did not significantly affect the degree of hydrogenation. Moreover, gel inhibitors, hydroquinone, also decreased the degree of hydrogenation.

1.3.3 Vulcanization

Vulcanization is a process generally applied to rubbery or elastomeric material [74]. It involves chemical bonding or crosslinking of rubber chains, usually by the reaction of sulfur and accelerators under pressure at elevated temperature to form three-dimensional structures. The network junctures are generated by the insertion of closslinks between polymer chains. A crosslink may be obtained by a group of sulfur atoms in a short chain, a single atom, a carbon to carbon bond, a polyvalent organic radical, an ionic cluster, or a polyvalent metal ion. Vulcanization increases elasticity but decreases plasticity. The formation of a crosslinked molecular network is shown in Figure 1.7.

Vulcanization is a chemical modification process that is very useful in rubber field for tires and mechanical goods. Unvulcanized rubber is generally not very strong, deficient in elastic recovery, sensitive to temperature and greatly swollen or dissolved by many organic solvents. Thus, vulcanization is required to improve the weak properties of the rubber. The favorite vulcanization method of NR latex is sulfur vulcanization. Vulcanization of NR latex using sulfur as a crosslinking agent can be carried out in two ways: pre-vulcanization and post-vulcanization.

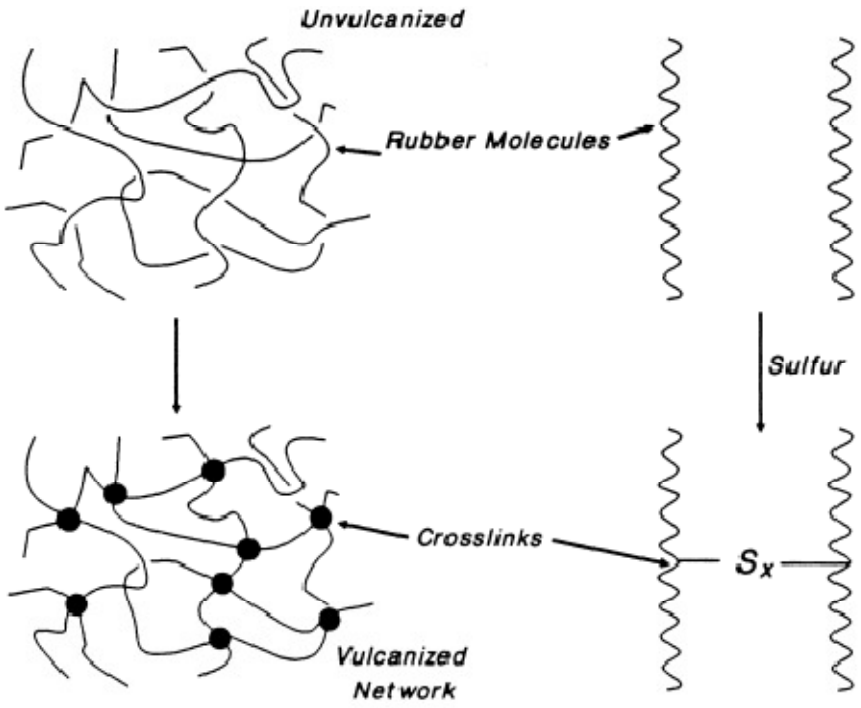

Figure 1.7 Network formation [74].

In the first method, NR latex is vulcanized with the rubber latex still remaining in the dispersed phase. Pre-vulcanized latex is carried out by mixing suitably stabilized latex with vulcanization ingredients (sulfur, accelerators and activators). The crosslink reaction is occurrs with maturation over a temperature range of 20°C to 90°C for appropriate periods. The rate of pre-vulcanization varies with different vulcanization systems and the extent of pre-vulcanization has an influence on the final vulcanization properties. After drying the latex, a vulcanized film with good strength properties is obtained without further heating because the rubber particles in pre-vulcanized latex have already been chemically crosslinked. For post-vulcanization, the compounded latex is vulcanized after it has been dried down to give a film with better resistance to oils, greases and solvents when compared to pre-vulcanized film. Moreover, the mechanical properties of post-vulcanized latex film are similar to or better than those of the film which is prepared from pre-vulcanization. In addition, the thickness of the compounded latex film has an

influence on the temperature and vulcanization time to achieve the required degree of crosslinking.

For the sulfur vulcanization of NR latex, many researchers have reported the influence of process variables on rubber properties. Claramma et al. [75] investigated the effect of temperature on sulfur prevulcanization of NR latex. The vulcanization was carried out under a ratio of S:ZDEC:ZnO dispersion in formulation of latex compound as 3:2:0.4 phr. The maximum crosslink density of the latex film was achieved when the vulcanization of the rubber latex was conducted at 80°C for 2 h or 90°C for 1 h. It was also found that the rate of vulcanization was slow at low temperatures. Moreover, the tensile strength and elongation at break were decreased when the vulcanization time increased at each temperature.

Ho et al. [76] studied the surface morphology of prevulcanized NR latex film by atomic force microscopy. The effect of pre-vulcanized NR latex maturation duration on the properties and morphology of latex films was also investigated. It was found that the crosslink density of latex films increased with increasing maturation duration. The maximum crosslink density of 6.14×10^{-6} mol/cm^3 was achieved under maturation for 8 days. Furthermore, the surface morphology of latex films showed that the vulcanization mechanism was controlled by the relative rates of the diffusion of vulcanizing reagents and the crosslink reaction within the latex particles.

Sasidharan et al. [77, 78] elucidated the effect of the vulcanization time and storage on the stability and physical properties of NR film. The mechanical propeties, the tensile strength and modulus increased but the elongation at break decreased with increasing vulcanization time. The change in the stability and physical properties were due to the crosslinking of rubber particle during vulcanization. While the mechanical stability time values of all vulcanized latex increased during storage for 120 days and thereafter the mechanical stability time slightly decreased at periods of storage between 0 to 300 days.

1.4 Objective and scope of dissertation

The synthesis of nanosized polymers has gained much more attention in recent years. One interesting topic involving polymeric materials is the preparation of polyisoprene nanoparticles by differential microemulsion polymerization, which is a new attractive method. Polyisoprene is a diene polymer which contains unsaturated carbon-carbon double bonds in its configuration. The unsaturated carbon-carbon double bonds in the rubber deteriorate when exposed to sunlight, ozone and oxygen. Chemical modification such as graft copolymerization and hydrogenation are necessary to improve the week rubber properties. This research work will give overviews of the preparation of nanosized polyisoprene by differential microemulsion polymerization method and modification of nanosized polyisoprene latex through a grafting reaction with vinyl monomer and diimide hydrogenation. For these modifications of nanosized polyisoprene, high grafting efficiency and a high degree of hydrogenation are targeted. Moreover, the potential uses of latex polyisoprene nanoparticles and modified nanosized polyisoprene and natural rubber are investigated.

Chapter I provide a historic overview of the understanding of the methods for preparation of polymer nanoparticles, graft copolymerization in emulsion system, diimide hydrogenation of diene polymers and modification of the polymer by vulcanization.

In Chapter II, the experimental information such as detail of materials, experimental procedures are presented. Moreover, the characterization methods utilized are also given in this chapter.

In Chapter III, the synthesis of nanosized polyisoprene via differential microemulsion polymerization is described. An experimental design was used to study the effect of process variables such as amount of initiator and surfactant, monomer to water ratio, reaction time and stirring speed on polyisoprene nanoparticle size and monomer conversion. Moreover, univariate experiments were used to study the effect of surfactant concentration and monomer to water ratio on polyisoprene

nanoparticle size. The rate of isoprene polymerization and characterization of nanosized polyisoprene were also reported in this chapter.

In Chapter IV and V, the results of the synthesis of the graft copolymers of methyl methacrylate or styrene onto nanosized polyisoprene by using cumene hydroperoxide/tetraethylene pentamine as redox initiator were described. The effects of process parameters such as the amount of initiator, monomer to rubber ratio, reaction temperature on grafting efficiency by experimental design were discussed. Univariate experiments were also used to study the effect of monomer concentration and polyisoprene nanoparticle size on grafting efficiency and conversion. In addition, the monomer conversion profile, the grafting efficiency profile and the characterization of graft copolymer were also reported.

In Chapter VI, the diimide hydrogenation of nanosized polyisoprene latex in the presence of cupric ion was presented. The hydrogenated nanosized polyisoprene was characterized using ^{1}H-NMR spectroscopy. The effects of the polyisoprene nanoparticle size, hydrazine concentration, hydrogen peroxide concentration and rubber concentration on degree of hydrogenation were explored.

In Chapter VII, the objective is to study the mechanical properties of the compound film of natural rubber filled with nanosized polyisoprene and natural rubber filled with modified nanosized polyisoprene. Pre-vulcanization was used to prepare the latex compound. Physical properties of pre-vulcanized rubber latex compound and mechanical properties of vulcanized film were described.

Finally, the important conclusions resulting from this study are summarized and the recommendations for future work are provided in Chapter VIII.

CHAPTER II

EXPERIMENTAL AND CHARACTERIZATION

2.1 Materials

2.1.1 Preparation of Nanosized Polyisoprene

Isoprene monomer (IP, Aldrich, 99%) and de-ionized water were used for all polymerization experiments. Sodium persulfate (SPS, Aldrich, 99%), ammonium persulfate (APS, Aldrich, 99%) and 2, 2'-azoisobutyronitrile (AIBN, Polyscience, AR grade) were used as initiators, sodium dodecyl sulfate powder (SDS, J.T.Baker, 99.7%) as a surfactant, sodium bicarbonate (SHC, BDH Inc., 99.7%) as a buffer, and a small amount of *n*-dodecyl mercaptan (*n*-DM, Aldrich, 97%) was used as a chain transfer agent. Methyl ethyl ketone (MEK, Fisher) was used as a coagulation agent.

2.1.2 Preparation Nanosized Methyl Methacrylate Graft Polyisoprene and Nanosized Styrene Graft Polyisoprene

Nanosized polyisoprene (nanosized PIP) and de-ionized water were used for all graft copolymerizations of methyl methacrylate (MMA) or styrene (ST) onto nanosized PIP. Reagent grade MMA monomer (purity > 99%, MERCK) and reagent grade ST monomer (purity > 99%, Aldrich) were destabilized in a conventional way by washing with 10% aqueous solution of sodium hydroxide (NaOH) and then with de-ionized water until neutrality was reached. The emulsifier SDS powder (99.7%, J.T.Baker), the stabilizer isopropyl propanol, the buffer potassium hydroxide (KOH, Ajax Finechem), the redox initiation system, cumene hydroperoxide (CHPO, 80%, Aldrich) and activator agent tetraethylene pentamine (TEPA, ACROS) were used as received.

2.1.3 Preparation of Nanosized Hydrogenated Polyisoprene

Nanosized PIP and de-ionized water were used in all diimide hydrogenation experiments. Hydrazine hydrate (>99%) was ordered from Sigma-Aldrich while hydrogen peroxide (30% aqueous solution,), copper sulfate and d-chloroform (for analysis) were purchased from Merck Co. Ltd. (Bangkok, Thailand). Silicone oil was used as received from Ajax Finechem (Auckland, New Zealand). Methylethylketone was obtained from Fisher Scientific (Fair Lawn, NJ).

2.1.4 Pre-vulcanization

Nanosized PIP and nanosized styrene graft onto PIP were used in rubber film pre-vulcanization. The commercial high-ammonia NRL comprised almost entirely of cis-polyisoprene had 60% by weight dry rubber content and was obtained from Rubber Research Institute of Thailand. Vulcanizing agents such as sulfur, zinc oxide (ZnO), zinc diethyl dithiocarbamate (ZDEC) were produced in dispersion by Rubber Research Institute of Thailand. Ammonia (25% aqueous solution, BDH Inc.) and de-ionized water were used throughout the work.

2.2 Synthesis of Nanosized Polyisoprene via Differential Microemulsion Polymerization

Differential microemulsion polymerization of isoprene was carried out in a 300-mL Parr reactor. In this work, SPS or APS or AIBN was used as initiator. 0.20-0.80 %wt initiator, 2.12-2.48 %wt sodium dodecyl sulfate, 0.60 %wt sodium bicarbonate and 0.20 %wt n-dodecyl mercaptan were dissolved in de-ionized water and charged into the reactor. After that the mixture was heated to the desired reaction temperature, the specified amount of isoprene monomer, 20.67-23.92 %wt was added continuously to the reactor. Generally the monomer was fed very slowly with continuous dropping of monomer droplets using a peristaltic pump at a flow rate of 0.6 mL/min for a designated time. After the addition of monomer was completed, the reaction system was kept at the reaction temperature with constant agitation for another hour in order to obtain a higher conversion of the microemulsion polymer. A

schematic of the apparatus used for the synthesis of nanosized polyisoprene is provided in Figure 2.1

The unreacted isoprene monomer was displaced from the product latex by nitrogen gas at ambient temperature. The resultant polymer was precipitated using an excess of MEK solvent and was dried in a vacuum oven.

The monomer conversion and dry rubber content of polyisoprene were determined by a gravimetric method and calculated using equation (2.1) and (2.2).

$$\text{Conversion} \quad (\%) \quad = \frac{\text{Weight of monomer reacted}}{\text{Weight of monomer charged}} \times 100 \tag{2.1}$$

$$\%\ \text{Dry Rubber Content} \quad (\%\text{DRC}) \quad = \frac{\text{Weight of dry polymer}}{\text{Weight of polymer}} \times 100 \tag{2.2}$$

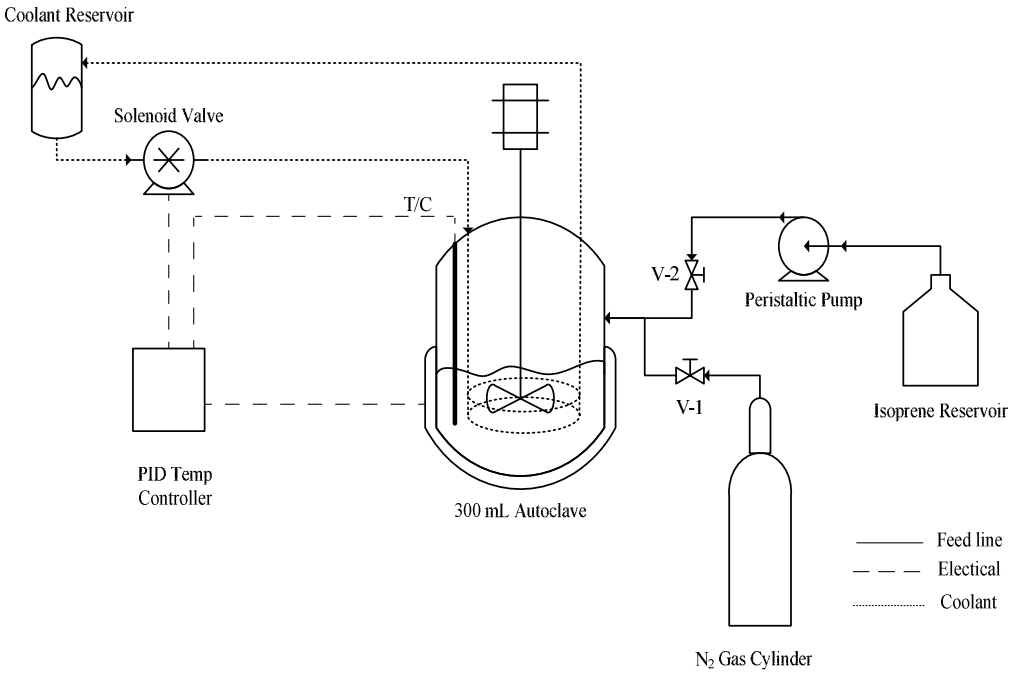

Figure 2.1 Schematic of the synthesis of nanosized polyisoprene apparatus.

2.2.1 Factorial Design Experiments

The multiple independent variables involved in nanosized polyisoprene synthesis give rise to factorial design experiments. In this work, five process variables, which are expected to have an effect on the synthesis of nanosized polyisoprene, were considered. These variables include the concentrations of initiator and surfactant, the IP/H_2O ratio, the reaction temperature and the stirring speed. The effects are complex and may include some interactions. When using two level fractional factorial design, the number of experiments can be reduced without loss of information about the main effects. In this case, a two level fractional factorial design was chosen, since the higher-order interactions were expected to be negligible. Process variables were varied according to a 2_V^{5-1} design. For each variable, a lower "-1 level" and higher "+1 level" were chosen over the range to be studied. The low level and high level of each design were coded as -1 and +1, respectively. The independent variables listed in Table 2.1 shows the low level and high level values of initiator concentration (AIBN), surfactant concentration (SDS), monomer-to-water ratio (IP/H_2O), reaction temperature (TEMP) and stirring speed (SS). The experiments all conditions of 16 runs are listed in Table 2.2

Table 2.1 Synthesis of nanosized polyisoprene: low and high level of design factors.

Factors	Name	Amount (Low = -1)	Amount (High = +1)
[AIBN]	2, 2'-Azoisobutyronitrile	0.33 %(w/v)	1.11 %(w/v)
[SDS]	Sodium dodecyl sulfate	2.78 %(w/v)	3.33 %(w/v)
IP/H_2O	Isoprene/Water ratio	0.4	0.5
TEMP	Reaction Temperature	60 °C	70 °C
SS	Stirring Speed	100 rpm	300 rpm

Table 2.2 Design matrix of experimental design for synthesis of nanosized polyisoprene.

Experiment	Basic Design				
	[AIBN]	[SDS]	IP/H_2O	TEMP	SS
PIP1	-1	-1	+1	-1	-1
PIP2	-1	-1	-1	+1	-1
PIP3	+1	-1	+1	-1	+1
PIP4	-1	+1	-1	+1	+1
PIP5	+1	+1	-1	+1	-1
PIP6	+1	-1	-1	+1	+1
PIP7	+1	+1	-1	-1	+1
PIP8	-1	-1	-1	-1	+1
PIP9	-1	+1	-1	-1	-1
PIP10	+1	+1	+1	+1	+1
PIP11	-1	+1	+1	+1	-1
PIP12	-1	-1	+1	+1	+1
PIP13	+1	-1	-1	-1	-1
PIP14	-1	+1	+1	-1	+1
PIP15	+1	+1	+1	-1	-1
PIP16	+1	-1	+1	+1	-1

Conditions: [SHC] (%wt) = 0.60; [*n*-DM] (%wt) = 0.20, Time 20 h.

2.2.2 Univariate Synthesis of Polyisoprene Nanoparticle

From the factorial design results, univariate experiments were formulated and performed. The influences of surfactant concentration over the range

of 0.43-3.34 %wt (SDS/IP: 0.01-0.12) and isoprene-to-water ratio range of 0.2-0.8 (SDS/IP: 0.04-0.18) on the polyisoprene nanoparticle size and the monomer conversion were also investigated.

2.3 Graft Copolymerization of Methyl Methacrylate onto Nanosized Polyisoprene

The graft copolymerization was carried out in a 500 mL four-necked round bottom flask, equipped with magnetic stirrer, condenser and nitrogen inlet. Nanosized polyisoprene latex and an aqueous solution, containing de-ionized water, 10 phr (10 parts per 100 parts of dry rubber content, by weight) i-propanol as stabilizer, and 1 phr SDS as an emulsifier, were charged to the reactor and the dissolved oxygen in the ingredients was removed by purging with nitrogen gas for at least 30 min, while continuously providing a stable latex. A potassium hydroxide solution, as a buffer, was added to maintain the pH of the latex above 10. The MMA monomer was fed to the reactor. The polyisoprene seed latex was then swollen with the monomer for 30 min at the reaction temperature before adding the initiator. The CHPO initiator was added to the system and then TEPA was added as an activator agent (CHPO:TEPA = 1:1). The polymerization reaction was performed with a stirring speed of 200 rpm at the desired temperature for 8 h. Graft copolymer samples were taken at intervals which were cast at room temperature in open trays to determine the degree of conversion of monomer to polymer gravimetrically.

The graft nanosized polyisoprene was recovered and dried to a constant weight. A soxhlet extraction procedure was carried out to assess the amounts of the graft copolymer, free nanosized polyisoprene and free homopolymer in the final product. The free nanosized PIP was removed with light petroleum ether and the free poly(methyl methacrylate) was extracted using acetone.

2.3.1 Design Experiments for Graft Copolymerization

The multiple independent variables involved in graft copolymerization suggest factorial design experiments. In this work, three process variables, which are

expected to have an effect on the graft copolymerization, are considered. These variables include the concentrations of initiator, MMA monomer content and the reaction temperature. Process variables were varied according a 2^3 design. For each variable, a lower "-1 level" and higher "+1 level" were chosen over the range to be studied. The independent variables listed in Table 2.3 are initiator concentration (INT), monomer concentration (MMA) and reaction temperature (TEMP). The experiments (a total of 8 runs) are listed in Table 2.4.

2.3.2 Univariate Experiments for Graft Copolymerization

From factorial design results for the synthesis of nanosized MMA-g-PIP using a redox initiator system, the effects of initiator concentration, monomer concentration and reaction temperature on graft copolymerization were presented in the previous section. From these results, univariate experiments were formulated and performed. The influences of monomer concentration (40, 60 and 100 phr), reaction time and particle size of the nanosized PIP (25, 40 and 60 nm) on the grafting MMA onto polyisoprene were also explored.

Table 2.3 Graft copolymerization of methyl methacrylate onto nanosized polyisoprene: Low and high level of design factors.

Factors	Name	Amount (Low = -1)	Amount (High = +1)
[INT]	Cumene hydrogenperoxide	1 phr	2 phr
[MMA]	Methyl methacrylate	40 phr	60 phr
TEMP	Reaction Temperature	50 ^{o}C	70 ^{o}C

Table 2.4 Design matrix of preparation nanosized MMA-g-PIP experimental design.

Experiment	Basic Design		
	[INT] (phr)	[MMA] (phr)	Temp (^{o}C)
MMAgPIP1	+1	+1	+1
MMAgPIP2	+1	-1	+1
MMAgPIP3	+1	-1	-1
MMAgPIP4	-1	-1	+1
MMAgPIP5	-1	-1	-1
MMAgPIP6	-1	+1	-1
MMAgPIP7	-1	+1	+1
MMAgPIP8	+1	+1	-1

Grafting conditions: Stirring speed = 200 rpm, [SDS] = 1 phr; reaction time = 8 h.

PIP synthesis condition: [AIBN] = 0.25 %wt; [SDS] = 2.53 %wt; IP/H_2O = 0.4; [SHC] = 0.60 %wt; [*n*-DM] = 0.20 %wt; temperature = 70 ^{o}C; stirring speed = 300 rpm; reaction time = 20 h; $D_{n\ (PIP)}$ = 25-27 nm

2.4 Graft Copolymerization of Styrene onto Nanosized Polyisoprene

The graft copolymerization of styrene onto nanosized polyisoprene latex was carried out similar to the preparation of nanosized MMA-g-PIP mentioned in section 2.3. The influences of monomer concentration (60, 100 and 150 phr), reaction temperature (40, 50, 60 and 70 °C) and particle size of the nanosized PIP (25, 40 and 60 nm) on the grafting of ST onto polyisoprene were investigated. The polymerization reaction was performed with a stirring speed of 200 rpm at the desired temperature for 8 h. Samples were taken at intervals to determine the degree of conversion of monomer to polymer.

The nanosized graft polyisoprene was recovered and dried to a constant weight. A Soxhlet extraction procedure was carried out to assess the amounts of the graft copolymer, free nanosized polyisoprene and free homopolymer in the final product. The free nanosized PIP was washed out with light petroleum ether. To remove free polystyrene, the residue was removed by methyl ethyl ketone.

The schematic of the apparatus used for the graft copolymerization of vinyl monomer (MMA or ST) onto nanosized polyisoprene is provided in Figure 2.2 and the experimental procedure followed is outlined in Figure 2.3.

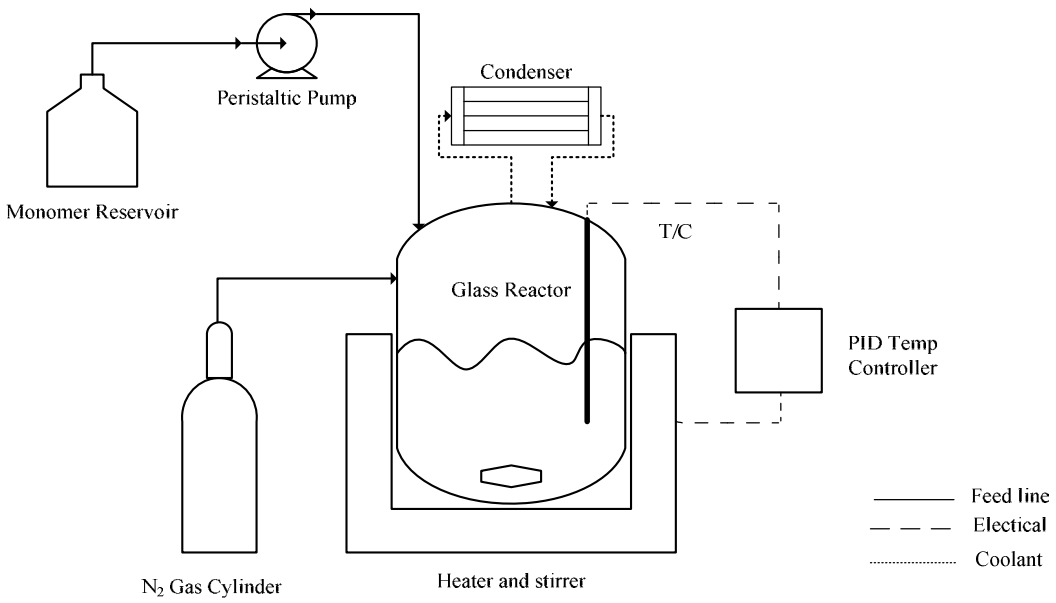

Figure 2.2 Schematic of apparatus used for graft copolymerization of MMA or ST onto nanosized polyisoprene.

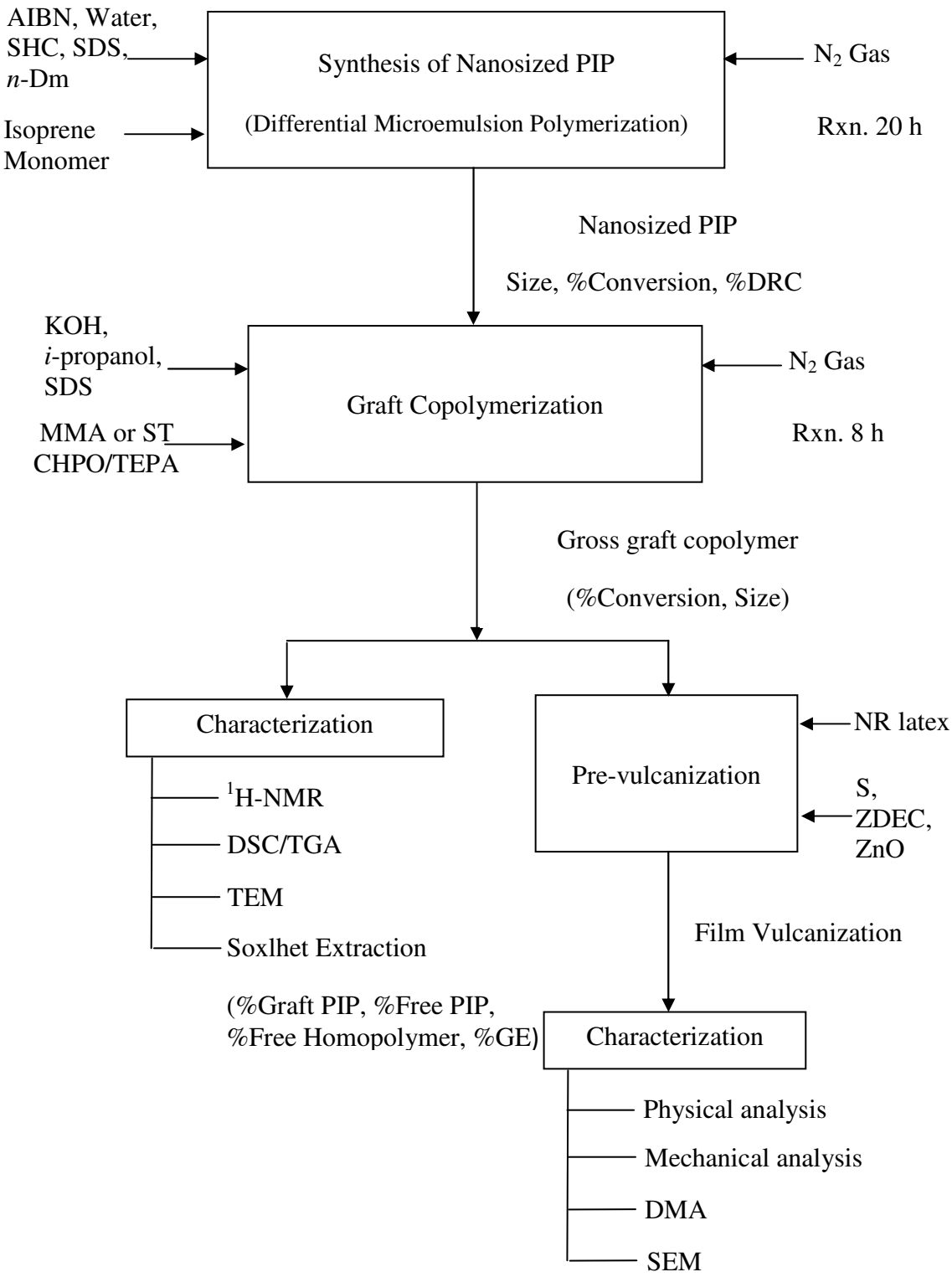

Figure 2.3 The experimental procedure for graft copolymerization and vulcanization.

2.5 Diimide Hydrogenation of Nanosized Polyisoprene

The nanosized PIP latex was added to a 500 mL four-necked flask. After stirring for 30 min, copper sulfate and hydrazine hydrate were added respectively, and stirred for 60 min. Then, the mixture was heated to the reaction temperature. Hydrogen peroxide was added dropwise at a rate such that the temperature of the mixture did not increase. During the addition of hydrogen peroxide, if too many bubbles were formed, a small amount of silicone oil as an antifoaming agent was added. After a reaction time of 6 h, the mixture was post-reacted for 30 min while cooling to room temperature. The nanosized hydrogenated polyisoprene latex was coagulated in methyl ethyl ketone (MEK) and dried under vacuum.

The schematic of the apparatus used for diimide hydrogenation of nanosized polyisoprene is shown in Figure 2.4 and the experimental procedure is summarized in Figure 2.5.

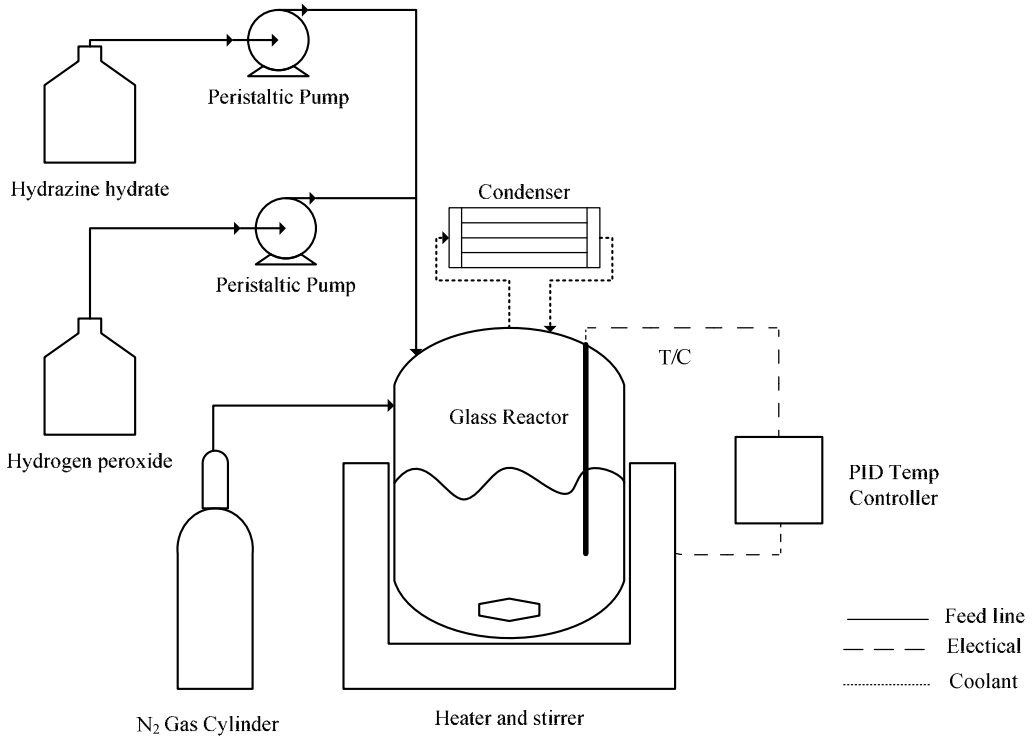

Figure 2.4 Schematic of diimide hydrogenation of nanosized polyisoprene apparatus**.**

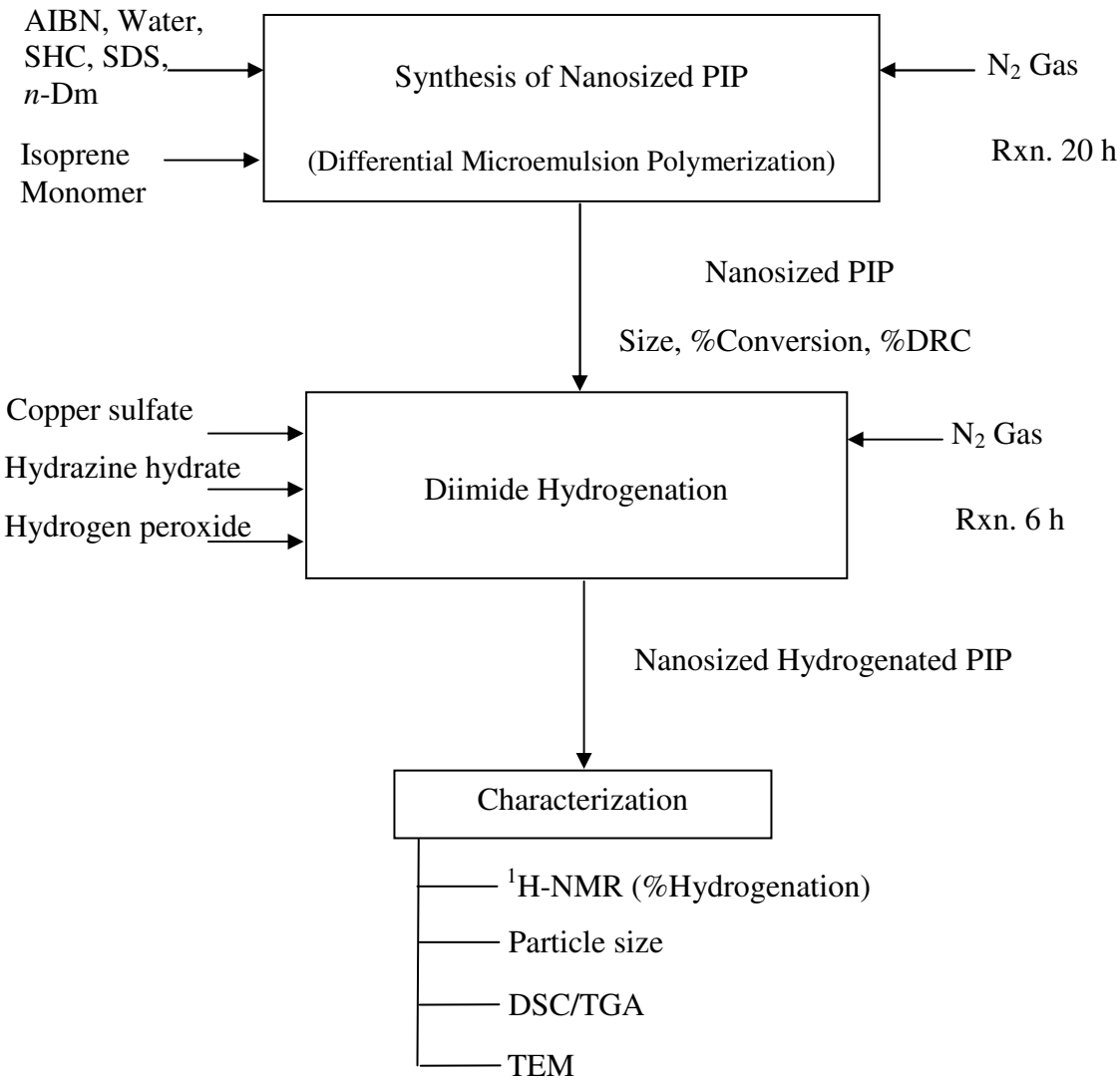

Figure 2.5 The experimental procedure for diimide hydrogenation.

2.6 Blending and Vulcanization

2.6.1 Latex Compound Preparation

Latex compounds of varying composition (0–30%) at 15% intervals by weight were prepared as nano-PIP, nano-graft PIP products. Vulcanizing agent dispersion (50%) of commercial chemicals was used as received. The latex was mixed with the compounding ingredients according to the formulation given in Table 2.5. The latex compounds were prevulcanized in a water bath at 60°C and stirred well for 2 h providing a homogeneous mixture. After that the compounded latex was cooled to room temperature. The compounded latex was then matured (keeping overnight to facilitate the diffusion of added chemicals), which ensures latex films of uniform properties. The compounded latex was cast on raised glass plates having a dimension of 13 cm × 13 cm × 2 mm. The cast film was then allowed to dry in air until transparent and then vulcanized at 70°C for 4 h in an air circulated oven.

Table 2.5 Formulation of the NR Latex Compound.

Ingredients	Dry (parts by weight, phr)
60% Natural rubber latex	Variable
	100, 85, 70
20% DRC of Nano-PIP latex or	Variable
50%GE of Nano-Graft PIP latex	0, 15, 30
50% Sulfur dispersion	1.0
50% ZDEC dispersion	1.5
50% Zinc oxide	2.0

2.6.2 Accelerated Thermal Ageing of Vulcanized Products

Vulcanized rubber specimens were aged at 100°C for 24 h in an air-circulating ageing oven and the tensile properties of the aged samples were determined according to ASTM D 573 (1994). Tensile test (ASTM D 412-99) was carried out on a tensile dumbell test specimen before and after ageing to estimate ageing resistance.

2.7 Characterization Methods

2.7.1 Fourier Transform Infrared Spectroscopic Analysis

The structure of polyisoprene was characterized using Fourier Transform Infrared Spectroscopy (FTIR, Bio–Rad FTS 3000X spectrometer). The FTIR samples were prepared by dissolving the polyisoprene in toluene (2% w/v) and then cast as a film on a sodium chloride (NaCl) disk. The solvent was evaporated at ambient temperature before recording the infrared spectra.

2.7.2 ^{1}H-NMR Analysis

Nuclear Magnetic Resonance spectroscopy (^{1}H-NMR, Bruker 300 MHz spectrometer) was used to characterize the structure of the polymer. The ^{1}H-NMR samples were dissolved in $CDCl_3$ at atmospheric pressure and room temperature and ^{1}H-NMR spectra were recorded.

For graft copolymerization, the presences of functional groups within the graft copolymer were quantified by ^{1}H-NMR spectra. The graft PIP samples were also dissolved in $CDCl_3$ and the ^{1}H-NMR spectrum was recorded.

For hydrogenation, the final degree of hydrogenation was evaluated by ^{1}H-NMR spectroscopy. The ^{1}H-NMR spectra of the rubber sample dissolved in $CDCl_3$ at room temperature was recorded on a Bruker 300 MHz spectrometer. The extent of hydrogenation was calculated from the ^{1}H-NMR spectra by the change in the integral of the peaks representing protons for the hydrogenated rubber latex. The

lump peak area for the saturated protons (-CH_2- and –CH_3) in the range of 0.8–2.3 ppm and the unsaturated protons peak area around 4.5-5.2 ppm were measured in order to calculate the %hydrogenation using equation (2.3):

$$\text{Hydrogenation (\%)} = \frac{\text{A - 7B}}{\text{A + 3B}} \times 100 \tag{2.3}$$

where A was the lump peak area of saturated protons and B was peak area of unsaturated protons. An example for the %hydrogenation calculation is provided in Appendix B.

2.7.3 Number-average Diameter Measurement

The number-average diameter (D_n) of the polymer particles was measured using a dynamic light scattering technique (DLS, Nanotrac Instrument).

2.7.4 Molecular Weight Measurement

Average molecular weights (M_n and M_w) and the molecular weight distribution were determined using a gel permeation chromatography system (GPCMALLS, Wyatt Technology) which consisted of a Waters 1515 isocratic HPLC pump and Waters 2414 refractive index detector (RID). Breeze software was used for data collection and processing. HPLC grade tetrahydrofuran (Lab Scan Asia) was used as the mobile phase at a flow rate of 1.0 mL/min. The samples of 0.1 % (w/v) rubber solution were filtered through a 0.45 μm pore size filter and then 100 μL of the filtered samples were injected into the GPC for analysis.

2.7.5 Thermogravimatic Analysis (TGA)

Thermogravimetric analysis (TGA) was performed on a Perkin-Elmer Pyris Diamond thermogravimetric/differential thermal analysis instrument. The samples were placed into a platinum pan. The temperature was raised under a nitrogen atmosphere from room temperature to 800^{o}C at a constant heating rate of 10^{o}C/min.

The nitrogen gas flow rate was 50 mL/min. The initial decomposition temperature (T_{id}) and the temperature at the maximum of mass-loss rate (T_{max}) were evaluated.

2.7.6 Differential Scaning Calorimetry (DSC)

Differential scanning calorimetry (DSC) was carried out on a TA Instrument DSC Model 2920. The instrument signal was derived from the temperature difference between the sample and the reference. The polyisoprene and graft copolymer samples were cooled to –100°C with liquid nitrogen and then heated to 200°C at a constant rate of 20°C/min. The hydrogenated sample was cooled to –100°C with liquid nitrogen and then heated to 30°C at a constant rate of 20°C/min. The glass transition temperature (T_g) was calculated from the midpoint of the base-line shift of the DSC thermogram.

2.7.7 Morphological Study

The morphology of latex particle was observed by transmission electron microscopy (TEM). A small amount of sample was dispersed in water and dropped on the grid. The samples were stained with OsO_4 vapor for 24 h before observation. The samples were examined using a JEOL JEM-2100 (200 KV) transmission electron microscope (Tokyo) at 120 kV.

The morphology of the vulcanized film was explored using a scanning electron microscope (SEM). The fracture surfaces after tensile testing were cut and stitched on a SEM stub using double-sided tape. Then, the sample was sputter – coated with gold and examined using a scanning electron microscope, JEOL model JSM – 6480 LV operated at 15 kV.

2.8 Determination of Grafting Efficiency and Grafting Properties

The gross graft copolymer was cast in an open tray and dried at ambient temperature. The ungraft nanosized PIP was extracted with petroleum ether using a soxhlet extractor for 24 h. To remove free homopolymer, poly(methyl methacrylate) (PMMA), the residue was extracted in acetone for 24 h. While

removing free polystyrene (PS), methyl ethyl ketone was used to extract the residue for 24 h. Weight of both initial samples and the extracted samples were measured for the determination of the graft copolymer and free copolymer contents. The monomer conversion (C, %) and grafting efficiency (GE, %) were estimated from the following equations [79-81]:

$$\text{Grafting efficiency (GE) (\%)} = \frac{\text{Total weight of polymer formed}}{\text{Weight of grafted monomer}} \times 100 \quad (2.4)$$

$$\text{Graft PIP (\%)} = \frac{\text{Weight of graft copolymer}}{\text{Weight of gross polymer}} \times 100 \quad (2.5)$$

$$\text{Homopolymer (\%)} = \frac{\text{Weight of free homopolymer}}{\text{Weight of gross polymer}} \times 100 \quad (2.6)$$

2.9 Properties of Pre-vulcanized Latex Determination

2.9.1 Equilibrium Swelling of Pre-vulcanized Latex [82]

The equilibrium swelling of a vulcanized rubber in a solvent was dependent on the density of crosslink, the nature of the solvent and the rubber. Equilibrium swelling values were determined by immersing a thin film of the rubber sample (10 x 10 x 2 mm) in the toluene solvent for 48 hours and measuring the increase in weight at equilibrium. Equilibrium swelling ratios are usually calculated using equation (2.7).

$$Q = \frac{W_2 - W_1}{W_1} \quad (2.7)$$

where Q = swelling index, W_1 = initial weight, W_2 = equilibrium swelling weight. The variation of 'Q' with crosslink density, for conventionally-cured natural rubber in toluene, may be broadly described as follows:

Unvulcanized rubber, Q = >15

Lightly vulcanized, Q = 7-15

Moderately vulcanized, Q = 5-7

Fully vulcanized, Q = <5

2.9.2 Crosslink Density of Pre-vulcanized Latex

The crosslink density efficiency of the sample was elucidated in terms of crosslink density using an equilibrium solvent swelling test method. The specimens (10 x 10 x 2 mm) were accurately weighed and then were immersed in toluene and allowed to swell in close vessels for 7 days. After that, the surface of the swollen samples was quickly wiped and the sample was weighed (w_1). After drying at 40°C for 48 h, the dried rubber samples were weighed again (w_2) to determine the amount of absorbed toluene inside the samples. The volume fraction of polymer in the swollen specimens (v) was calculated using equation (2.8).

$$v = \frac{w_2\,(\delta_r\,)^{-1}}{w_2\,(\delta_r\,)^{-1} + (w_1 - w_2)(\delta_S\,)^{-1}} \tag{2.8}$$

where δ_r and δ_S are the density of rubber and solvent, respectively. The crosslink density of the specimens was calculated based on the Flory-Rhener [83] equation (2.9)

$$-[\ln(1-v) + v + \chi v^2] = V_0 n[v^{\frac{1}{3}} - \frac{v}{2}] \tag{2.9}$$

where n is the number of elastically active chains per unit volume (mol/cm^3). V_0 is the molar volume of the solvent (106.3 cm^3/mol for toluene) and χ is the Flory-Huggins polymer solvent interaction term. For this experiment an assumed value of $\chi = 0.39$ (χ of NR-toluene) was used for all calculations [82, 84].

2.9.3 Chloroform Number Test in Pre-vulcanized Latex [82]

The chloroform test was performed by mixing an equal part (ca. 5 g) of prevulcanized latex and chloroform and then stirring until coagulation was completed. The state of vulcanization could therefore be judged from the appearance of the coagulum. An arbitrary number, known as the chloroform number, was assigned to the latex on the basis of appearance. Four stages of latex vulcanization were usually distinguished by this test, and were assigned as chloroform numbers as follows, the perceived degree of vulcanization increased with increasing chloroform number as follows:

State	Coagulum form
No.1	Uncrosslinked rubber tacky lump
No.2	Lightly vulcanized rubber tender lumps, breaks short
No.3	Moderately vulcanized rubber non-tacky crumbs
No.4	Fully vulcanized rubber fine dry crumbs

2.10 Mechanical Properties of Vulcanized Rubber

The mechanical properties in terms of tensile strength and hardness of pre-vulcanized rubber were evaluated. The tensile test of all pre-vulcanized film samples was carried out on a Universal Testing Machine (LLOYD model LR5K) at 500 mm/min of the cross-head speed. This test method followed the standard method ASTM D412. Testing specimens were cut using a die C and the average of three specimens was considered as the representative value. The cutting die punched the

specimen into dumbbell samples which were 25 mm in gauge length, 25 mm in width and 2.0 mm in thickness. The elongations at break were also measured.

The hardness testing was measured at the room temperature using Durometer Shore-type-A according to ASTM D2240. The measurements were taken from five different points distributed over the sample and the reported values were based on an average of five measurements.

2.11 Dynamic Mechanical Properties of Vulcanized Rubber

Dynamic mechanical properties such as storage modulus and loss modulus of the rubber samples after the vulcanization process were examined using a GABO QUALIMETER EPLEXOR 25N with tension mode. The temperature scan was run at an oscillation frequency of 4 Hz with a heating rate of 10 °C/min. The vulcanized rubber samples were cut as strips of 10 mm width, 10 mm length and 2 mm thickness.

CHAPTER III

SYNTHESIS NANOSIZED POLYISOPRENE VIA DIFFERENTIAL MICROEMULSION POLYMERIZATION

3.1 Introduction

Emulsion polymerization plays a large role in attempts to produce rubber latex, a material which has gained great importance. The rubber latex e.g. natural rubber, is a dispersion of polymer particles in water with a particle size ranging from 100 nm up to 2000 nm (2 μm), stabilized by surface proteins and lipid surfactants [85]. The polyisoprene synthesis using redox initiators in emulsion polymerization was investigated and it was found that the polymerizations initiated with the potassium persulfate/sodium bisulfite (KPS/SBS) redox couple had a significant inhibition period and provided a low yield [86]. For isoprene polymerization initiated by the tert-butylhydroperoxide/tetraethylene pentamine redox couple, the results showed resonable yields and no apparent inhibition. It was proposed that the lipophilic nature of the t-butyl group plays a favorable role in the entry of hydroperoxide-initiated oligomeric radicals, while persulfate initiated radicals are more likely to undergo aqueous phase termination before entry. Moreover, the preparation of polyisoprene latex using benzoyl peroxide (BPO) and KPS were also investigated and the results showed that polymerization using oil- soluble initiator (BPO) gave lightly cross-linked polyisoprene latex while, polymerization using water-soluble initiator (KPS) and high SDS/IP weight ratio, provided a small particle size around 30-40 nm with high gel content. For the seed polyisoprene synthesis using sodium persulfate (SPS) as an initiator and sodium bicarbonate as a buffer in the emulsion polymerization, a small seed of polyisoprene of 59.4-137 nm was obtained [87].

As described in Chapter 1, the microemulsion polymerization is a common method used to synthesize polymer nanoparticles. The particle size from

microemulsion polymerization is considerably smaller, usually 10-50 nm, as opposed to conventional emulsion polymerization. The major disadvantage of microemulsion polymerization is the necessity of using a high amount of surfactant. Surfactants are not only expensive but also have a significant negative impact on the properties of the synthesized polymer. However, differential microemulsion polymerization is a practical technical route in that the amount of surfactant required could be decreased while still maintaining the nanoparticle size. Therefore, the differential microemulsion polymerization could be applied for the synthesis of nanosized rubber latex.

The purpose of this work was to prepare nanoparticles of polyisoprene by a differential microemulsion polymerization method, and to clarify the effects of process variables on rubber nanoparticle size and monomer conversion. Due to a complexity of the investigation, in view of the great number of variables involved, among which are the initiator and surfactant concentration, monomer-to-water ratio, reaction temperature, stirring speed and reaction time, factorial design experiments are very useful in identifying the main effects of process variables on nanosized polyisoprene synthesis.

3.2 Preliminary Study of Nanosized Polyisoprene Synthesis

Effect of initiator type, stirring speed and reaction temperature on monomer conversion and PIP nanoparticle size were investigated in the preliminary study. The results of the initial study are provided in Table 3.1 and Table 3.2 and will be subsequently discussed.

The results of isoprene polymerization using the SPS initiator at different reaction temperatures and stirring speeds are presented in Table 3.1. The dry rubber content (DRC) and monomer conversion increased with increasing reaction temperature and stirring speed. This can be explained in that the higher stirring speed caused a decrease in monomer droplet size resulting in a larger interfacial area for emulsion polymerization. Moreover, increasing reaction temperature increased the degree of micelle ionization while the agglomeration number of sodium dodecyl

sulfate (SDS) decreased [88]. Hence, the stabilizing activity of SDS increased with the temperature. This behavior led to the production of a high yield of nanosized polyisoprene. Similar behavior was also observed in synthesis of butyl acrylate via microemulsion polymerization initiated by ammonium persulfate (APS) [89].

Table 3.1 Effect of reaction tempearature and stirring speed on synthesis of nanosized polyisoprene

Polymer Code	Temp (^{o}C)	Stirring Speed (rpm)	DRC (%)	Conversion (%)	D_n (nm)
PIP_S_1	60	100	11.1	47.6	15.2
PIP_S_2	70	100	15.5	68.8	17.4
PIP_S_3	60	200	22.3	98.9	19.3
PIP_S_4	70	200	19.5	91.5	19.0

Condition: SPS initiator concentration = 0.20 %wt, Time = 20 h.

Table 3.2 Effect of initiator types on synthesis of nanosized polyisoprene

Polymer Code	Initiator	Gel Content (%)	DRC (%)	Conversion (%)	$\overline{M_W}$ (x10^{-6})	$\overline{M_N}$ (x10^{-6})	PDI ($\overline{M_W}/\overline{M_N}$)	D_n (nm)
PIP_S	SPS	85	12.1	49.3	1.29	3.13	4.12	16.2
PIP_A	APS	48	10.3	42.0	0.68	0.12	5.44	15.0
PIP_AI	AIBN	30	12.4	54.9	3.06	2.42	1.27	20.9

Condition: Temperature = 60 °C, Stirring speed = 100 rpm, Initiator concentration = 0.20 %wt, Time = 20 h.

Water soluble initiators are commonly used, but there are many reports of microemulsion polymerization instigated using oil soluble initiators. In this work, a water soluble initiator system (SPS, APS) and an oil soluble initiator system 2, 2'-azoisobutyronitrile (AIBN) were selected for the synthesis of nanosized polyisoprene. Table 3.2 illustrates the influence of initiator type on the microemulsion polymerization of isoprene using SDS as a surfactant. The polymerization condition was kept constant with a temperature of 60 °C and a stirring speed of 100 rpm. For isoprene polymerization, AIBN as an initiator was the most suitable system because the AIBN initiator system gave the highest monomer conversion, dry rubber content and molecular weight compared with the SPS and APS initiator systems. The AIBN initiator system also gave a much lower gel content and polydispersity index (PDI) as a measurement of the distribution of molecular mass in polyisoprene. The gel fraction of polyisoprene was obtained by dissolving the dried polymer in excess toluene for 1-week, after which the solid fraction was collected by filtration and weighed to give an estimated amount of the gel fraction [87, 90, 91]. From Table 3.2, isoprene polymerization using AIBN as initiator gave a PDI value around 1.27 and then, it approached unity (PDI = 1) as the polymer chains approached homogeneous chain length. However, the rubber particle size from polymerization using an oil soluble initiator system, 20.9 nm, was slightly larger than using a water soluble initiator system. The appearances of nanosized polyisoprene emulsion prepared by different initiators are shown in Figure 3.1. The nanosized polyisoprene emulsion was quite transparent.

These results were also consistent with other work, which describes how AIBN is a suitable initiator for emulsion or microemulsion polymerization and more economical than the system using a water soluble initiator [27]. For the emulsion polymerization of methacrylate monomers such as 2-hydroxyethyl methacrylate (HEMA), methyl methacrylate (MMA) and butyl methacrylate (BMA), more hydrophobic monomers, the hydrophobic initiators lead to much better polymerization results, with much less coagulum and smaller particles, than the hydrophilic potassium peroxodisulfate [92]. Most notably, the water-soluble HEMA stable latexes were only obtained by using hydrophobic initiators such as AIBN or

dibenzoyl peroxide in combination with alkyl sulfate surfactants. Furthermore, the synthesis of polyurethane emulsion showed that using oil-soluble AIBN was better than using water-soluble potassium persulfate (KPS) because the different initiator initiated the free radical reaction via a different mechanism [93]. The free radicals of AIBN could diffuse into emulsion particles from the water phase because the free radicals which originate from AIBN decomposition were lipophilic and hydrophobic. For the microemulsion copolymerization of ethylacrylate and MMA, the KPS initiator resulted in a much larger particle size and lower particle stability, whereas the emulsion system initiated with KPS at identical conditions resulted in stable colloidal polymer particles of very small particle size with a higher solid content [94]. In contrast, AIBN-initiated microemulsion generated stable nanolatex as compared to the emulsion system.

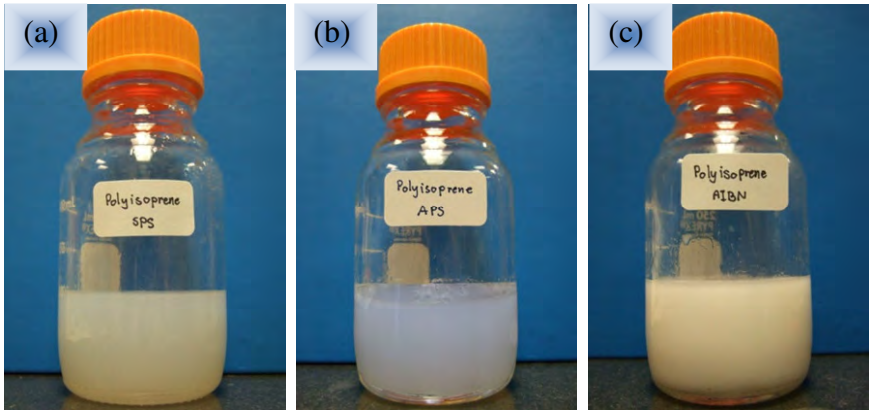

Figure 3.1 Appearance of nanosized polyisoprene emulsions with 20% DRC: (a) using SPS as initiator, (b) using APS as initiator and (c) using AIBN as initiator.

3.3 Statistical Analysis using Two-level Factorial Design Experiments

The experiments of a 2_V^{5-1} factorial experimental design (a total of 16 runs) are listed in Table 3.3. Within this famework, the effect of process variables, the amount of initiator, surfactant, the IP/H_2O ratio, the reaction temperature and the stirring speed were examined. Statistical analysis was used to study the influence of each process variable irrespective of and in combination with the other process variables on the synthesis of nanosized polyisoprene. A statistical method based on analysis of the variance (ANOVA) was used to determine the statistical significance of the effects and interactions comparing the mean square with an approximation of experimental error. The data of polymer particle size and monomer conversion was used to do the ANOVA analysis. In this work, the effects and interactions with P-values less than 0.05 indicate that they are significantly different from zero at the 95.0% confidence level. From these results, the PIP5 experiment gave the smallest particle size of 15.4 nm, while the PIP4 experiment gave the highest monomer conversion of 99.7%.

3.3.1 Response Variable of Polyisoprene Particle Size

The effect of the process variables on the particle size is presented in Table 3.3. From these results, it can be seen that the nanosized polyisoprene particle size ranged from 15.4–39.6 nm depending on the process conditions. Table 3.4 shows the ANOVA analysis of the process variables on the polyisoprene particle size. In this project, the main effect of initiator concentration, reaction temperature and stirring speed were significant because those parameters had P-values of less than 0.05. Some investigators reported that the surfactant concentration also had a significant effect on controlling the nanoparticle size [95, 96].

Table 3.3 Design matrix of experimental design and effect of process variables on monomer conversion, dry rubber content, particle size and molecular weight

Expt.	Basic Design					%Con	%DRC	$\overline{D_n}$ (nm)	$\overline{M_W}$ ($\times10^{-6}$)	$\overline{M_N}$ ($\times10^{-6}$)
	[AIBN]	[SDS]	IP/H_2O	Temp	SS					
PIP1	-1	-1	+1	-1	-1	46.4	13.1	21.5	4.68	2.64
PIP2	-1	-1	-1	+1	-1	68.0	15.2	17.7	1.53	0.46
PIP3	+1	-1	+1	-1	+1	96.1	24.0	34.1	3.15	1.80
PIP4	-1	+1	-1	+1	+1	99.7	22.7	27.7	2.37	1.86
PIP5	+1	+1	-1	+1	-1	66.9	15.1	15.4	3.01	0.18
PIP6	+1	-1	-1	+1	+1	90.9	20.1	22.9	1.63	0.38
PIP7	+1	+1	-1	-1	+1	83.9	17.9	28.0	0.91	0.16
PIP8	-1	-1	-1	-1	+1	93.6	20.2	39.6	3.14	2.22
PIP9	-1	+1	-1	-1	-1	59.2	13.5	19.0	3.28	1.28
PIP10	+1	+1	+1	+1	+1	85.3	22.1	26.5	3.56	1.42
PIP11	-1	+1	+1	+1	-1	65.8	17.6	19.7	3.79	1.74
PIP12	-1	-1	+1	+1	+1	89.7	23.4	36.8	9.45	7.76
PIP13	+1	-1	-1	-1	-1	55.4	12.6	16.9	1.64	0.34
PIP14	-1	+1	+1	-1	+1	95.7	24.0	37.8	4.17	3.13
PIP15	+1	+1	+1	-1	-1	53.6	14.5	16.2	2.33	0.35
PIP16	+1	-1	+1	+1	-1	64.9	17.4	16.6	1.71	0.17

[AIBN] (%wt): 0.25(-1), 0.80(+1); [SDS] (%wt): 2.12(-1), 2.48(+1); IP/H_2O: 0.4(-1), 0.5(+1); Temp (^oC): 60(-1), 70(+1); Stirring speed, SS (rpm): 100(-1), 300(+1)

Conditions: [SHC] (%wt) = 0.60; [*n*-DM] (%wt) = 0.20, Time 20 h.

Table 3.4 Analysis of variance (ANOVA) on the particle size using factorial design

Source	Sum of Squares	D.F.	Mean Square	F-Value	P-Value	
Model	979.83	5	195.97	25.57	< 0.0001	significant
A, [AIBN]	116.75	1	116.75	15.23	0.0029	
B, [SDS]	15.96	1	15.96	2.08	0.1796	
C, IP/H_2O	30.14	1	30.14	3.93	0.0755	
D, Temp.	55.50	1	55.50	7.24	0.0227	
E, SS.	761.48	1	761.48	99.36	< 0.0001	
Residual	76.64	10	7.66			
Total(Correlation)	1056.48	15				

R^2 = 0.9275; R^2-(ad) = 0.8912; standard error of estimation = 2.7684.

In these factorial design experiments, the surfactant concentration is not a significant process parameter due to the narrow range of surfactant concentration investigated. The equation which describes particle size in term of coded factors is as follows:

$$\text{Particle size} = 24.7738 - 2.7013A - 0.9988B + 1.3725C - 1.8625D + 6.8988E \quad (3.1)$$

The R^2 of this equation is 0.9275, indicating that the fitting was quite good. According to the definition, the main effects of the controlled independent variable are the mean of the difference between the values at high level (+1) and the values at low level (-1). The rubber particle size was inversely proportional to the AIBN (A), SDS (B) concentration and reaction temperature (D) but was directly proportional to the IP/H_2O ratio (C) and stirring speed (E).

Figures 3.2(a) and 3.2(b) show the response surface developed by the model of initiator concentration and stirring speed relation at high and low reaction temperature, respectively. These plots offer a visual means of understanding how main factors influence the change of nanoparticle size. This optimal relation was observed denoting that a high AIBN initiator concentration level, high reaction temperature level and low stirring speed level yielded the smaller polyisoprene particle size. High reaction temperature increased the stabilizing activity of SDS micelle and high AIBN initiator concentration increased the interfacial area for polymerization; thus, polymerization proceeded very well at many loci of the system. However, the low stirring speed delayed the polymerization rate in the polyisoprene particle relating to the growing polymer chains and the nanosized polyisoprene particles could be controllably synthesized. Table 3.3 shows how the results of M_N ranged from 0.16-7.76×$10^6$and M_W ranged from 1.53-9.45×10^6 depending on the process conditions.

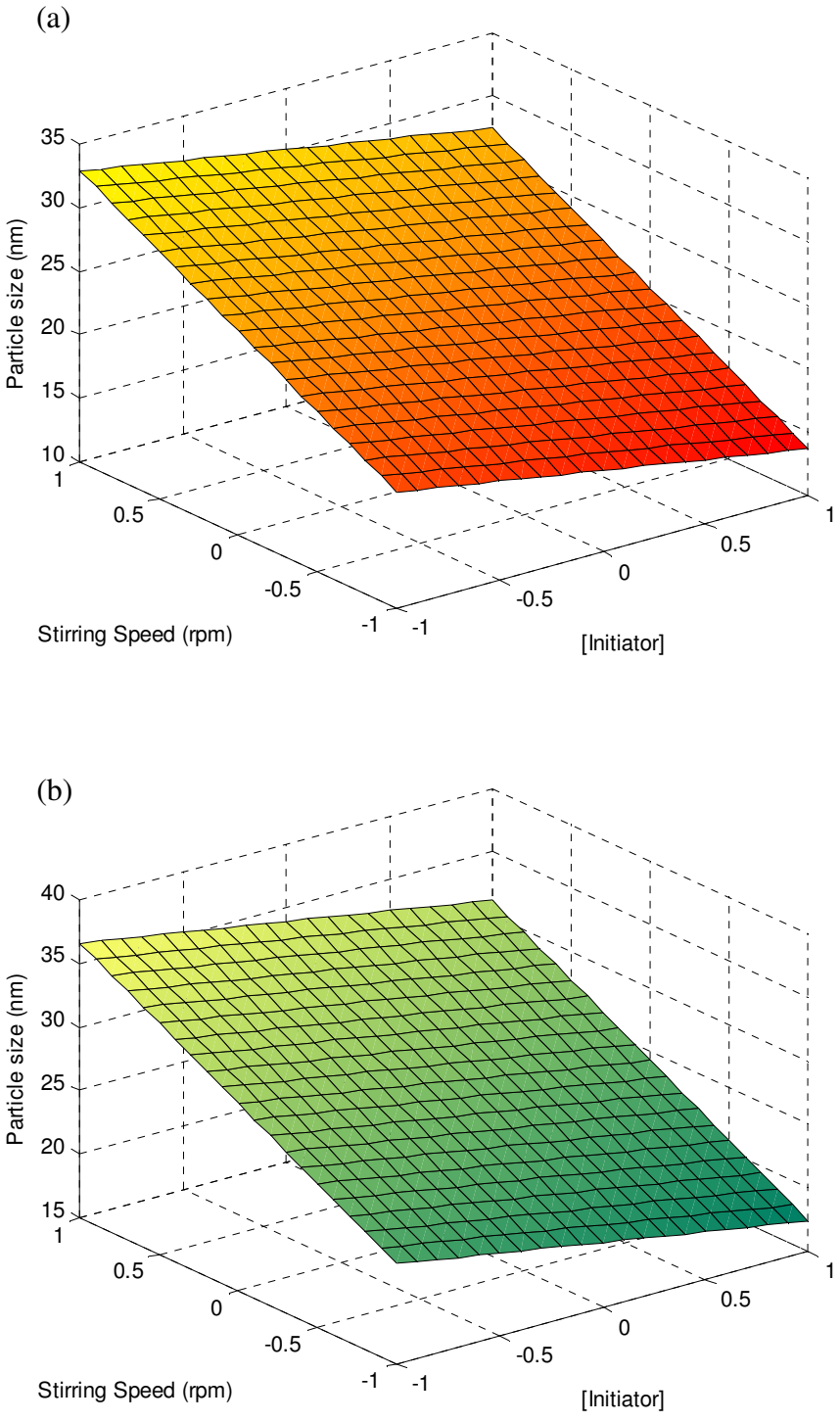

Figure 3.2 Response surface developed by the model of initiator concentration and stirring speed relation (a) Response at high reaction temperature and (b) Response at low reaction temperature.

3.3.2 Response Variable of Isoprene Monomer Conversion

Table 3.3 presents the effect of the process variables on the monomer conversion. From these results, it can be seen that the isoprene conversion ranged from 46.4–99.7% depending on the process condition. Table 3.5 shows the ANOVA analysis of the process variables on the monomer conversion. The significant effects on isoprene conversion in this model were reaction temperature (D), stirring speed (E) and interaction between reaction temperature and stirring speed (DE) over the range of this design because those parameters have P-values of less than 0.05. Equation (3.2) describes the conversion in terms of significant variables as follows:

$$\text{Conversion} = 75.8994 + 3.0006D + 15.8706E - 3.3731DE \quad (3.2)$$

The fitting of this equation is quite good (R^2 = 0.9329). Variances of every factor and their importance can be obtained by ANOVA showing only significant parameters at a 95% confidence level.

Table 3.5 Analysis of variance (ANOVA) on conversion using factorial design

Source	Sum of Squares	D.F.	Mean Square	F Value	P Value	
Model	4356.14	3	1452.05	55.58	< 0.0001	significant
D, Temp.	144.06	1	144.06	5.51	0.0368	
E, SS.	4030.03	1	4030.03	154.26	< 0.0001	
DE	182.05	1	182.05	6.97	0.0216	
Residual	313.50	12	26.12			
Total(Correlation)	4669.64	15				

R^2 = 0.9329; R^2-(ad) = 0.9161; standard error of estimation = 5.1113.

The main effects of the controlled independent variable are the mean of the difference between the values at high level (+1) and the values at low level (-1). The conversion was influenced by reaction temperature, stirring speed and their interaction. Figure 3.3 shows the response surface of the mean conversion developed by the model for reaction temperature and the stirring speed relation. In this case, reaction temperature and stirring speed have a non-linear behavior showing an optimal relation with the maximum conversion. This optimal relation of the maximum conversion depended significantly on the stirring speed. The reaction temperature also had a minor effect on conversion. Increased conversion was due to increasing the interfacial area for microemulsion polymerization, which increased with increasing stirring speed because the monomer droplet size decreased and the initiator radical was generated at a high reaction temperature [89, 97]. Table 3.3 also presents the results for dry rubber content (DRC) which ranged from 13.1–24.0% depending on the process conditions.

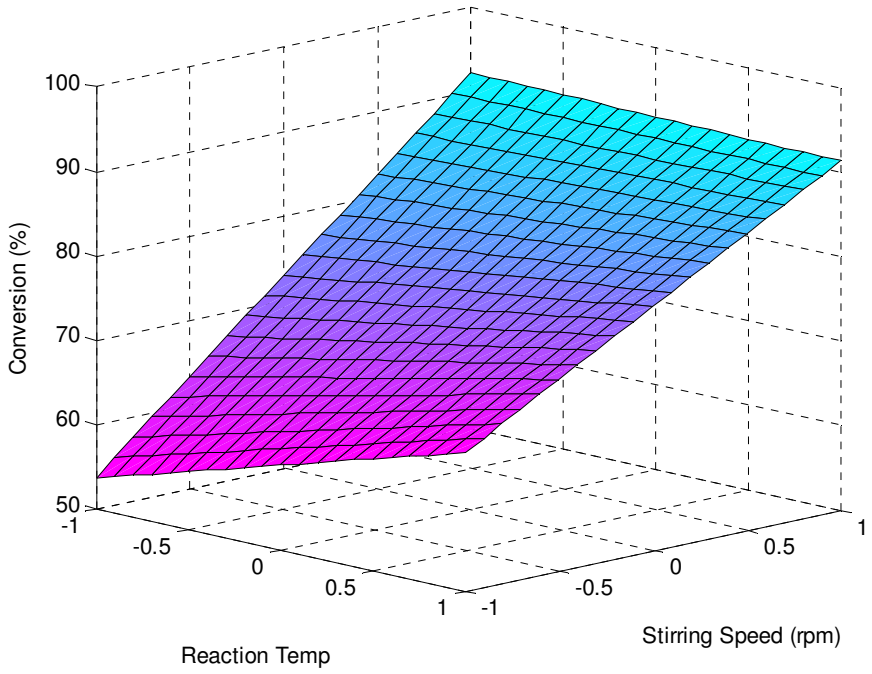

Figure 3.3 Response surface developed by the model for reaction temperature and stirring speed relation.

3.4 Univariate Experiment for Synthesis of Polyisoprene Nanoparticle

From the results of factorial design, the univariate experiments were formulated and performed to investigate the influences of surfactant concentration and isoprene-to-water ratio on the polyisoprene nanoparticle size and the monomer conversion.

3.4.1 Dependence on Surfactant Concentration

The effect of surfactant concentration over the range of 0.43 %wt and 3.34 %wt (SDS/IP: 0.01-0.12) was studied. The influence of SDS concentration on the particle size of nanosized polyisoprene is shown in Figure 3.4. It can be seen that the rubber particle size was inversely proportional to the surfactant concentration. The particle size of nanosized polyisoprene decreased with increasing surfactant concentration, and did not significantly change when SDS concentration was above 3.34 %wt (SDS/IP = 0.12). The results were similar to thoses obtained for the preparation of poly(methy methacrylate) (PMMA) nanoparticles initiated by AIBN via differential microemulsion polymerization [27]. For preparation of nanosized polyisoprene particle size around 20 nm, the required surfactant amount could be as low as 0.09 of the isoprene monomer amount in weight. For comparison of nanosized polyisoprene synthesis of 30-60 nm, SDS/IP ratio required by differential polymerization was 0.03 which was lower than that required by emulsion polymerization (SDS/IP ratio = 0.11) [87]. Moreover, the results implied that the polyisoprene nanoparticle size could be controlled by the amount of surfactant. This behavior had a similar trend with the synthesis of nanosized poly(vinyl acetate) via microemulsion polymerization (41.5-89.2 nm) [95] and polystyrene via emulsion polymerization (62.5-94.0 nm) [97].

From Figure 3.4, the monomer conversion increased with increasing surfactant concentration and reached a maximum around 90% at SDS concentration of 3.34 %wt. For dry rubber content (DRC), increasing SDS concentration also increased DRC of nanosized polyisoprene. The maximum DRC of around 24% was also acheived at 3.34 %wt SDS concentration. This phenomenon suggests that the

conversion and solid content in differential microemulsion polymerization was determined by the micelle numbers and there were no monomer droplets [26]. The nanosized polyisoprene synthesis initiated by oil-soluble initiator is believed to occur in micelles. Micelle numbers increased with increasing SDS concentration, and as each micelle became small. The small micelles caused a decrease in diffusion resistance resulting in the fast polymerization rate. For synthesis of nanosized polyisoprene, a higher SDS concentration resulted in higher conversion and DRC similar to that observed for the synthesis of PMMA [27]. From these results, the appropriate SDS concentration was 2.53 %wt (SDS/IP = 0.09) for synthesis of nanosized polyisoprene with high conversion of 80%, high DRC of 22% and small polyisoprene nanoparticle size of around 20 nm.

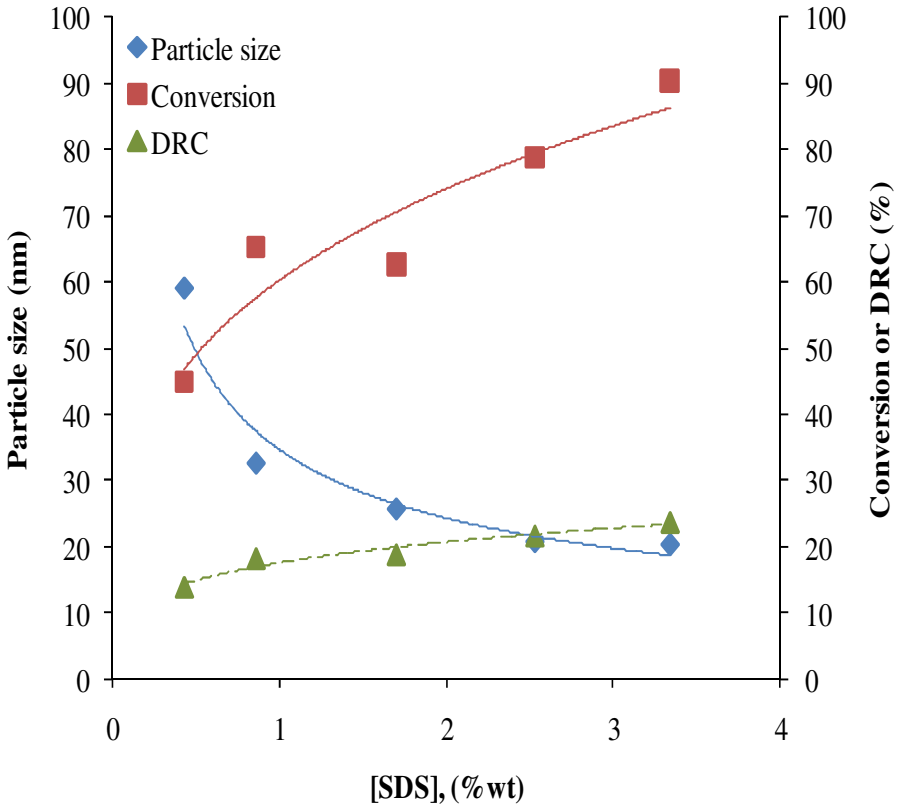

Figure 3.4 Effect of SDS concentration on the particle size, monomer conversion and dry rubber content (DRC) of nanosized polyisoprene latex: [AIBN] = 0.25 %wt; IP/H_2O = 0.4; [SHC] = 0.60 %wt; [*n*-DM] = 0.20 %wt; temperature = 70 °C; stirring speed = 300 rpm; time = 20 h.

3.4.2 Dependence on Isoprene Monomer-to-Water Ratio

The effect of IP/H_2O ratio on particle size of nanosized PIP was studied for IP/H_2O range of 0.2-0.8 (SDS/IP: 0.04-0.18). The influences of IP/H_2O ratio on the particle size and monomer conversion are shown in Figure 3.5. This indicated that the rubber particle size was directly proportional to the IP/H_2O ratio. The nanosized polyisoprene particle size decreased with decreasing IP/H_2O ratio similar to the results of the factorial design experiment. In this work, a hydrophobic initiator was used and isoprene is an oil-soluble monomer. Therefore, the nucleations are most likely occurring within the micelles. The size of the micelle increased with increasing isoprene monomer concentration. Thus, the ratio of monomer/water significantly affected the particle size. This behavior had a similar trend to that observed for the synthesis of nanosized PMMA via differential microemulsion polymerization initiated by ammonium persulfate, even though the nucleation mainly occurred in the water phase since MMA is a slightly water-soluble monomer [26].

However, the appropriate IP/H_2O ratio for synthesis of nanosized PIP was 0.4 (at SDS/IP ratio = 0.09). This optimum condition gave a small nanosized PIP particle size of around 20 nm, monomer conversion of 82% and DRC of 22%. Furthermore, increasing the IP/H_2O ratio to higher than 0.4 caused an increase in the micelles size and diffusion resistance resulting in a slow polymerization rate and a decrease in the stabilization of nanoemulsion. Thus, monomer conversion decreased with increasing IP/H_2O ratio. Figure 3.5 shows that the DRC increased with increasing isoprene monomer ratio. However, DRC was in the range of 10 to 30% depending on the process conditions. This could imply that DRC was directly proportional to the IP/H_2O ratio and monomer conversion.

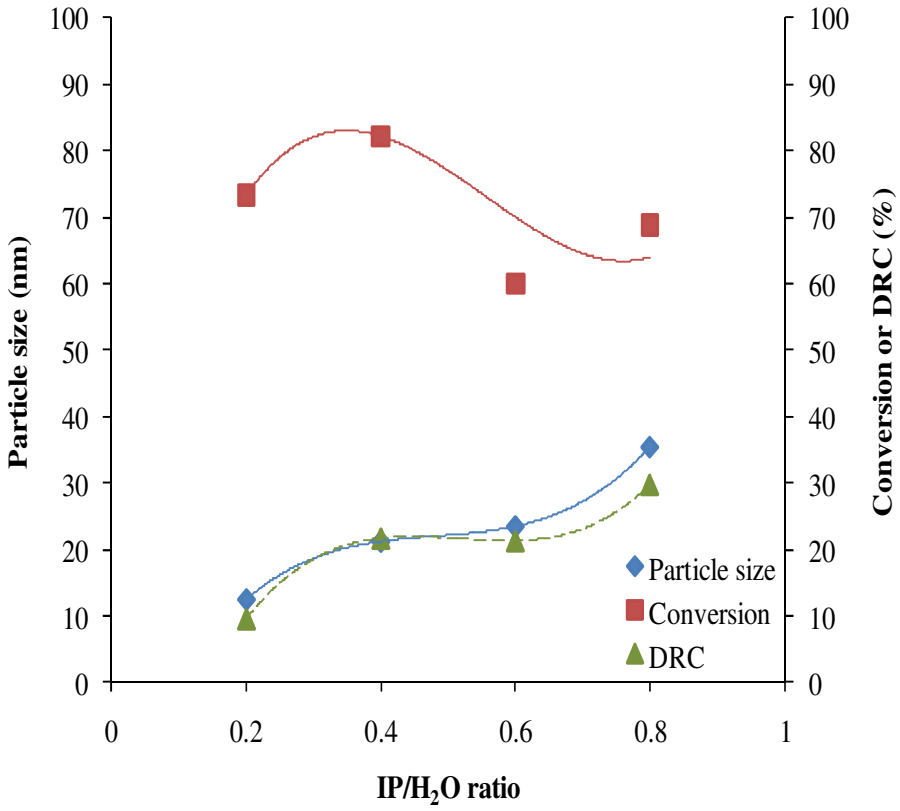

Figure 3.5 Effect of IP/H_2O ratio on the particle size, monomer conversion and dry rubber content (DRC) of nanosized polyisoprene latex: [AIBN] = 0.25 %wt; [SDS] = 2.53 %wt; [SHC] = 0.60 %wt; [*n*-DM] = 0.20 %wt; temperature = 70 °C; stirring speed = 300 rpm; time = 20 h.

3.5 Rate of Isoprene Polymerization

Using a factorial strategy for nanosized polyisoprene synthesis and using AIBN as initiator, PIP2 and PIP4 experiments (Table 3.3) were selected to study the polymerization rate at different stirring speeds. PIP2 and PIP4 experiments were carried out under the same conditions including low AIBN concentration, low IP/H_2O ratio and high temperature. The difference between the PIP2 and PIP4 experiments were that the PIP2 had a low SDS concentration and low stirring speed, while the PIP4 had a high SDS concentration and high stirring speed. However, the amount of SDS did not affect the polymer particle size and monomer conversion as

described earlier. Figure 3.6(a) shows the effect of stirring speed on the rate of microemulsion polymerization of isoprene. The high stirring speed gave a higher conversion than the low stirring speed. For PIP2 (100 rpm), the conversion increased linearly with time and reached around 70% in 20 h. For PIP4 (300 rpm), the conversion increased sharply and reached a maximum of around 90% in 8 h as a result of the high polymerization rate. This behavior confirms that stirring speed has a main effect on escalating conversion. At high stirring speed, monomer droplet size was decreased and interfacial area for polymerization was increased. Thus, the contact time between monomer and radical initiator increased. These behaviors lead to increased conversion.

The number of polymer chains per particle (N) was calculated according to Equation (3.3)

$$N = \frac{4}{3}\pi(D/2)^3 \rho N_A / M_W \tag{3.3}$$

where D is the diameter of the particle, ρ is the density of particle, assuming that all monomers in the particle have been polymerized. N_A is Avogadro number and M_w is the weight average molecular weight. For PIP the density is 0.93 g/cm^3. Figure 3.6(b) shows the number of polymer chains per particle (N) depending on time. For PIP2, one nanosized particle contained one polymer chain from 2 h to 20 h of reaction time. For PIP4, the nanosized particle initially contained 3-4 polymer chains and then decreased to ca. 1 polymer chain per particle after 10 h (see Figure 3.6(c)). These behaviors show that high stirring speed improves the dispersion of isoprene monomer with the micelle and the micelle acts as a monomer reservoir. With increasing time, polymerization continued with polymer chain growth. The number of polymer chains within the particle decreased; however, while the particle size and average molecular weight still increased. These results also implied that the nanosized particles could be prepared with high molecular weight, having uniform chain numbers in the particles.

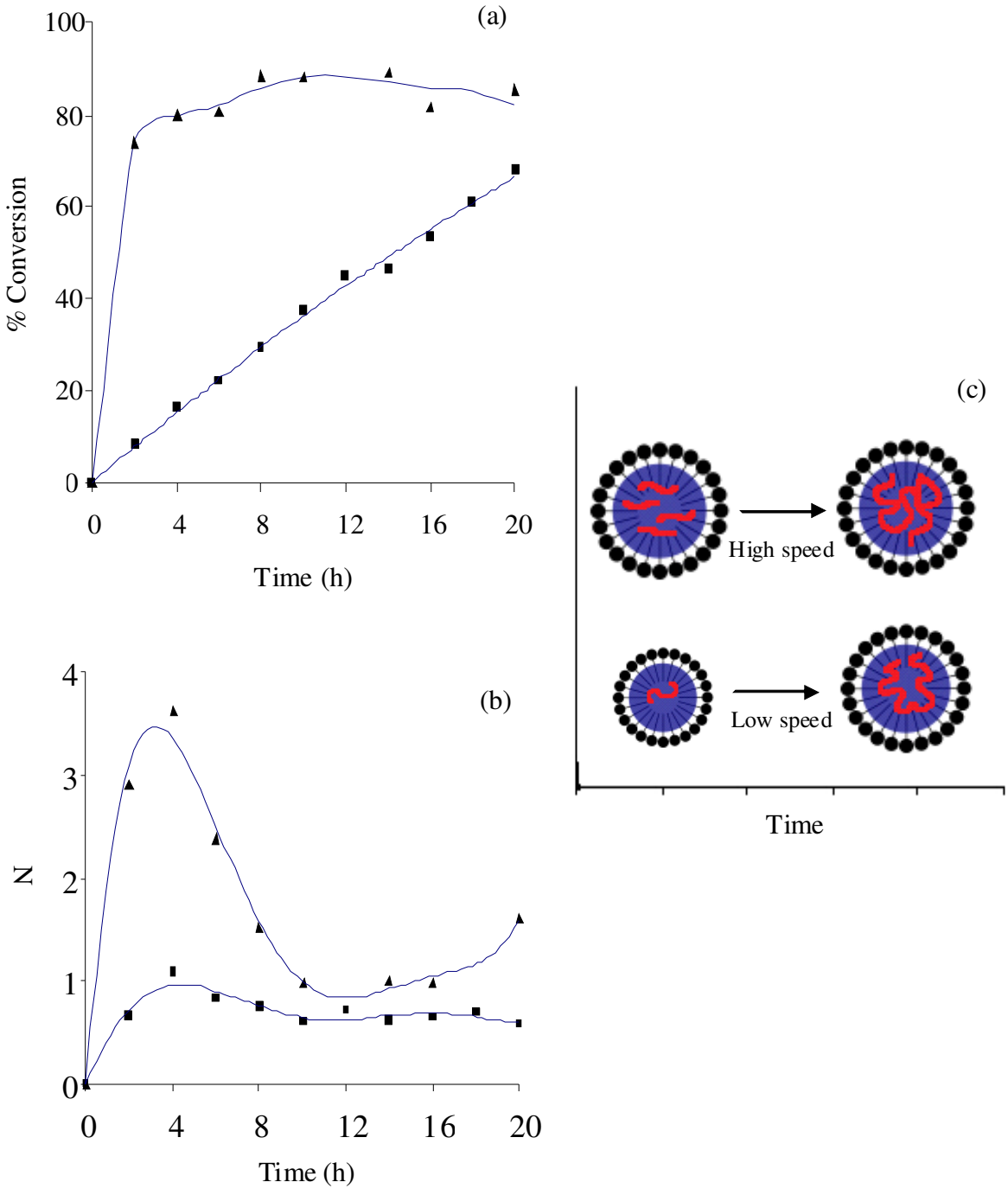

Figure 3.6 (a) Conversion as a function of time. (b) Number of polymer chain per particle (N) as a function of time. (c) Model of Molecular chain and particle size. AIBN initiator concentration = 0.25 %wt, Temperature = 70 °C: (■) PIP2, stirring speed 100 rpm; (▲) PIP4, stirring speed 300 rpm.

The effect of reaction time on molecular weight and particle size were also investigated. Average molecular weight is an important characteristic which has an influence not only on mechanical properties of the polymer formed, but also on the film formation process involved in many applications of polymer latexes. From Table 3.6, the percentage of dry rubber content and average molecular weight, M_n and M_w increased with reaction time. For PIP_2, the M_w increased with time corresponding to an increase in particle size during a polymerization time of 4-20 h. Since the isoprene monomer was dissolved slowly, the conversion and molecular weight were slightly increased. For PIP_4, the particle size remained the same over a polymerization time of 2-20 h, while M_w increased with time corresponding to the decreasing number of polymer chains per particle. This behavior is due to the fact that when the polymerization rate increased with time, the microemulsion viscosity also increased, leading to decreasing mass transfer of isoprene. However, the particle size remained the same and the average molecular weight increased slightly.

Table 3.6 Effect of reaction time and stirring speed on isoprene polymerization

Polymer Code	Stirring speed (rpm)	Time (h)	DRC (%)	$\overline{M_W}$ (x10^{-6})	$\overline{M_N}$ (x10^{-6})	D_n (nm)
PIP2	100	2	2.1	0.19	0.04	7.5
PIP2	100	4	4.2	0.56	0.09	12.7
PIP2	100	6	5.5	0.66	0.10	12.2
PIP2	100	8	7.2	0.92	0.09	13.3
PIP2	100	10	8.9	1.36	0.22	14.0
PIP2	100	12	10.8	1.79	0.36	16.4
PIP2	100	14	10.9	1.79	0.31	15.5
PIP2	100	16	12.4	2.21	0.71	16.9
PIP2	100	18	14.2	2.21	1.21	17.3
PIP2	100	20	15.4	2.98	0.91	18.0
PIP4	300	2	16.4	1.75	0.43	25.9
PIP4	300	4	18.1	1.37	0.23	25.6
PIP4	300	6	18.0	2.20	0.48	26.1
PIP4	300	8	19.9	4.48	1.80	28.5
PIP4	300	10	19.3	5.27	2.55	26.0
PIP4	300	14	19.8	5.06	1.99	25.9
PIP4	300	16	19.0	5.17	1.92	25.8
PIP4	300	20	18.7	4.57	1.86	29.2

Condition: AIBN initiator concentration = 0.25 %wt, Temperature = 70 °C.

3.6 Characterization of Synthesis Polyisoprene

The physical appearance of nanosized polyisoprene synthesized by differential microemulsion polymerization using AIBN as initiator is showed in Figure 3.7. This figure shows a comparison of nanosized polyisoprene, skim natural rubber latex and natural rubber latex contains 20 and 60% DRC. The synthesis nanosized polyisoprene latex with 20% DRC was more transparent than skim natural rubber latex and natural rubber latex with equal or higher DRC.

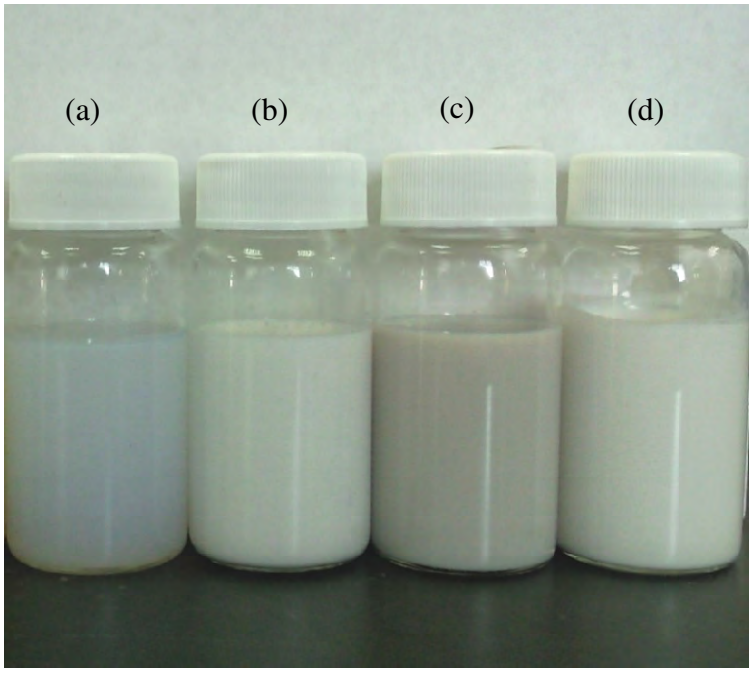

Figure 3.7 Appearance of rubber latex samples: (a) emulsion of nanosized polyisoprene (20 nm) with 20% DRC, (b) dilute natural rubber latex with 20% DRC, (c) skim natural rubber latex with 3–10% DRC and (d) natural rubber latex with 60% DRC.

The structure of synthesized polyisoprene latex was analyzed by FTIR and ^{1}H-NMR spectroscopy. The nanosized polyisoprene synthesized by using AIBN could have various isomeric structures with cis-1,4, tran-1,4, 3,4 or 1,2 connection which affects the physical properties of the rubber. From Figure 3.8, the FTIR spectrum shows the methylene stretching at 2,925 and 2,854 cm^{-1}, the methyl stretching at 2,962 cm^{-1}, the methyl deformations at 1,450 and 1,377 cm^{-1} and the prominent =C-H out-of-plane wag at 837 cm^{-1}. The distinctive peaks existed at 3,035 cm^{-1} for the =C-H stretching, 2,727 cm^{-1} for the overtone of the methyl deformation and 1,664 cm^{-1} for C=C stretching. From the ^{1}H-NMR spectrum as shown in Figure 3.9, the sharp chemical shift from the methyl protons of cis-1,4 (d) and trans-1,4 units (j) were observed at 1.58 and 1.68 ppm, respectively. The olefinic protons signal of cis- and trans-1,4 was observed at 5.13 ppm. The signal at 4.60-4.78 ppm were attributed to olefinic protons of 3,4-addition. The peaks at 4.80-4.95 and 5.70-5.80 ppm indicated the olefinic protons of 1,2-addition. These peaks confirm the formation of 1,4-polyisoprene, 3,4-polyisoprene and 1,2-polyisoprene.

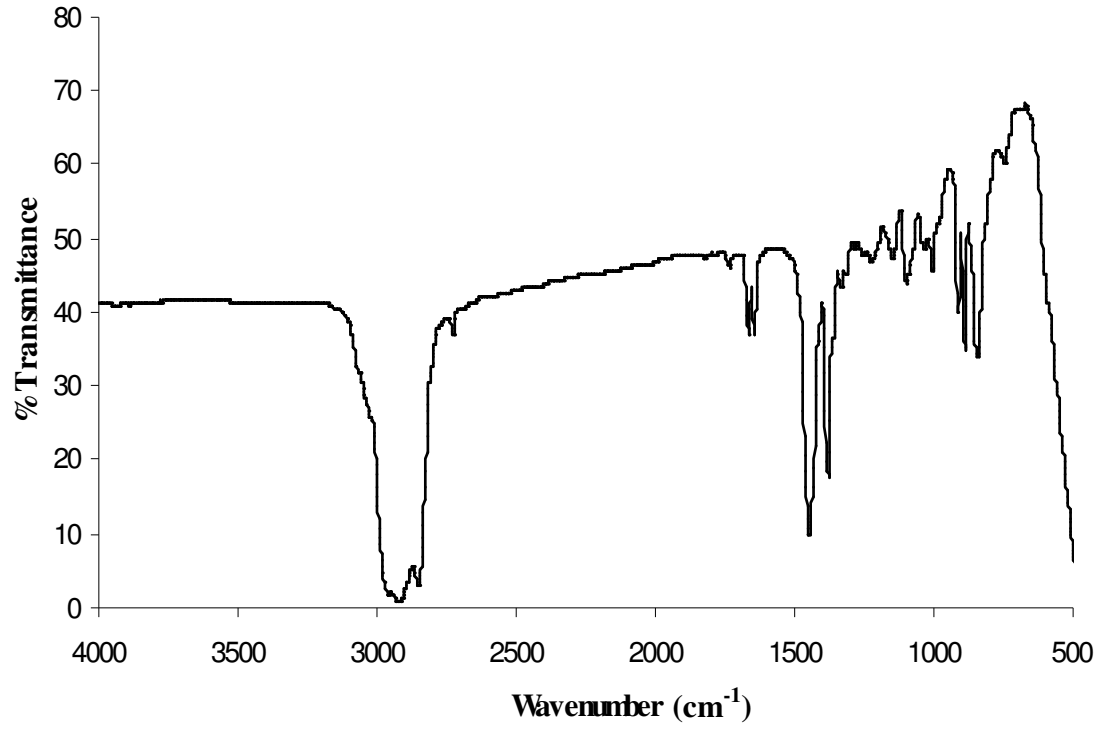

Figure 3.8 FTIR spectra of nanosized polyisoprene.

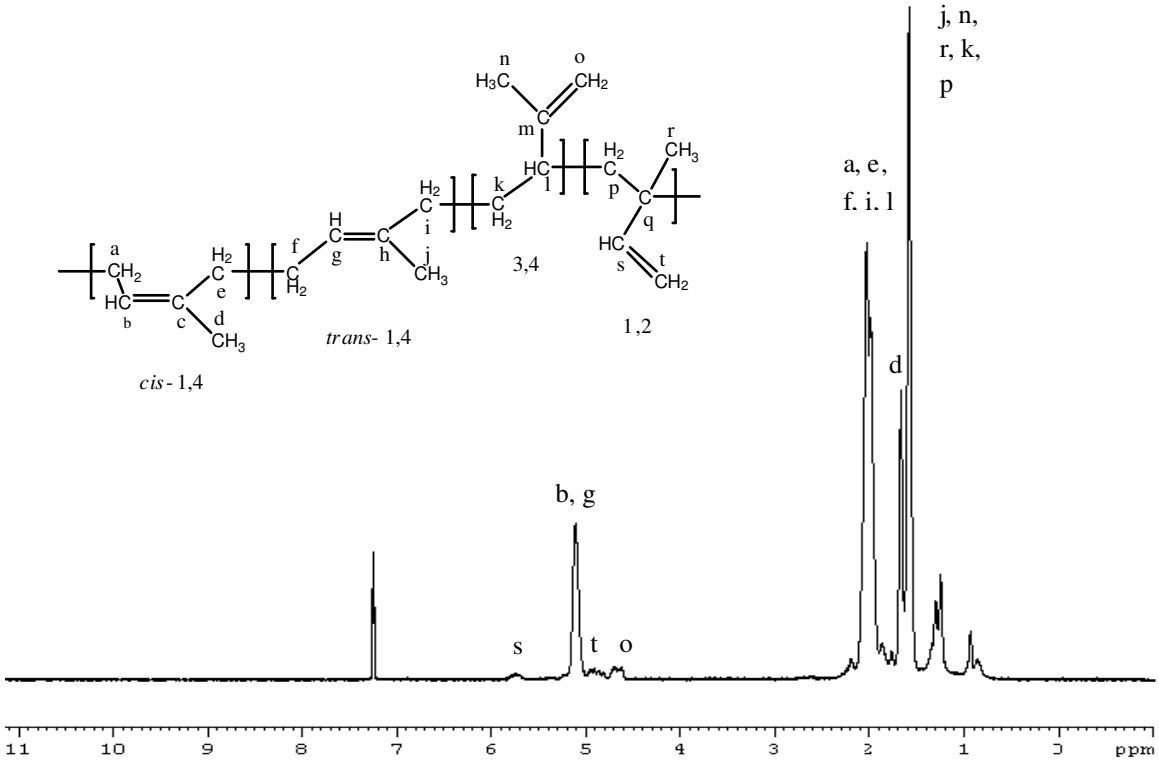

Figure 3.9 ^{1}H-NMR spectra of nanosized polyisoprene in $CDCl_3$

3.7 Thermal Properties of Nanosized Polyisoprene

Thermal analysis was used to investigate the physical properties of substrates as a function of temperature. These experiments were carried out using thermal gravimetric analysis (TGA) to find the initial decomposition temperature (T_{id}) and the maximum decomposition temperature (T_{max}). TGA of *cis*-1,4-polyisoprene (CPIP), PIP2 (D_n = 17.7 nm, $M_w = 1.53\times10^6$), PIP4 (D_n = 27.7 nm, $M_w = 2.37\times10^6$) and PIP8 (D_n = 39.6 nm, $M_w = 3.14\times10^6$) was conducted under a nitrogen atmosphere. T_{id} was determined from the intersection of two tangents at the onset of the decomposition temperature. T_{max} was obtained from the peak maxima of the derivative of the TG curves. Table 3.7 summarizes the degradation temperature (T_{id} and T_{max}) of all rubber samples. The results show that the degradation temperatures of nanosized polyisoprene samples are very close to CPIP.

Table 3.7 Glass transition temperature and decomposition temperature of rubber samples

Rubber sample	T_g (^oC)	T_{id} (^oC)	T_{max} (^oC)
CPIP*	-63.4	363.6	384.6
PIP2	-60.5	355.6	391.7
PIP4	-61.9	358.8	393.2
PIP8	-55.6	362.1	398.5

*High-molecular-weight CPIP with 97% cis isomer (Natsyn) was provided by Bayer, Inc. (Sania, Canada).

Differential scanning calorimetry (DSC) was used to determine the glass transition temperature (T_g). T_g is the transition temperature related to the motion in the amorphous section of the polymer. It was established from the midpoint of the base line shift of the DSC thermogram. The DSC thermogram of the nanosized polyisoprene indicated a one step base line shift. This implies that the nanosized polyisoprene samples have a single glass transition temperature. T_g values obtained from the DSC thermogram are presented in Table 3.7. The T_g of CPIP and nanosized polyisoprene are nearly the same, which exhibit rubber properties at room temperature and glass properties below T_g. Consequently, from these results it can be concluded that the nanoparticle had no appreciable effect on T_g of the synthesized polyisoprene.

3.8 Morphology of Nanosized Polyisoprene

The morphologies of nanosized polyisoprene and skim natural rubber examined by TEM are shown in Figure 3.10. The surface morphology of rubber samples were studied by OsO_4 staining of the carbon–carbon double bonds of the rubber samples to increase the contrast and gradation of the particles. Figure 3.10(a) shows the nanosized polyisoprene latex with a particle size around 25 nm. The morphology of the polyisoprene nanoparticle was spherical having a smooth surface. From Figure 3.10(b), the particle size of skim natural rubber was larger than 1000 nm.

(a)

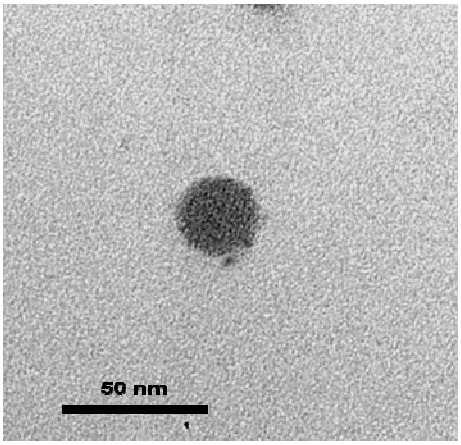

(b)

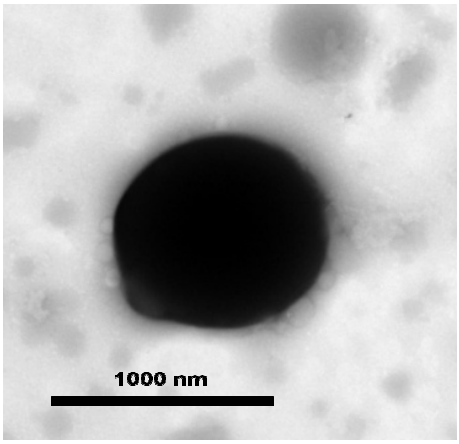

Figure 3.10 Transmission electron micrographs: (a) nanosized polyisoprene (~25 nm), (×50,000) and (b) skim natural rubber (~1000 nm), (×2,500).

CHAPTER IV

GRAFT COPOLYMERIZATION OF METHYL METHACRYLATE ONTO NANOSIZED POLYISOPRENE USING REDOX INITIATOR SYSTEM

4.1 Introduction

The chemical modification of rubber by grafting with vinyl monomers combines the desirable properties of the polymer of that of the graft monomer . The graft rubber-based composite latex particles have some properties better than those of the inherent ones and can be used as impact modifiers in thermoplastics [43-45, 98]. The graft copolymerization of vinyl monomers such as methyl methacrylate (MMA) onto natural rubber has been reported by many investigators as described in Section 1.3 and the influence of various process variables on grafting reactions was described.

However, the graft copolymerization of natural rubber (*cis*-1,4-polyisoprene) was suppressed by side reactions with proteins present in the natural rubber latex [99]. To increase grafting efficiency, it is necessary to remove the proteins and reduce particle size of the rubber latex. The graft copolymerization of styrene onto urea-deproteinized NR latex showed high conversion and high grafting efficiency [100]. For graft copolymerization onto synthetic polyisoprene latexes by using two-component redox initiation system, the modified latex particles were postulated to possess a 'hairy layer' of surface-graft poly(DMAEMA) chains and it was formed via an abstraction reaction between cumyloxy radicals and the isoprene moieties present in the seed polymer [87].

Graft copolymerization of nanosized polyisoprene (nanosized PIP) was expected to have high monomer conversion and high grafting efficiency compared with grafting on NR since the nanoparticles have large surface area. In Chapter III, the nanosized PIP latex was synthesized by differential microemulsion polymerization using 2, 2'-Azoisobutyronitrile (AIBN) as an initiator. The optimum conditions gave

the highest monomer conversion of 90% and an average particle size of PIP of 27 nm. The aims of this work were to prepare the nanosized particles of MMA graft PIP and to elucidate the effects of process variables on grafting properties and monomer conversion.

4.2 Statistical Analysis using Two-level Factorial Design Experiments

The results of a 2^3 factorial experimental design (a total of 8 runs) are presented in Table 4.1. Within this framework, the effect of process variables, the amount of initiator, monomer concentration and the reaction temperature were investigated. The statistical analysis was used to study the influence of each process variable irrespective and in combination with the other process variables on the graft copolymerization of MMA onto nanosized PIP. A statistical method based on analysis of the variance (ANOVA) was used to determine the statistical significance of effects and interactions by comparing the mean square with an estimation of experimental error. The results of percentage graft PIP and percentage free poly(methyl methacrylate) (PMMA) were used to perform the ANOVA analysis. In this work, the effects and interactions with P-values less than 0.05 indicate that they are significantly different from zero at the 95.0% confidence level.

4.2.1 Response Variable of %Graft polyisoprene

From Table 4.1, the percentage graft nanosized PIP ranged from 53-72% depending on the process conditions and MMAgPIP6 has the highest percentage graft PIP of 72.4%. Table 4.2 shows the ANOVA analysis of the process variables on the percentage graft PIP. In this design, the main effect of monomer concentration (B), reaction temperature (C) and interaction between initiator concentration and reaction temperature (AC) were significant because those parameters had P-values of less than 0.05. This indicated that they were significantly different from zero at the 95.0% confidence level. Equation (4.1) describes the percentage graft PIP in term of significant variables as follows:

$$\text{Graft PIP (\%)} = 62.975 + 1.575A + 3.525B - 2.85C + 2.65AC \qquad (4.1)$$

The R^2 of this equation was 0.9576, indicating that the fitting was quite good. According to the definition, the main effects of the controlled independent variable were the mean of the difference between the values at high level (+1) and the values at low level (-1). The percentage graft PIP was directly proportional to the cumene hydroperoxide concentration (A), MMA concentration (B) but was inversely proportional to the reaction temperature (C).

Table 4.1 Design matrix of experimental design and effect of process variables on grafting properties

Exp.	Basic Design			%Graft PIP	%Ungraft PIP	% Free PMMA	$\overline{D_n}$ MMA-g-PIP (nm)
	A, [INT] (phr)	B, [MMA] (phr)	C, Temp (^oC)				
MMAgPIP1	+1	+1	+1	67.5	16.0	16.5	31.8
MMAgPIP2	+1	-1	+1	61.2	19.2	19.6	35.3
MMAgPIP3	+1	-1	-1	62.4	25.5	12.2	30.4
MMAgPIP4	-1	-1	+1	53.2	27.3	19.5	32.0
MMAgPIP5	-1	-1	-1	61.4	22.3	16.4	28.1
MMAgPIP6	-1	+1	-1	72.3	13.3	14.5	31.0
MMAgPIP7	-1	+1	+1	58.6	21.1	20.5	30.9
MMAgPIP8	+1	+1	-1	67.5	16.0	16.5	29.9

[INT] (phr): 1(-1), 2(+1); [MMA] (phr): 40(-1), 60(+1); Temperature (^oC): 50(-1), 70(+1).

Grafting conditions: Stirring speed = 200 rpm, [SDS] = 1 phr; reaction time = 8 h.

PIP synthesis condition: [AIBN] = 0.25 %wt; [SDS] = 2.53 %wt; IP/H_2O = 0.4; [SHC] = 0.60 %wt; [*n*-DM] = 0.20 %wt; temperature = 70 ^oC; stirring speed = 300 rpm; reaction time = 20 h; $D_{n\,(PIP)}$ = 25-27 nm

Table 4.2 Analysis of variance (ANOVA) on the percentage graft PIP using factorial design

Source	Sum of Squares	D.F.	Mean Square	F-Value	P-Value	
Model	240.41	4	60.10	16.94	0.0213	significant
A, [INT]	19.85	1	19.85	5.59	0.0990	
B, [MMA]	99.41	1	99.41	28.01	0.0132	
C, Temp.	64.98	1	64.98	18.31	0.0234	
AC	56.18	1	56.18	15.83	0.0284	
Residual	10.65	3	3.55			
Total(Correlation)	251.06	7				

R^2 = 0.9576; R^2-(ad) = 0.9011; standard error of estimation = 1.8837.

Figure 4.1(a) and 4.1(b) show the response surface of the percentage graft PIP developed by the model of initiator concentration and reaction temperature at high and low MMA concentration, respectively. These figures offer a visual means of understanding how main factors influence the change of percentage graft PIP. In this case, initiator concentration and reaction temperature have a non-linear behavior showing an optimal relation with the maximum percentage graft PIP. This optimal relation was observed denoting that low CHPO initiator concentration level; low reaction temperature level but high MMA concentration level yielded the highest percentage of nanosized graft PIP. It was originally surmised that the amount of grafting would depend on the amount of monomer present in the reaction at the conditions described in Table 4.1.

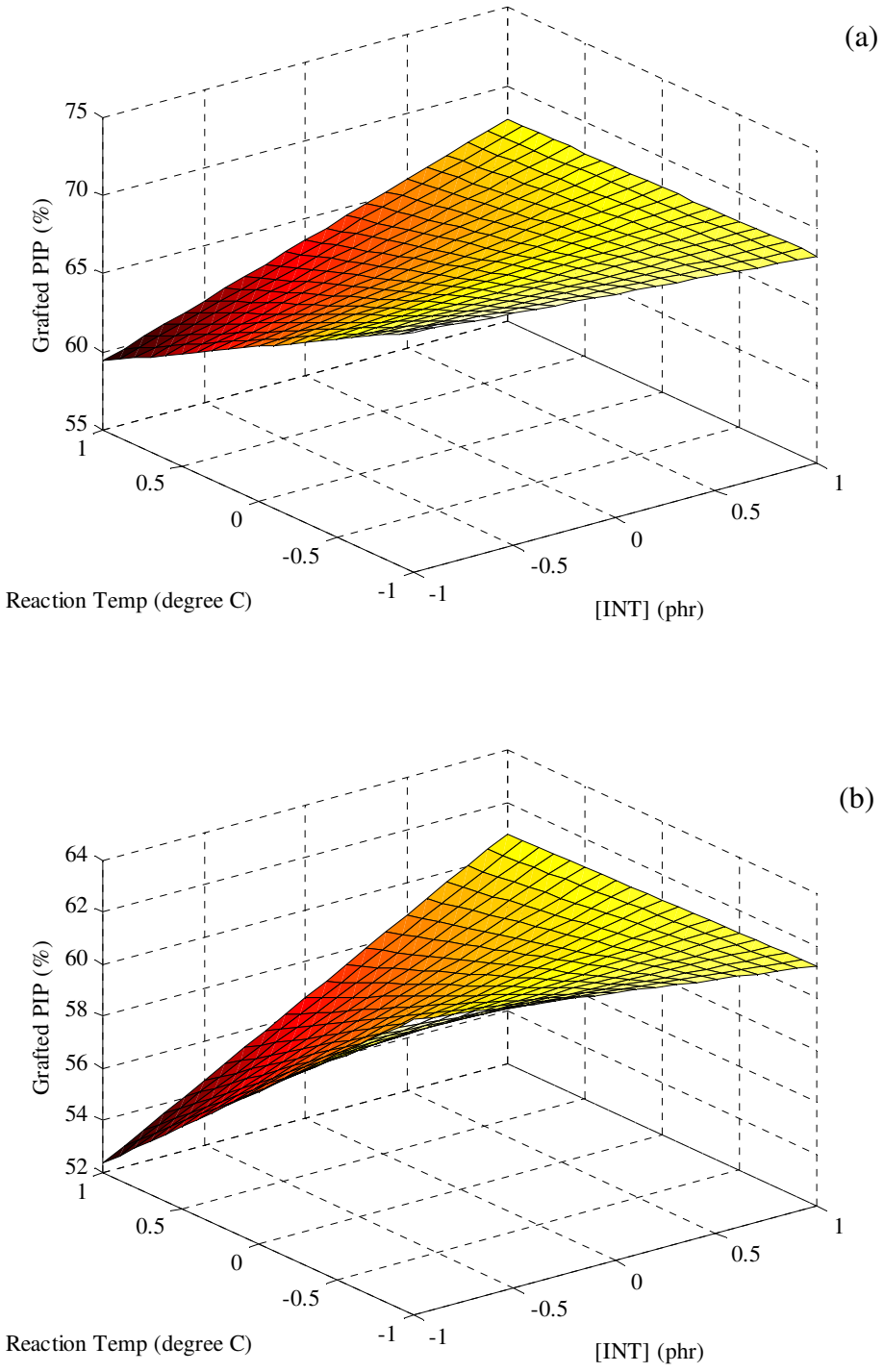

Figure 4.1 Response surface of nanosized graft PIP developed by the model of initiator concentration and reaction temperature relation: (a) response at high monomer concentration and (b) response at low monomer concentration.

The effect of initiator concentration on grafting MMA onto PIP at high and low monomer concentration were investigated. Figure 4.1(a) and 4.1(b) show similar results. At a low reaction temperature level, increasing the amount of initiator led to a decrease in the percentage of graft PIP while at high reaction temperature level, percentage graft PIP increased with increasing initiator concentration. These phenomena can be explained in that increasing initiator concentration at high reaction temperature produced more radicals to initiate and propagate the MMA molecules to graft onto nanosized PIP or to self polymerize toward homopolymer. This is also due to the fact that the radicals transfer to nanosized PIP or monomer, producing macroradicals and it is probable that the numbers of graft sites are increased [52, 79, 80]. For the response at low reaction temperature, high amount of initiator generated high free homopolymer so the percentage graft PIP decreased.

The effect of reaction temperature on grafting of MMA onto PIP was also elucidated from the response surfaces shown in Figure 4.1(a) and 4.1(b). The percentage graft polyisoprene decreased when the polymerization temperature was high. The initiator decomposition increased with increasing temperature resulting in instantaneously providing an abundance of free radicals. The radicals underwent either recombination or other side reactions such as a chain transfer reaction; the initiator efficiency for grafting was thus reduced at higher temperature. Thus, a high amount of free homopolymer (free nanosized PIP and free PMMA) produced more than graft PIP at high polymerization temperatures [51, 52]. The results of this experimental design agreed with earlier work and the highest percentage graft PIP was obtained at the low reaction temperature level and low initiator concentration level.

4.2.2 Response Variable of %Free Poly(methyl methacrylate)

From Table 4.1, the percentages of free PMMA ranged from 12.5-20.5% depending on the process conditions and MMAgPIP3 had the lowest percentage free PMMA of 12.5%. Table 4.3 shows the ANOVA analysis of the process variables on the percentage free PMMA. The significant effect on percentage free PMMA in this design was reaction temperature (C) because this parameter had P-values of less than 0.05. Moreover, the Model F-value of 6.02 could imply that the model was significant. There was only a 4.66% chance that the "Model F-Value" was high due to noise. Equation (4.2) describes the percentage graft PIP in terms of the significant variables as follows:

$$\text{Free PMMA (\%)} = 16.98 - 0.70A + 2.08C \quad (4.2)$$

However, the R^2 of this equation was 0.7066, indicating that the fitting was not good resulting in a low Adj-R^2 value of 0.5892. According to the definition, the main effects of the controlled independent variable were the mean of the difference between the values at high level (+1) and the values at low level (-1). Figure 4.2 shows the mean percentage free PMMA of nanosized MMA-g-PIP latex as a response to the two variables investigated. The percentage of free PMMA was directly proportional to the reaction temperature (C) but was inversely proportional to the initiator concentration (A). While MMA concentration did not affect the percentage of free PMMA in this design. The optimal relation was determined denoting that low CHPO initiator concentration level and low reaction temperature level yielded the lowest percentage of free PMMA.

Table 4.3 Analysis of variance (ANOVA) on the percentage free PMMA using factorial design

Source	Sum of Squares	D.F.	Mean Square	F-Value	P-Value	
Model	38.36	2	19.18	6.02	0.0466	significant
A, [INT]	3.92	1	3.92	1.23	0.3.178	
C, Temp.	34.44	1	34.44	10.81	0.0218	
Residual	15.93	5	3.19			
Total(Correlation)	54.30	7				

R^2 = 0.7066; R^2-(ad) = 0.5892; standard error of estimation = 1.7849.

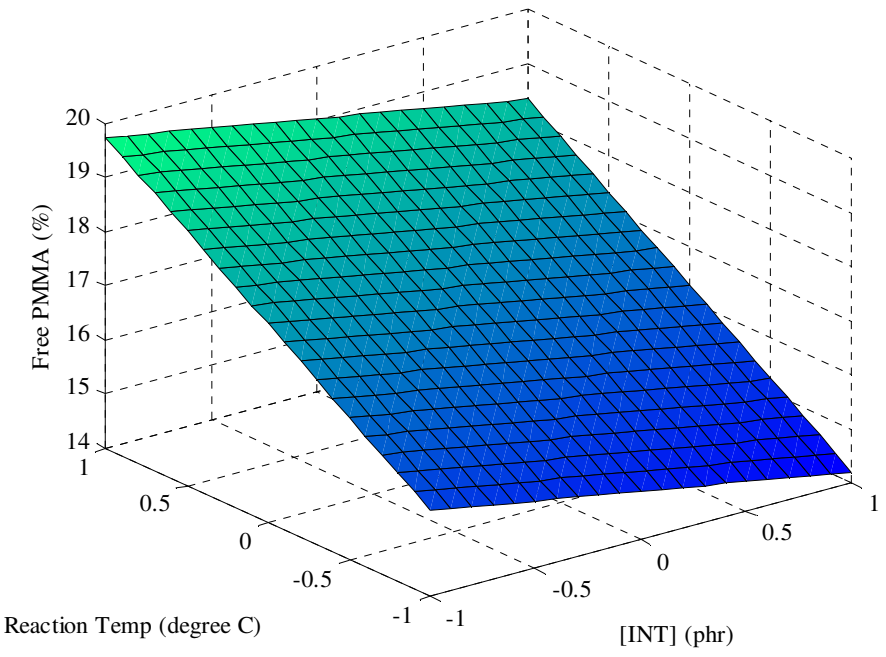

Figure 4.2 Response surface of free PMMA developed by the model of initiator concentration and reaction temperature relation.

4.2.3 Response Variable of % Ungraft PIP (Free PIP)

From Table 4.1, the percentages of ungraft PIP ranged from 13.0-27.3% depending on the process conditions. MMAgPIP6 had the lowest percentage of free PMMA. Table 4.4 shows the ANOVA analysis of the process variables on the percentage of ungraft PIP. The significant effects on percentage of free nanosized PIP in this design were MMA concentration (B) and interaction between initiator concentration and reaction temperature (AC) because those parameters had P-values less than 0.05. It indicated that they were significantly different from zero at the 95.0% confidence level. Equation (4.3) describes the percentage of ungraft PIP in terms of the significant variables as follows:

$$\text{Ungraft PIP } (\%) = 20.075 - 0.9A - 3.5B + 0.8C - 2.375AC \quad (4.3)$$

The R^2 of this equation was 0.9248, indicating that the fitting was quite good. According to the definition, the main effects of the controlled independent variable were the mean of the difference between the values at high level (+1) and the values at low level (-1). The percentage of ungraft PIP was inversely proportional to the initiator concentration (A), MMA concentration (B) but was directly proportional to the reaction temperature (C).

Figure 4.3(a) and 4.3(b) show the response surface of the percentage of ungraft PIP developed by the model of initiator concentration and reaction temperature at high and low MMA concentration, respectively. In this case, initiator concentration and reaction temperature have a non-linear behavior showing an optimal relation with the minimum percentage of ungraft PIP. This optimal relation was observed denoting that a low CHPO initiator concentration level; low reaction temperature level but high MMA concentration level yielded the lowest percentage of ungraft PIP.

Table 4.4 Analysis of variance (ANOVA) on the percentage ungraft PIP using factorial design

Source	Sum of Squares	D.F.	Mean Square	F-Value	P-Value	
Model	154.73	4	38.68	9.22	0.0493	significant
A, [INT]	6.48	1	6.48	1.54	0.3023	
B, [MMA]	98.00	1	98.00	23.35	0.0169	
C, Temp.	5.12	1	5.12	1.22	0.3500	
AC	45.13	1	45.13	10.75	0.0465	
Residual	12.59	3	4.20			
Total(Correlation)	167.32	7				

R^2 = 0.9248; R^2-(ad) = 0.8244; standard error of estimation = 2.0486.

The effects of initiator concentration on ungraft PIP at high and low monomer concentrations are similar as shown in Figure 4.3(a) and 4.3(b). At low reaction temperature level, increasing amount of initiator led to an increase in the percentage of ungraft PIP while at a high reaction temperature level, the percentage of ungraft PIP decreased with increasing initiator concentration. For the effect of reaction temperature on ungraft PIP, the response surfaces of Figures 4.3(a) and 4.3(b) show that the percentage of ungraft PIP decreased at low polymerization temperature.

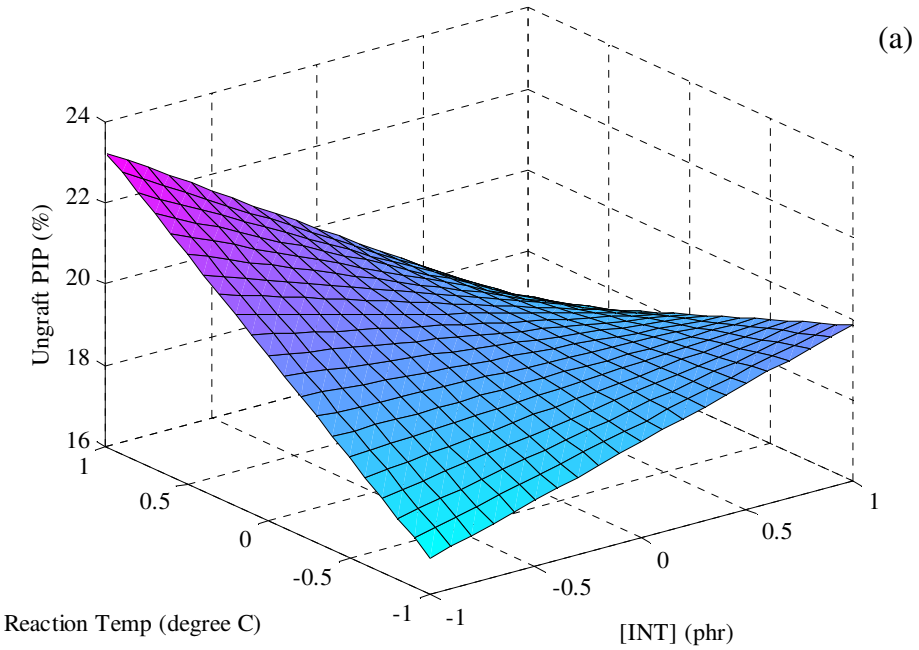

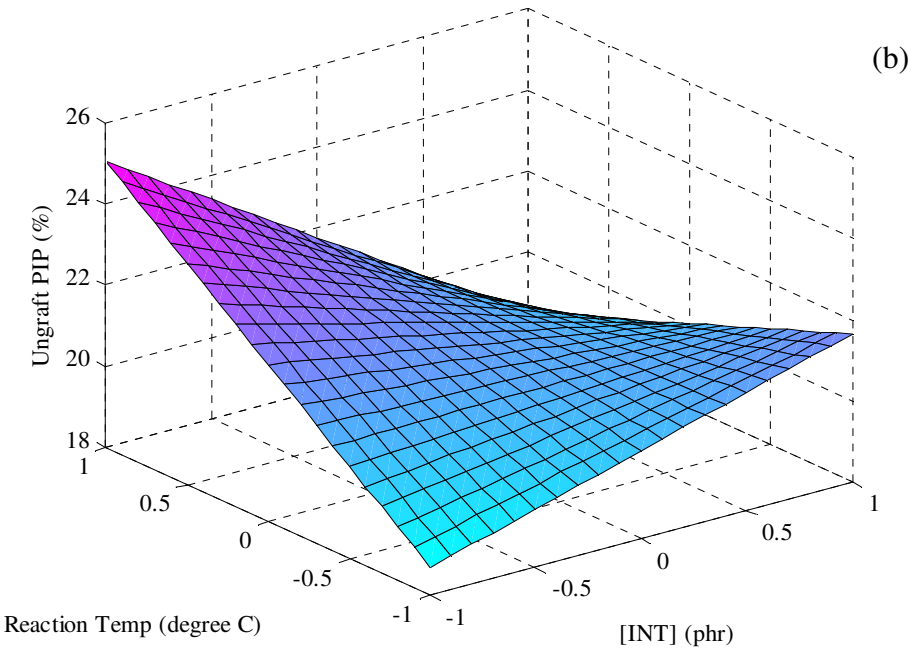

Figures 4.3 Response surface of ungraft PIP developed by the model of initiator concentration and reaction temperature relation: (a) response at high monomer concentration and (b) response at low monomer concentration.

4.3 Univariate Experiment of Graft Copolymerization

From factorial design experiments for the synthesis of nanosized MMA-g-PIP using a redox initiator system, the effects of initiator concentration, monomer concentration and reaction temperature on graft copolymerization were presented in previous section. From these results, univariate experiments were formulated and performed. The influences of monomer concentration and particle size of the nanosized PIP on the MMA grafting onto PIP were also explored. The results of univariate experiments are provided in Table 4.5 and Table 4.6 and will be subsequently discussed.

4.3.1 Effect of Monomer Concentration

From the factorial design experiments in the previous part, the percentage of graft PIP and conversion increased with increasing monomer concentration. Table 4.5 presents the effect of MMA concentration on graft copolymerization at 1 phr CHPO concentration as initiator, reaction temperature of 50 $^{\circ}$C and reaction time of 8 h. The percentage graft PIP increased from 61.4 up to 68.6% and conversion increased from 66.4 up to 97.1% with increasing the amount of monomer from 40 up to 100 phr. It could be noted that the rate of graft copolymerization was high at high monomer concentration. Moreover, this was also explained by the surface-controlled process that the nanosized polyisoprene seed has higher reaction surface and a higher number of graft sites than natural rubber as seed in the system [46, 52, 53].

4.3.2 Effect of Polyisoprene Nanoparticle Size

The effect of PIP nanoparticle size on graft copolymerization was also investigated by using variable PIP nanoparticle sizes (20, 40 and 60 nm). The initiator concentration of 1 phr, the MMA concentration of 100 phr, the SDS concentration of 1 phr, the reaction temperature of 50 °C and the reaction time of 8 h were kept constant. From Table 4.6, it is seen that the average particle sizes of MMA graft PIP were slightly increased from initial PIP nanoparticles while monomer conversion and grafting efficiency (GE) were higher than 95% and 50%, respectively. From these results, the nanopolymer with smaller particle size and higher surface area exhibited higher grafting properties than those of large particle size, such as NR (100-2000 nm).

Thus, the high conversion and high degree of grafting could be acheived when the very small particle was used as core polymer.

Table 4.5 Effect of monomer concentration on graft copolymerization of MMA onto nanosized PIP.

Experiment	[MMA] (phr)	Size (nm)		%Conv.	Graft Properties		
		PIP	Graft PIP		%Graft PIP	%Ungraft PIP	%Free PMMA
40MMA-g-PIP_25	40	25.0	28.1	66.3	61.4	22.3	16.3
60MMA-g-PIP_25	60	25.1	31.0	73.8	66.3	21.1	12.6
100MMA-g-PIP_25	100	24.9	38.0	95.6	68.5	15.3	16.1

Grafting conditions: [INT] 1 phr; [SDS] = 1 phr; reaction temperature 50 ^{o}C; stirring speed = 200 rpm; reaction time = 8 h.

PIP synthesis condition: [AIBN] = 0.25 %wt; [SDS] = 2.53 %wt; IP/H_2O = 0.4; [SHC] = 0.60 %wt; [*n*-DM] = 0.20 %wt; temperature = 70 ^{o}C; stirring speed = 300 rpm; reaction time = 20 h.

Table 4.6 Effect of particle size on graft copolymerization of MMA onto PIP.

Experiment	Size (nm)		%Conv.	Graft Properties			%GE
	PIP	Graft PIP		%Graft PIP	%Ungraft PIP	%Free PMMA	
100MMA-g-PIP_25	24.9	37.9	97.1	65.0	15.9	19.2	59.3
100MMA-g-PIP_40	44.0	49.0	98.5	82.1	7.1	10.8	77.0
100MMA-g-PIP_60	62.3	78.8	99.4	77.7	6.7	15.7	68.2

Grafting conditions: [INT] = 1 phr; [MMA] = 100 phr; [SDS] = 1 phr; stirring speed = 200 rpm; reaction temperature = 50 ^{o}C; reaction time 8 h.

PIP synthesis condition: [AIBN] = 0.25 %wt; [SDS] = 0.43-3.34 %wt; IP/H_2O = 0.4; [SHC] = 0.60 %wt; [*n*-DM] = 0.20 %wt; temperature = 70 ^{o}C; stirring speed = 300 rpm; reaction time = 20 h.

However, the highest percentage of graft PIP and GE were obtained for PIP with an initial particle size of 40 nm. The nanosized PIP with an initial particle size of around 20 nm had low percentage of graft PIP, GE and conversion. The grafting of MMA onto 20 nm PIP resulted in high free ungraft nanosized PIP and high free nanosized PMMA because the MMA polymerization occurred rather than graft copolymerization. From Table 4.6, the optimum condition of graft copolymerization (100MMA-g-PIP_40) gave 82% graft PIP, 77% GE and 98.5% conversion. Figure 4.4(a) and 4.4(b) show the size histogram of the nanosized PIP latex and MMA-g-PIP latex, respectively. The particle size distribution of nanosized PIP and MMA-g-PIP were narrow for all experiments. These results implied that the nanoparticle of MMA-g-PIP could be controlled.

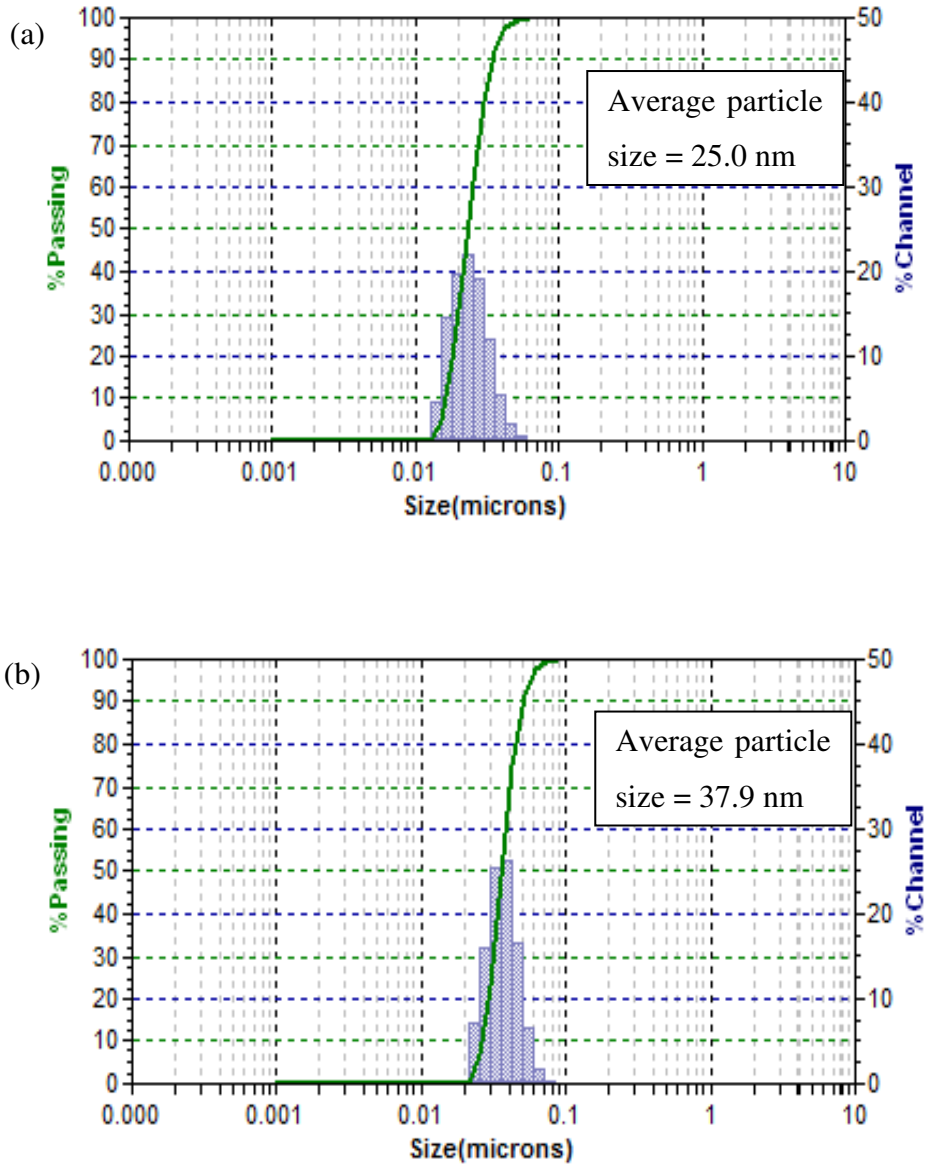

Figure 4.4 Polymer particle size distribution histograms: (a) nanosized PIP and (b) 100MMA-g-PIP_25.

4.4 Conversion and Grafting Efficiency Profile

The synthesis of 100MMA-g-PIP was carried out at low initiator concentration (1 phr), low reaction temperature (50 °C) and high monomer concentration (100 phr). Figure 4.5 shows monomer conversion and grafting efficiency as a function of reaction time. The monomer conversion increased with increasing reaction time and reached around 90% in 2 h as a result of the high copolymerization rate. The conversion reached a maximum around 96% in 8 h. This implied that the conversion during the first 1-2 h increased rapidly because most monomers were polymerized to form new polymeric radicals until the monomers were almost completely consumed, and it reached maximum conversion at that particular time. The monomer conversions increased with increasing reaction time and approached a constant conversion [80]. For grafting of nanosized PIP, grafting efficiency increased rapidly to 64% in 2 h and reached a maximum of around 67% at 8 h. This is due to the fact that the nanosized PIP seed particles have a high surface of active sites for grafting.

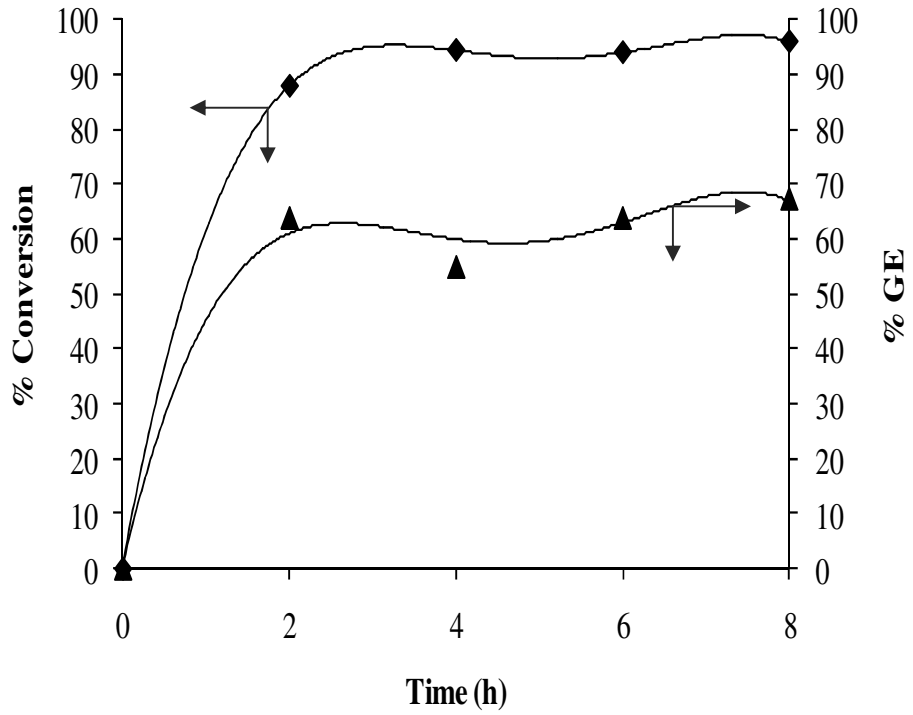

Figure 4.5 Conversion and grafting efficiency as a function of time for grafting of MMA onto nanosized PIP. [INT] = 1 phr, [MMA] = 100 phr, [SDS] = 1 phr, temperature = 50 °C, stirring speed = 200 rpm, reaction time = 8 h.

4.5 Characterization of Nanosized MMA-g-PIP

^{1}H-NMR spectroscopy was used to investigate the grafting of MMA onto nanosized PIP. A comparison between the ^{1}H-NMR spectrum of nanosized PIP and graft PIP is shown in Figure 4.6(a) and 4.6(b), respectively. From Figure 4.6(a), the nanosized PIP had various isomeric structures with *cis*-1,4, *tran*-1,4, 3,4 or 1,2 connection which affected the physical properties of the rubber. The ^{1}H-NMR chemical shifts of nanosized PIP are also shown as labeled in Figure 4.6(a). Figure 4.6(b) shows the ^{1}H-NMR of graft PIP which is attributed to $-CH_3$ (1.68 ppm), $-CH_2-$ (2.01 ppm), $-OCH_3$ (3.57 ppm), $C=CH_2$ (5.13 ppm), and the signal for the aliphatic protons of the alkane (1–2 ppm). The appearance of new peaks at 3.57 ppm is attributed to the methoxy protons of the acrylic group of the graft MMA onto nanosized PIP. This confirms that nanosized PIP was graft with MMA.

4.6 Morphology of Nanosized MMA-g-PIP

The morphologies of nanosized PIP and nanosized MMA graft PIP examined by TEM are shown in Figure 4.7. The surface morphology of the graft PIP was studied by OsO_4 staining of the carbon–carbon double bonds of the nanosized PIP to increase contrast and gradation of the particles. The darker areas represent the nanosized polyisoprene core regions and the lighter areas represent PMMA graft on nanosized polyisoprene as the shell. Figure 4.7(a) shows the nanosized PIP latex particles size were around 25 nm. The morphology of nanosized PIP particles are spherical having a smooth surface. The nanosized PIP was completely coated with PMMA by the grafting method. Figure 4.7(b), 4.7(c) and 4.7(d) show the core shell morphology of nanosized graft PIP and the thickness of the PMMA shell was around 2-10 nm depending on the GE level.

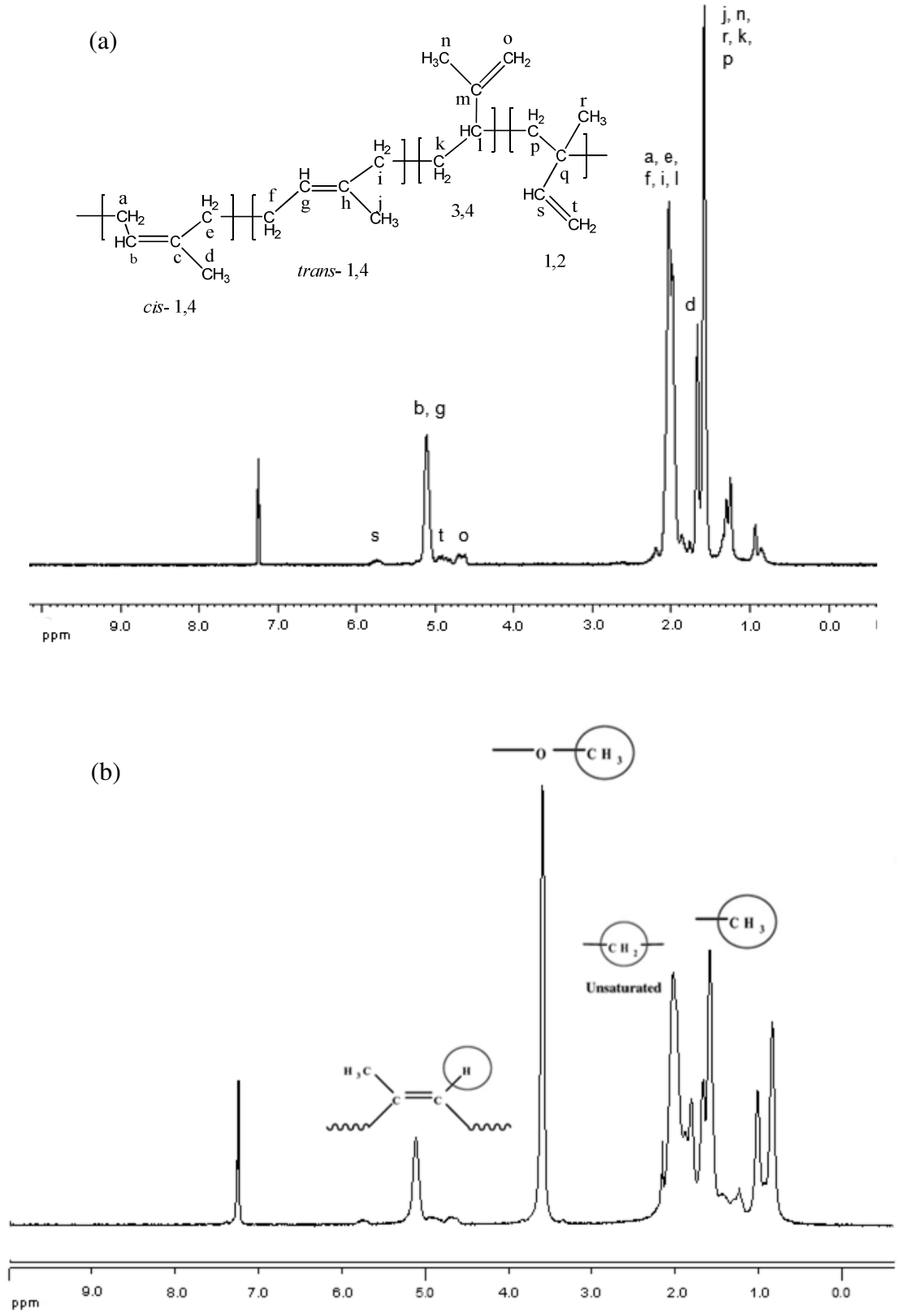

Figure 4.6 ^{1}H-NMR spectra: (a) nanosized polyisoprene and (b) nanosized MMA-g-PIP.

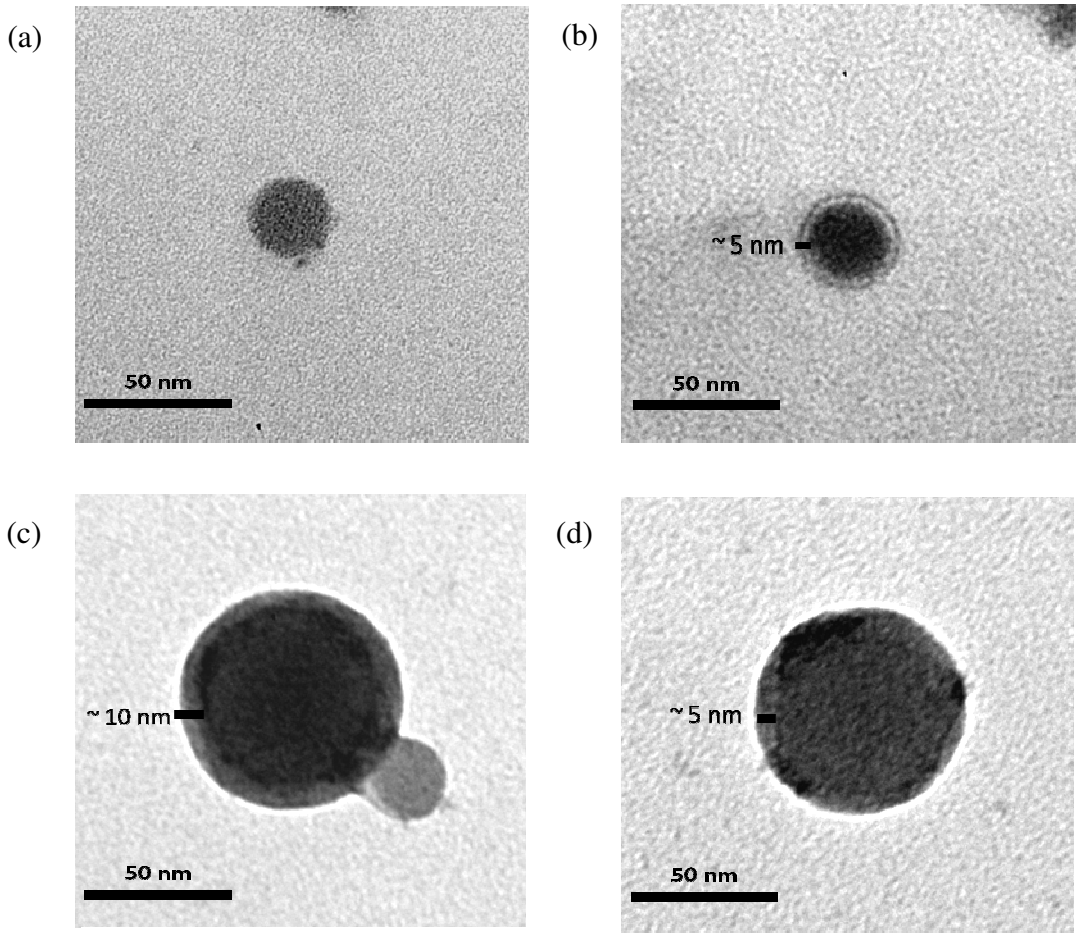

Figure 4.7 Transmission electron micrographs (×50,000) of nanosized MMA-g-PIP: (a) nanosized PIP (~25 nm), (b) 100MMA-g-PIP_25 (~30 nm), (c) 100MMA-g-PIP_40 (~60 nm) and (d) 100MMA-g-PIP_60 (~55 nm).

4.7 Thermal Properties of Nanosized MMA-g-PIP

Thermal analysis was used to investigate the physical properties of the graft polymer as a function of temperature. Thermal gravimetric analysis (TGA) was used to find the initial decomposition temperature (T_{id}) and the maximum decomposition temperature (T_{max}). TGA of nanosized PIP (D_n = 27.7 nm, M_w = 2.37×10^6) and MMA graft PIP samples at various conditions were conducted under a nitrogen atmosphere. T_{id} was determined from the intersection of two tangents at the onset of the decomposition temperature. T_{max} was obtained from the peak maxima of the derivative of the TG curves. From the TGA thermograms of MMA-g-PIP sample in Figure 4.8, the weight loss occurred between 250-500 °C due to the loss of volatile matter contained within the copolymer. The TGA curves of the samples showed only a one-step change and provided a smooth weight loss curve. These results are similar to the thermal properties behavior of ST-g-NR and MMA-g-NR [101, 102].

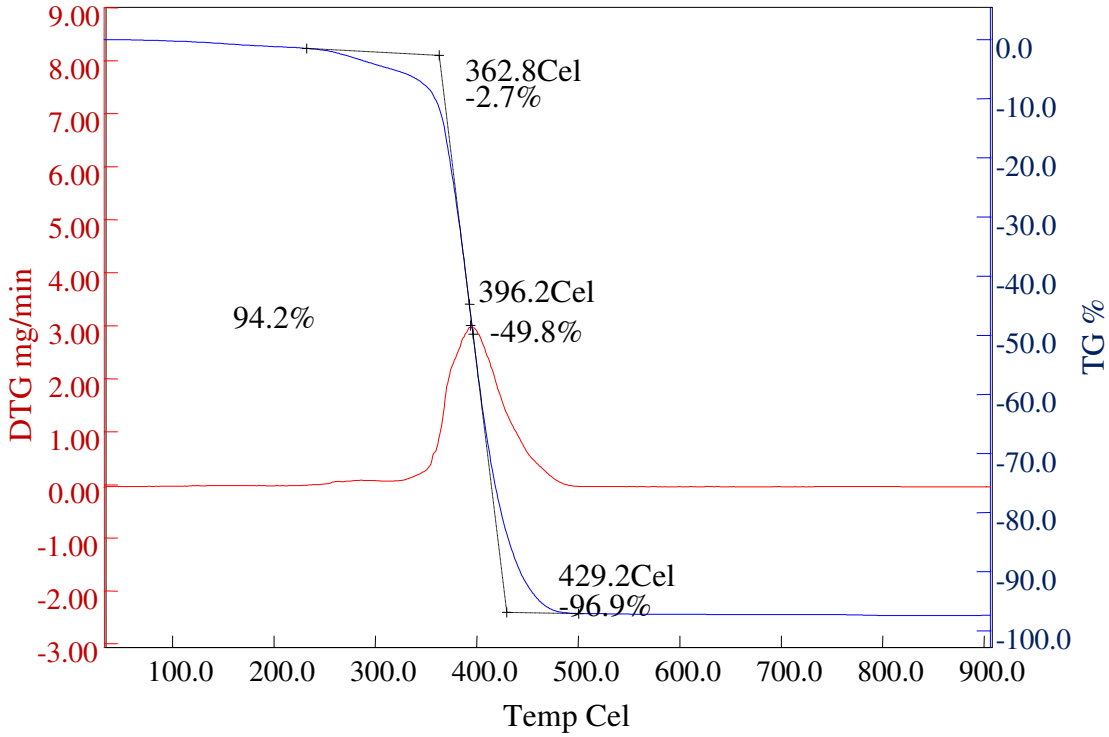

Figure 4.8 Thermogravimetric analysis curve of nanosized 100MMA-g-PIP_40.

Table 4.7 summarizes the degradation temperature (T_{id} and T_{max}) of all the rubber samples. The results show that the T_{max} of MMA graft PIP samples and nanosized PIP are nearly the same (increase ~3°C). However, T_{id} of MMA graft PIP samples were slightly increased (3-9°C) as shown in Table 4.7. The nanosized PIP particle size and MMA content was not found to have a significant effect on T_{id} and T_{max} of the MMA graft samples.

Table 4.7 Glass transition temperature and decomposition temperature of MMA-g-PIP

Rubber sample	[MMA] phr	Size (nm)		T_g (°C)	T_{id} (°C)	T_{max} (°C)
		PIP	Graft PIP			
Nanosized PIP	0	27.7	-	-61.9	358.8	393.2
40MMA-g-PIP_25	40	25.2	28.1	-56.5	361.6	399.9
60MMA-g-PIP_25	60	25.0	31.0	-57.3	369.3	408.2
100MMA-g-PIP_25	100	24.9	37.9	-59.5	365.1	396.1
100MMA-g-PIP_40	100	44.0	49.0	-58.8	362.8	396.2
100MMA-g-PIP_60	100	62.3	78.8	-59.8	367.0	396.5

Differential scanning calorimetry (DSC) was used to determine the glass transition temperature (T_g) which is one of the most important parameters for characterization of the polymer structure. T_g is the transition related to the motion in the amorphous section of the polymer. This value is affected by the size of side groups and mobility of the chain. Decreasing T_g would result by any factor disturbing the closest packing of main chain but increasing T_g would occur with any factor stiffening or increasing the interaction between chains [42]. From the DSC thermogram of grafting MMA-g-PIP, a two step base-line shift was observed as

shown in Figure 4.9. The lower T_g is the T_g of the PIP backbone and the upper T_g is belongs to the graft PMMA over the T_g range of 80-85 °C. From Table 4.7, the T_g of MMA graft PIP was slightly higher than that of nanosized PIP (increase 2-6 °C). These results showed that the majority of these graft copolymers have graft chains affecting the free volume backbone. Consequently, it can be concluded that the nanoparticle size of the primary polymer did not have an appreciable effect on the T_g of MMA graft polymer.

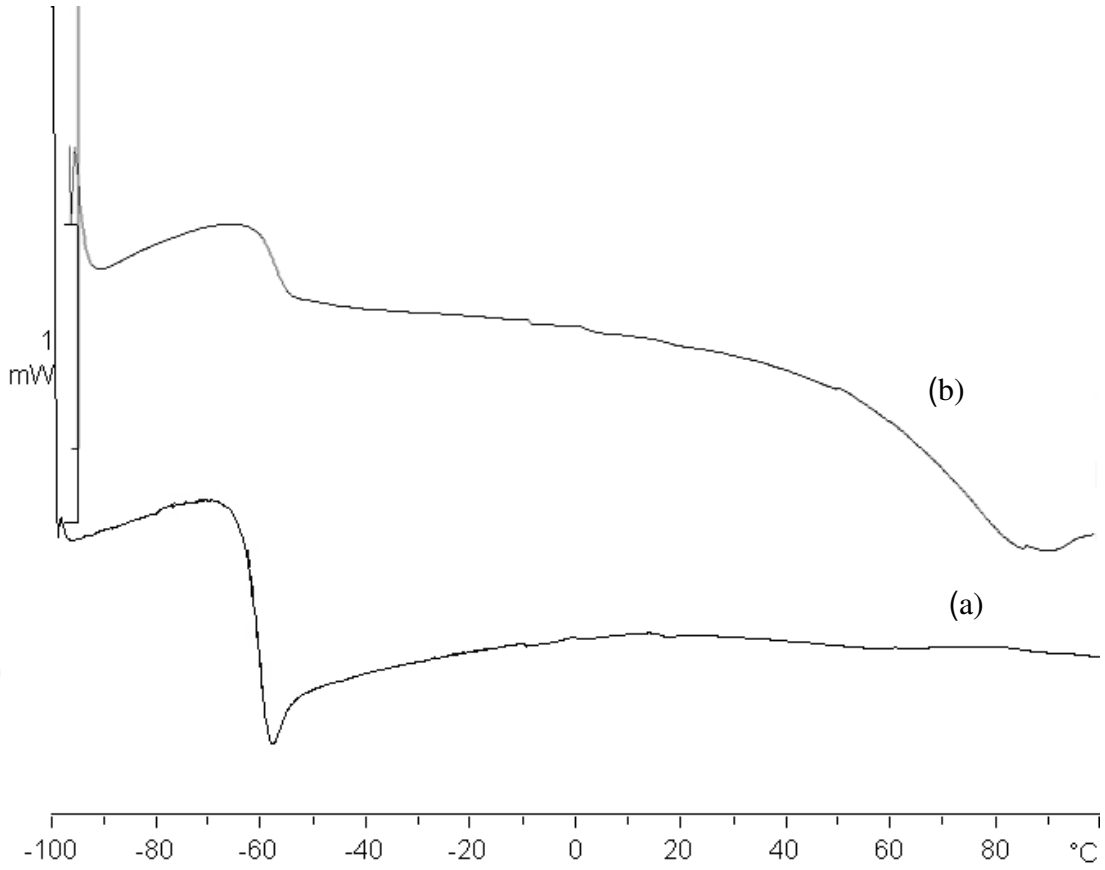

Figure 4.9 DSC thermograms of (a) nanosized PIP and (b) 100MMA-g-PIP.

CHAPTER V

GRAFT COPOLYMERIZATION OF STYRENE ONTO NANOSIZED POLYISOPRENE USING REDOX INITIATOR SYSTEM

5.1 Introduction

Graft copolymerization of vinyl monomers onto diene-based rubber has been widely studied in recent years. The initiator systems employed include water-soluble, oil-soluble and redox initiator systems. The most promising graft copolymer based on diene rubber is derived from methyl methacrylate (MMA) and styrene (ST). In Chapter IV, the graft copolymerization of methyl methacrylate (MMA) onto nanosized polyisoprene has been reported including the influence of various process variables on the grafting reaction. The graft copolymerization of polyisoprene was carried out in latex form, since the existence of double bonds in its chains, can be readily graft with a variety of monomers. Nanosized polyisoprene (nanosized PIP) has a narrow size distribution of particles and the particle size could be controlled by varying surfactant concentration or isoprene monomer to water ratio in the preparation step as reported in Chapter III.

Styrene graft PIP (STgPIP) latex is one type of specialty latex produced by chemical modification of PIP latex. The ST monomer is graft onto nanosized PIP latex using a redox couple initiator to produce graft copolymer. Graft copolymerization of ST onto nanosized PIP is expected to have high monomer conversion and high grafting efficiency because PIP nanoparticles have large surface area for grafting sites. Many investigators earlier reported the improvement of grafting efficiency by a modified backbone of the polymer as described in Chapter IV. To increase grafting efficiency, it is necessary to remove the impurities and reduce particle size of the rubber latex. For example, the graft copolymerization of styrene onto urea-deproteinized natural rubber latex showed high conversion and high grafting efficiency [99, 100].

The purpose of the present work was to synthesis the ST graft PIP by emulsion graft copolymerization using redox initiator. The effects of PIP nanoparticle size, reaction temperature and ST monomer concentration on grafting properties and monomer conversion were studied. The morphology and thermal properties of ST-g-PIP were determined.

5.2 Effect of Polyisoprene Particle Size

The effect of PIP nanoparticle size on graft copolymerization was investigated. The initiator concentration of 1 phr, the ST concentration of 100 phr, the SDS concentration of 1 phr, the reaction temperature of 50 °C and the reaction time of 8 h were kept constant. From Table 5.1, it can be seen that the average particle sizes of ST graft PIP were slightly increased from initial PIP particle size. For all particle sizes, the monomer conversion was around 90% and grafting efficiency (GE) was higher than 50%. The nanopolymers with smaller particle size and higher surface area exhibited higher grafting properties than those of large particle size, such as NR (100-2000 nm). This could imply that the high conversion and high degree of grafting could be obtained when the very small particle was used as core polymer. From Table 5.1, the optimum condition of graft copolymerization (100ST-g-PIP_40) gave 84.3% graft PIP, 75.9% GE and 90% monomer conversion. These results were similar to the preparation of nanoparticles of grafting MMA onto PIP. However compared with the synthesis of MMA-g-PIP, the optimum condition gave 82.1% graft PIP, 77.0% GE and 98.5% monomer conversion. Thus, the ST grafting gave lower monomer conversion and %GE than MMA grafting onto nanosized PIP. Since the polymerization system contained water as media and used low stirring speed, the hydrophilic MMA monomer was more compatible with water than the hydrophobic ST monomer.

Table 5.1 Effect of particle size on graft copolymerization of ST onto PIP.

Experiment	Size (nm)		%Conv.	Graft Properties			%GE
	PIP	Graft PIP		%Graft PIP	%Ungraft PIP	%Free PST	
100ST-g-PIP_25	24.4	27.6	89.1	68.2	11.7	20.1	51.1
100ST-g-PIP_40	38.5	41.5	90.0	84.3	8.3	7.4	75.9
100ST-g-PIP_50	51.1	60.2	93.6	66.9	11.3	21.8	51.3

Grafting conditions: [INT] = 1 phr; [ST] = 100 phr; [SDS] = 1 phr; stirring speed = 200 rpm; reaction temperature = 50 °C; reaction time 8 h.

PIP synthesis condition: [AIBN] = 0.25 %wt; [SDS] = 0.43-3.34 %wt; IP/H_2O = 0.4; [SHC] = 0.60 %wt; [*n*-DM] = 0.20 %wt; temperature = 70 °C; stirring speed = 300 rpm; reaction time = 20 h.

Figure 5.1(a) and 5.1(c) show the size histogram of nanosized PIP latex. While the size histrogram of ST-g-PIP latex show in Figure 5.1(b) and 5.1(d). The particle size distribution of nanosized PIP and ST-g-PIP were narrow for all experiments. This implied that the nanoparticle size of ST-g-PIP could be controlled.

(a) Average particle size = 24.4 nm

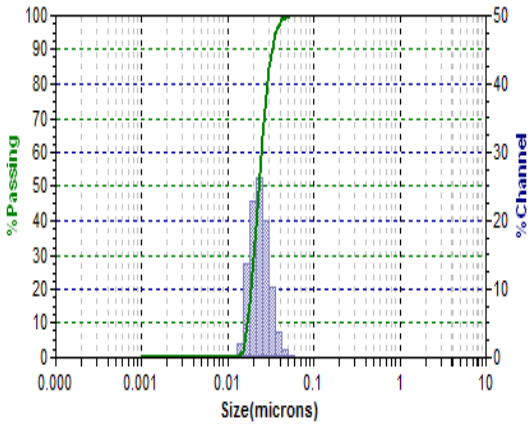

(b) Average particle size = 27.6 nm

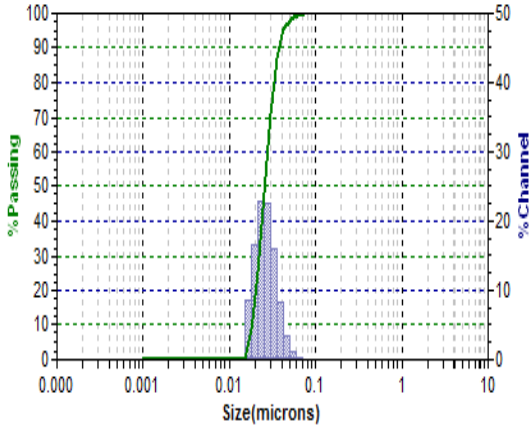

(c) Average particle size = 38.5 nm

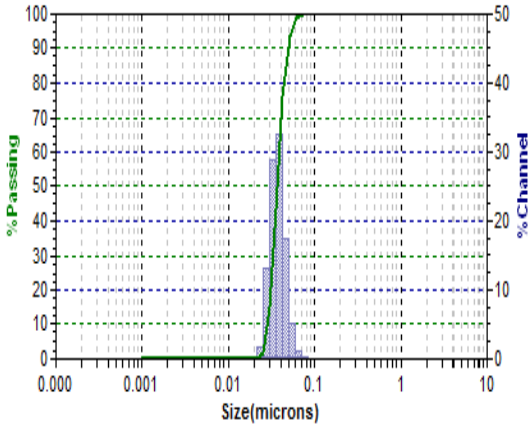

(d) Average particle size = 38.5 nm

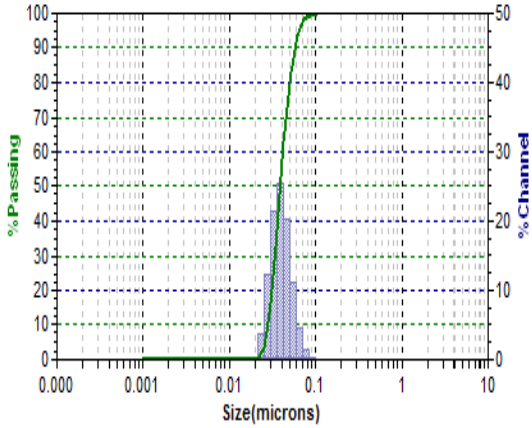

Figure 5.1 Polymer particle size distribution histograms: (a) PIP_25 (b) 100ST-g-PIP_25, (c) PIP_40 and (d) 100ST-g-PIP_40

5.3 Effect of Reaction Temperature

The effect of reaction temperature on the graft copolymerization was investigated. The conditions for ST grafting onto nanosized PIP were as follows: initiator concentration of 1 phr, ST concentration of 100 phr, SDS concentration of 1 phr, reaction temperature 40-70 °C and a reaction time of 8 h. For the temperature range of 40-70 °C, the polymerization temperature had a positive effect on grafting efficiency and monomer conversion as shown in Table 5.2. The grafting efficiency and monomer conversion increased with increasing reaction temperature. According to the Arrhenius relation, in radical polymerization started by thermal decomposition of an initiator, as temperature was increased, the rate of polymerization is strongly increased. In addition, when the temperature was raised, the diffusion rate of ST monomers into the nanosized PIP was enhanced, resulting in higher grafting efficiency. This result was similar to that reported for the graft copolymerization of MMA onto natural rubber [103] and the graft copolymerization of ST and MMA on to SBR [104]. However, some investigators reported a negative effect of high reaction temperature [47-49, 55, 57]. They explained that the decomposition of the initiator increased with increasing reaction temperature; which caused an increase in both the number of free radicals and the rate of polymerization. The free radicals went through either recombination or other side reactions such as a chain transfer reaction which it caused a decrease in the initiator efficiency for grafting. However, these phenomena did not occur in the graft copolymerization of ST onto nanosized PIP. It may be due to the fact that for the nanoparticles with higher surface area, the rate of polymerization was higher than rate of side reactions even though a high polymerization temperature was used.

At the appropriate temperature for graft copolymerization of ST onto nanosized PIP, the high % monomer conversion almost 84-92%, and %GE around 47-59% were over the range of 50 to 70 °C. This was one advantage of nanoparticle latex in that high % monomer conversion and %GE could be achieved by using low reaction temperature for graft copolymerization.

Table 5.2 Effect of reaction temperature on graft copolymerization of ST onto PIP.

Experiment	Temp (°C)	Size (nm)		%Conv.	Graft Properties			%GE
		PIP	Graft PIP		%Graft PIP	%Ungraft PIP	%Free PST	
ST-g-PIP_T40	40	20.2	25.4	84.9	65.3	14.3	20.5	47.1
ST-g-PIP_T50	50	24.4	27.6	89.1	68.2	11.7	20.1	51.1
ST-g-PIP_T60	60	22.9	28.2	93.7	69.3	10.1	20.6	53.9
ST-g-PIP_T70	70	24.5	27.5	92.7	69.3	13.4	17.4	59.2

Grafting conditions: [INT] 1 phr; [ST] = 100 phr; [SDS] = 1 phr; stirring speed = 200 rpm; reaction time = 8 h.

PIP synthesis condition: [AIBN] = 0.25 %wt; [SDS] = 2.53 %wt; IP/H_2O = 0.4; [SHC] = 0.60 %wt; [*n*-DM] = 0.20 %wt; temperature = 70 °C; stirring speed = 300 rpm; reaction time = 20 h.

5.4 Effect of Monomer Concentration

The effect of the monomer concentration on the percentage grafting efficiency and monomer conversion were explored. Experiments were performed at a ST monomer concentration of 60 to 150 phr (Monomer-to-rubber ratio of 0.6 to 1.5) when the initiator concentration of 1 phr, the SDS concentration of 1 phr, reaction temperature 50 °C, stirring speed 200 rpm and a reaction time of 8 h were kept constant. Figure 5.2(a) shows the conversion and grafting efficiency profile at various times for each monomer concentration. As the monomer concentration increased, the grafting efficiency and monomer conversion increased and reached a maximum at a ST monomer concentration of 100 phr. At a ST monomer concentration of 150 phr, the grafting efficiency and monomer conversion were lower than at 100phr.

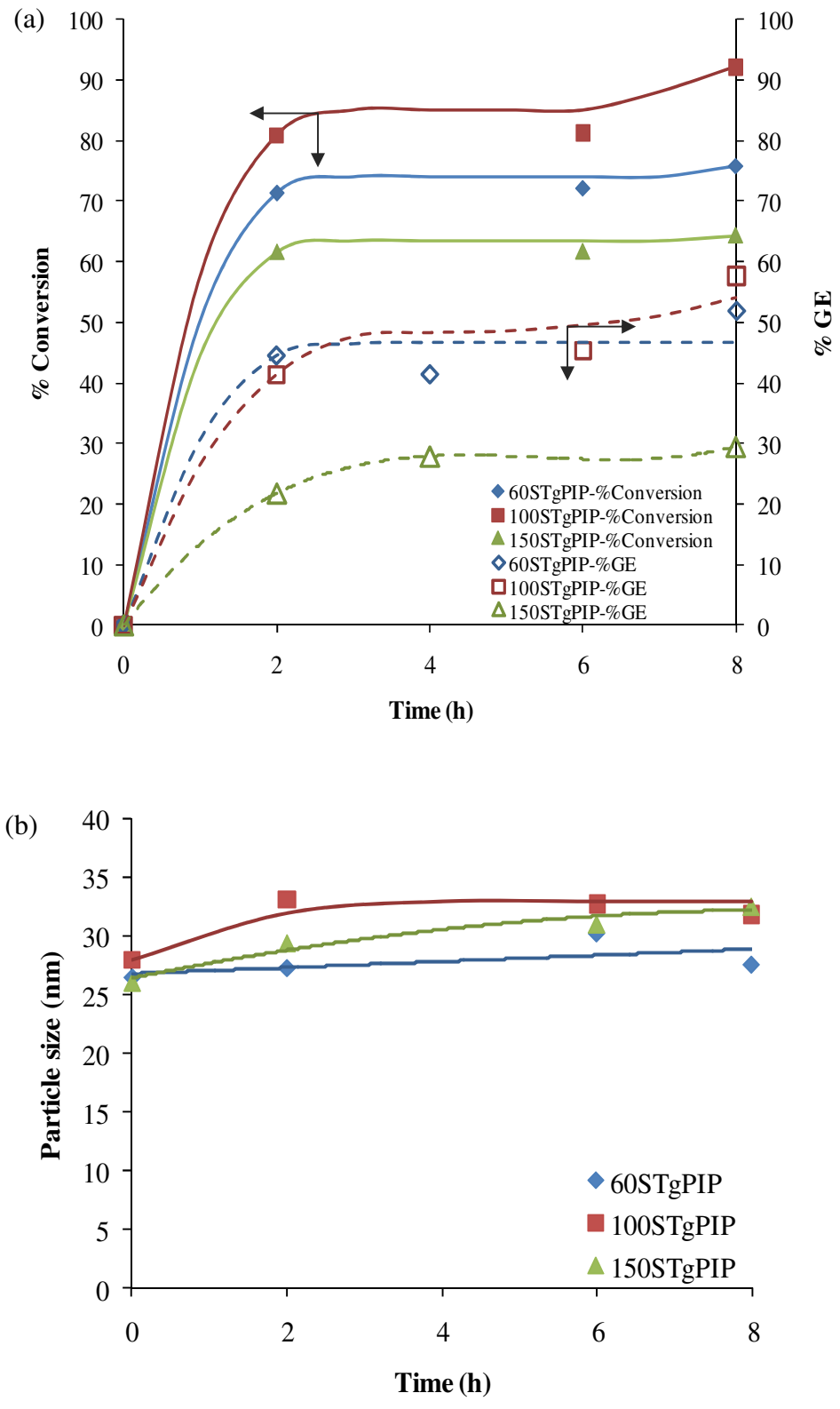

Figure 5.2 Graft ST onto nanosized PIP as a functional of time: (a) Conversion and grafting efficiency profiles and (b) Changing of particle size profile.

At higher monomer concentration (ST = 150 phr), the homopolymerization or chain transfer is more pronounced than graft copolymerization. Therefore, the graft copolymerization with high monomer concentration has a lower active surface area at the reaction site and the rate of homopolymerization is more favored than the polymeric radical transfer rate to nanosized PIP. This cause a lower grafting efficiency and monomer conversion when using high amount of monomer. This phenomenon was similar to the observations for vinyl monomer grafting onto natural rubber [48, 50, 52] and ST grafting onto deproteinized natural rubber [100, 105].

Figure 5.2(b) shows the variation of nanoparticle size of ST graft PIP at various times. The nanoparticle size was slightly increased from the initial PIP nanoparticle. The degree of increase in particle size increased with increasing monomer concentration. From the above discussion, the graft copolymerization with very high monomer concentration has a lower active surface area at the reaction site and the rate of homopolymerization is more favored than the polymeric radicals transfer rate to nanosized PIP. Then, these homopolymers (free PST) may attach to the polymer backbone and cause an increase in the particle size. These phenomena can be also explained by a mechanism of the graft copolymerization of styrene onto nanosized PIP particle at various monomer concentrations. At low monomer concentration (Figure 5.3(a)), a limited amount of monomer was consumed but active sites still remained. This led to low grafting efficiency and low monomer conversion, from the appropriate monomer condition (Figure 5.3(b)). At an appropriate amount of monomer, all monomer and active sites were consumed to produce high grafting efficiency and high monomer conversion with or without a small amount of free PST. With excess monomer or excess monomer (Figure 5.3(c)), long chains of PST may also affect the steric attraction which occurs at active grafting sites of polymer backbone. Thus, the grafting efficiency and monomer conversion were decreased at high monomer concentration.

(a) Low monomer concentration

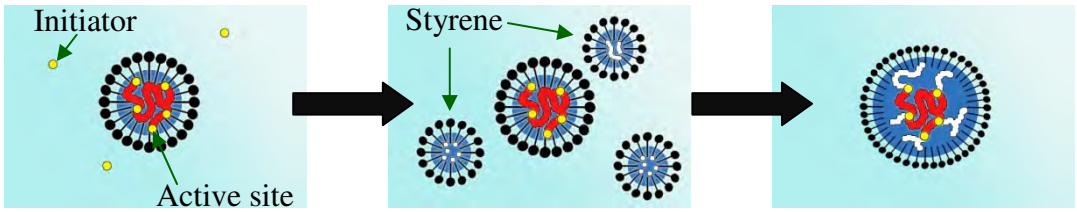

Low Grafting Efficiency
and Low conversion

(b) Appropriate monomer concentration

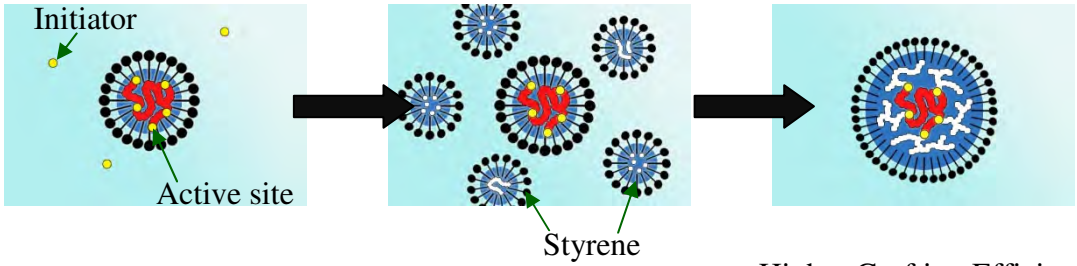

Higher Grafting Efficiency
and Higher conversion

(c) High monomer concentration

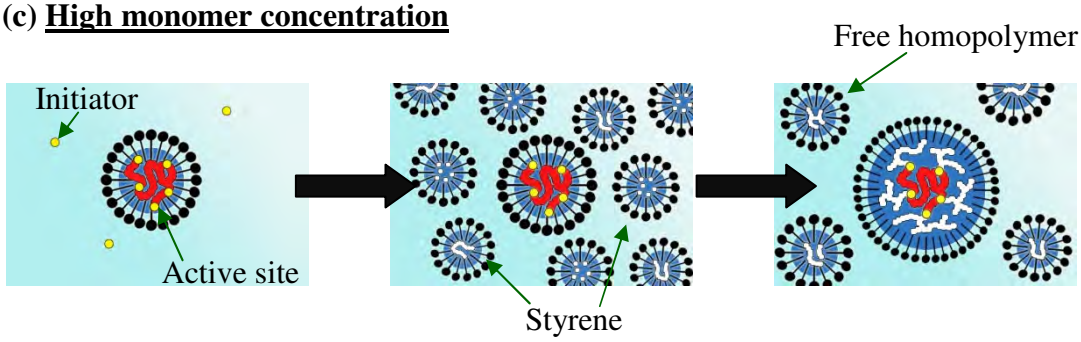

Lower Grafting Efficiency
and Lower conversion

Figure 5.3 Schematic representation of mechanism of graft copolymerization of styrene onto nanosized PIP particle at various monomer concentrations (adapted from Pukkate, N. et al. [105])

5.4.1 Conversion and Grafting Efficiency Profile

From Figure 5.2(a), the conversion and grafting efficiency increased sharply and reached a maximum in 2 h as a result of the high polymerization rate of PIP nanoparticles which has high interfacial area for polymerization. This implied that the conversion during the first 1-2 h increased rapidly because most of the monomer was polymerized to form new polymeric radicals until the monomer was completely consumed and it reached maximum conversion at that particular time. The monomer conversion increased with increasing time and approached a constant conversion [80]. The highest conversion and grafting efficiency was observed at a ST monomer concentration of 100 phr (100STgPIP). For grafting ST onto nanosized PIP, the monomer conversion increased with increasing time and reached around 85% in 2 h as a result of the high copolymerization rate. Then, the conversion reached a maximum around 90% in 8 h. While the grafting efficiency increased rapidly to 45% in 2 h and reached a maximum around 60% at 8 h. This is due to the fact that the nanosized PIP seed particle has a high surface as active sites for grafting. These results showed a similar trend with the graft copolymerization of MMA onto nanosized PIP reported in Chapter IV.

5.4.2 Grafting properties profile

Grafting properties were determined from the Soxhlet extraction analysis of gross graft copolymer. The grafting properties were related to the grafting efficiency. Figure 5.4 shows the grafting properties of ST graft PIP as a function of time at various ST concentrations. The percentage of graft PIP, ungraft PIP and free polystyrene (homopolymer) increased sharply and reached a maximum in 2 h and remained constant during 2-8 h. These grafting properties had the same trend with grafting efficiency and conversion. From Figure 5.4(a) the 60STgPIP had the highest percentage of graft PIP, around 68% after 8 h, but the 100STgPIP had the highest grafting efficiency. It can be seen that the 60STgPIP had a higher percentage of ungraft PIP than 100STgPIP at 8 h and had a high percentage of free polystyrene around 20% as shown in Figure 5.4(b) and 5.4(c), respectively.

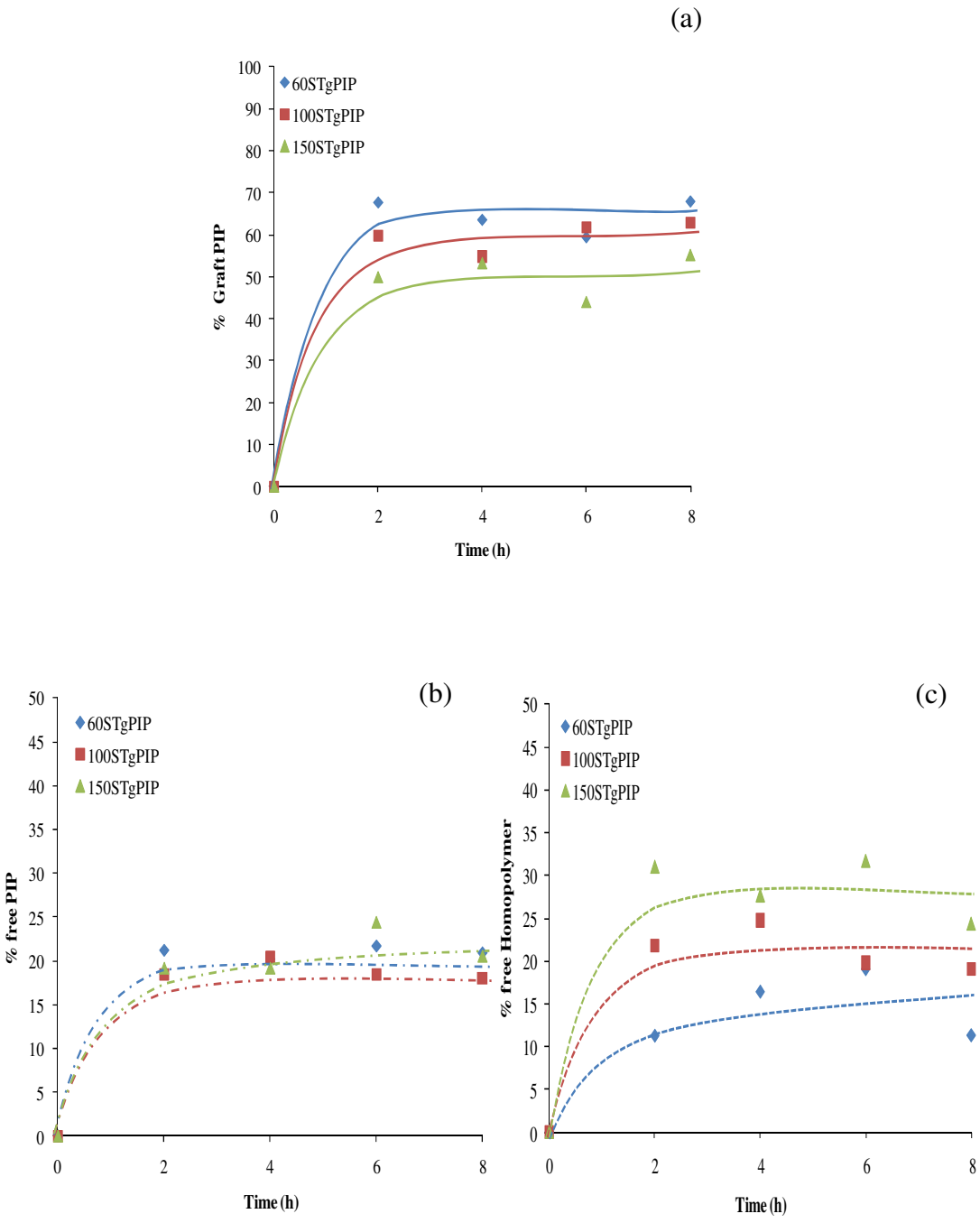

Figure 5.4 Grafting properties of ST graft onto nanosized PIP as a functional of time: (a) % graft nanosized PIP, (b) % free nanosized PIP and (c) % free polystyrene

The 150STgPIP had the lowest percentage of graft PIP because 150STgPIP had the highest percentage of ungraft PIP and free polystyrene as shown in the Figure 5.4. This resulted in low grafting efficiency and low monomer conversion. These behaviors can be explained by a mechanism of ST grafting onto nanosized PIP particles at a high amount of monomer as described in Figure 5.3.

From Figure 5.4, the appropriate ST concentration for graft copolymerization onto nanosized PIP was 100 phr (100STgPIP) and the high monomer conversion, grafting efficiency and graft PIP but a low percentage of ungraft PIP and free homopolymer could be obtained.

5.5 Characterization of Nanosized ST-g-PIP

^{1}H-NMR spectroscopy was used to investigate the ST grafting onto nanosized PIP. The ^{1}H-NMR spectra of nanosized PIP and graft PIP are illustrated in Figures 5.5(a) and 5.5(b), respectively. From Figure 5.5(a), the nanosized PIP had various isomeric structures with *cis*-1,4, *tran*-1,4, 3,4 or 1,2 connection representing the properties of the diene rubber. The ^{1}H-NMR chemical shifts of nanosized PIP are also shown as labeled in Figure 5.5(a). Figure 5.5(b) shows the ^{1}H-NMR of ST graft PIP which is attributed to $–CH_3$ (1.68 ppm), $–CH_2–$ (2.01 ppm), -aromatic (6.5-8.5 ppm), $C=CH_2$ (5.13 ppm), and the signal for the aliphatic protons of the alkane (0.9–2.0 ppm). The appearances of new peaks in the range of 6.5-8.8 ppm are attributed to aromatic protons of the graft ST onto PIP which confirms that the nanosized PIP was graft with ST.

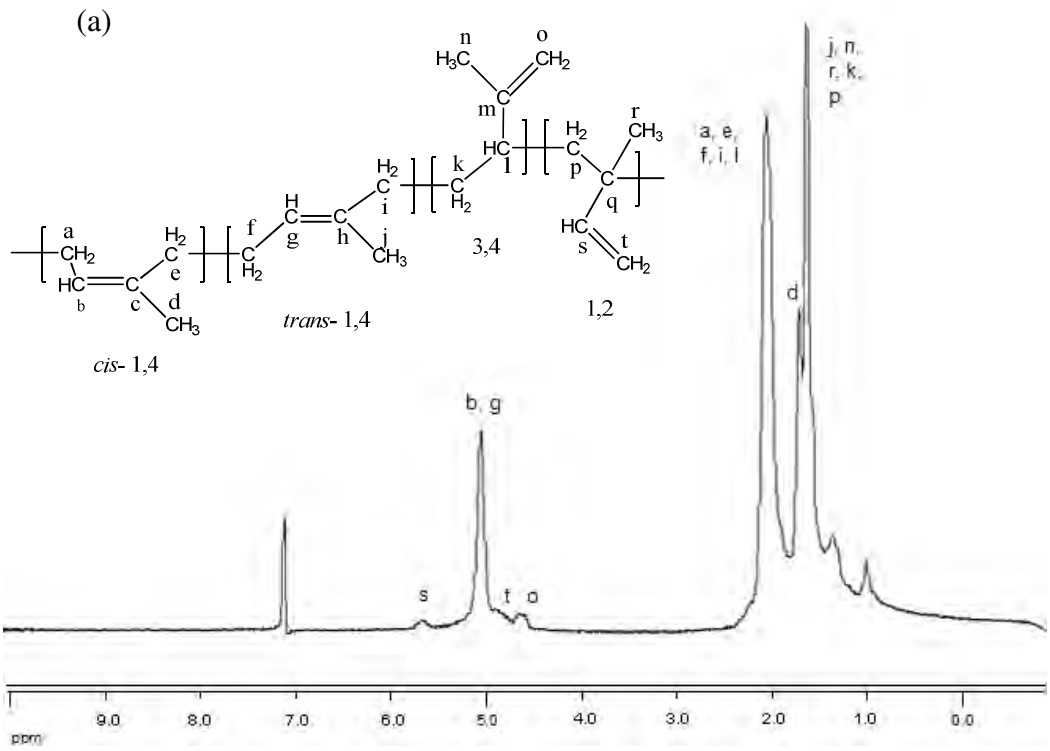

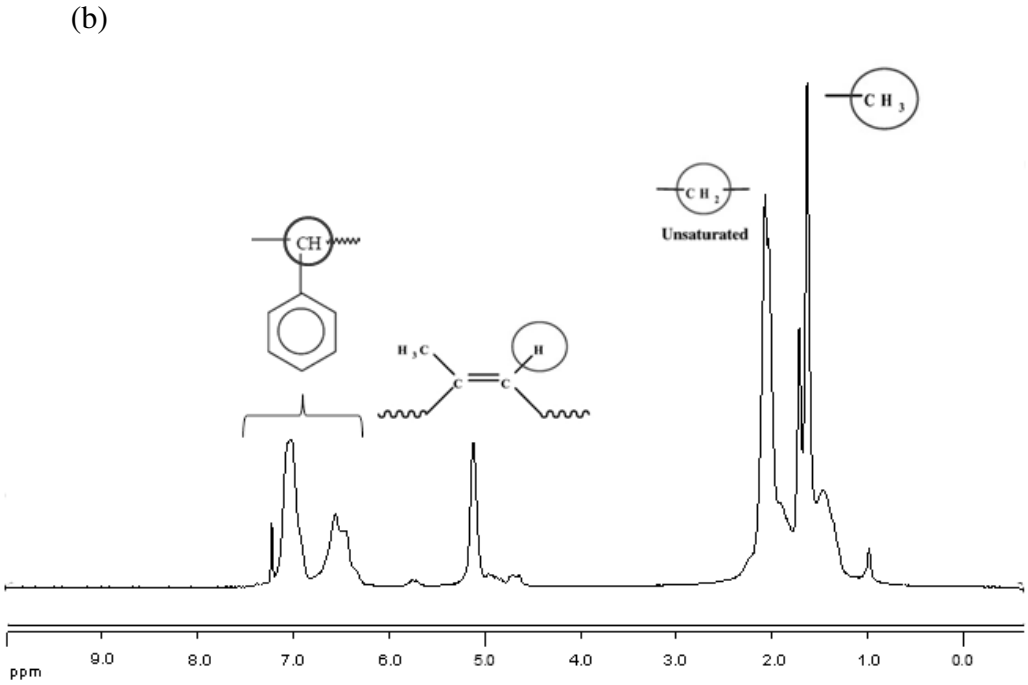

Figure 5.5 ^{1}H-NMR spectra: (a) nanosized polyisoprene and (b) nanosized ST-g-PIP.

5.6 Morphology of Nanosized ST-g-PIP

The morphologies of nanosized PIP and ST graft PIP examined by TEM are shown in Figure 5.6. The surface morphology of the graft PIP was observed by OsO_4 staining of the carbon–carbon double bonds of PIP to increase contrast and gradation of the particles. The darker areas represent the nanosized polyisoprene core regions and the lighter areas represent the ST graft on polyisoprene as the shell. From Figure 5.6 (a), the morphology of the nanosized PIP particles are spherical having a smooth surface. For the small PIP nanoparticles (100ST-g-PIP_25), it was completely coated with PST by the grafting method as shown in Figure 6.5 (b) which shows the core shell morphology of nanosized graft PIP. While the larger PIP nanoparticles (100ST-g-PIP_40 and 100ST-g-PIP_50) might not be completely coated with PST but the PST might be distributed like raspberry morphology in some portion of particle as shown in Figures 5.6(c) and 5.6(d). The thickness of ST shell was estimated to be around 10 nm depending on the GE level.

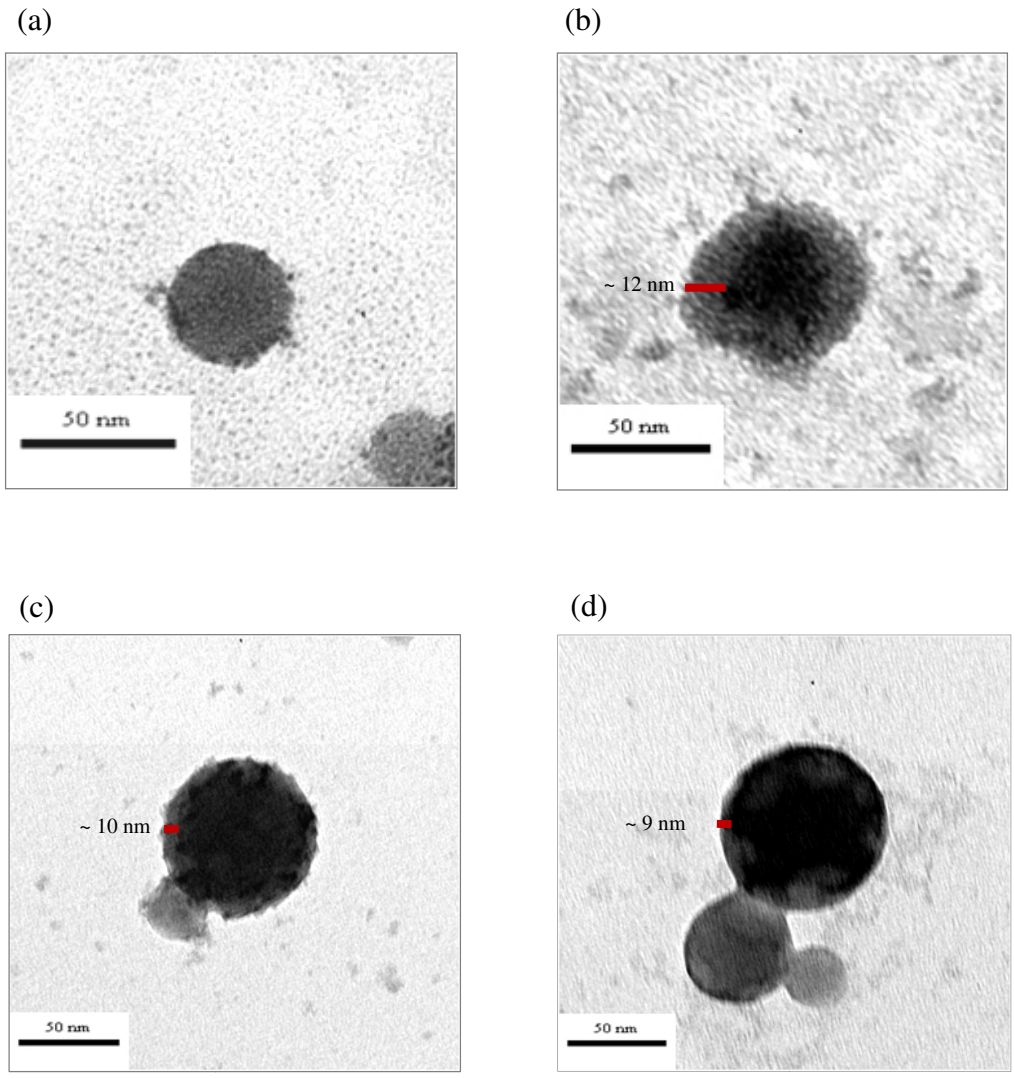

Figure 5.6 Transmission electron micrographs (×50,000) of nanosized ST-g-PIP: (a) nanosized PIP (~41 nm), (b) 100ST-g-PIP_25, (c) 100ST-g-PIP_40 and (d) 100ST-g-PIP_50.

5.7 Thermal Properties of Nanosized ST-g-PIP

Thermal analysis was used to investigate the physical properties of the polymers as a function of temperature. Thermal gravimetric analysis (TGA) was used to find the initial decomposition temperature (T_{id}) and the maximum decomposition temperature (T_{max}). TGA of nanosized PIP and ST graft PIP samples at various conditions conducted under a nitrogen atmosphere. T_{id} was determined from the intersection of two tangents at the onset of the decomposition temperature. T_{max} was obtained from the maximum peak of the derivative of the TG curves. Table 5.3 summarizes the degradation temperature (T_{id} and T_{max}) of all rubber samples. From the TGA thermograms in Figure 5.7, the weight loss occurred between 250-520 °C due to the loss of volatile matter contained within the copolymer. The degradation temperature increased with increasing ST concentration. From Table 5.3, the T_{max} of ST graft PIP samples were higher than that of nanosized PIP by around 10-30 °C. The T_{id} of ST graft PIP samples with high grafting efficiency were quite the same as PIP. The particle size of nanosized PIP had no significant effect on T_{id} and T_{max} while ST content had a significant effect on T_{id} and T_{max} of ST graft samples.

Differential scanning calorimetry (DSC) was used to determine the glass transition temperature (T_g) which is one of the most important parameters for characterization of the polymer structure. T_g is the transition related to the motion in the amorphous section of the polymer. This value is affected by the size of side groups and mobility of the chain. Decreasing T_g would by any factor disturbing the closest packing of main chain but increasing T_g would occur with any factor stiffening or increasing the interaction between chains [42].

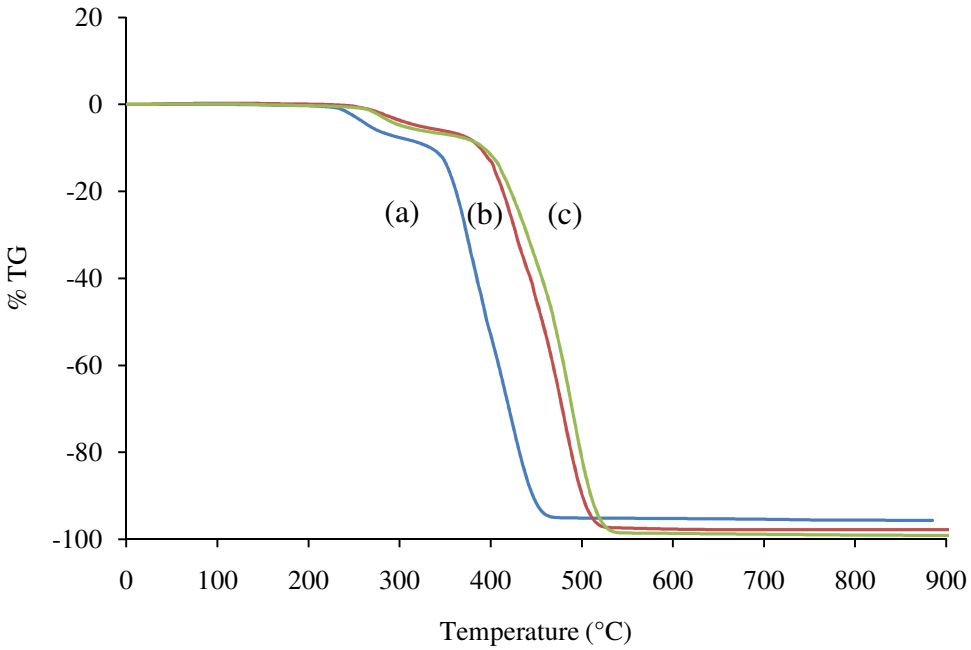

Figure 5.7 TGA thermograms of ST-g-PIP: (a) 60ST-g-PIP_25, (b) 100ST-g-PIP_25 and (c) 150ST-g-PIP_25.

Table 5.3 Glass transition temperature and decomposition temperature of ST-g-PIP

Rubber sample	[ST] phr	Size (nm)		T_g (°C)	T_{id} (°C)	T_{max} (°C)
		PIP	Graft PIP			
Nanosized PIP	0	27.7	-	-61.9	355.6	391.7
60ST-g-PIP_25	60	26.5	27.6	-58.2	340.8	395.5
100ST-g-PIP_25	100	28.0	31.9	-58.8	356.8	407.4
150ST-g-PIP_25	150	26.1	32.6	-59.9	355.7	426.8
100ST-g-PIP_40	100	38.5	41.5	-58.1	350.0	401.5
100ST-g-PIP_50	100	51.1	60.2	-58.2	352.2	401.1

From the DSC thermogram of graft ST-g-PIP, a two step base-line shift was observed as shown in Figure 5.8. Then, the lower T_g is the T_g of the PIP backbone and the upper T_gs belongs to the polystyrene graft chain which has range of 75-90 °C. The T_g of ST-g-PIP was slightly higher than that of PIP (increase = 2-4 °C). It could be explained that the majority of these graft copolymers have graft chains affecting the free volume backbone. Consequently, it can be concluded that the nanoparticle size of the primary polymer had no appreciable effect on the T_g of the ST graft polymer. The thermal behaviors of ST-g-PIP were similar to that of MMA-g-PIP reported Chapter IV.

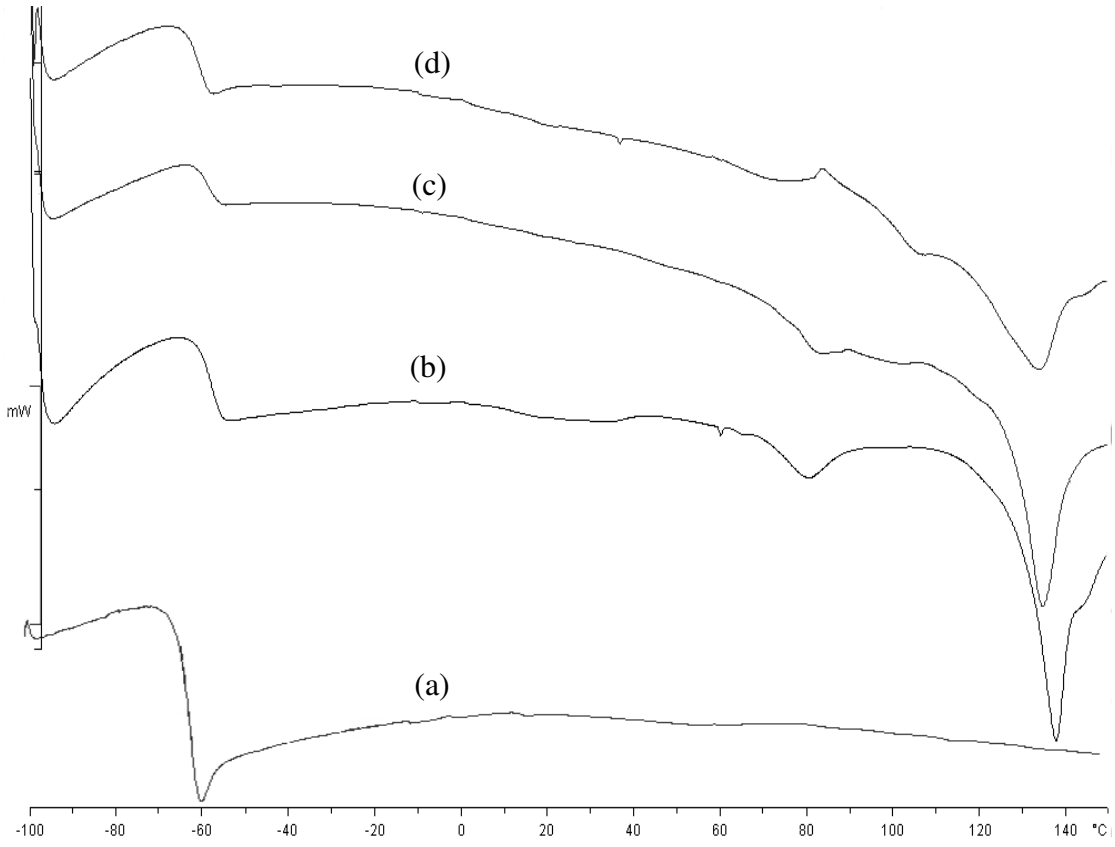

Figure 5.8 DSC thermograms of (a) nanosized PIP, (b) 60ST-g-PIP_25, (c) 100ST-g-PIP_25 and (d) 150ST-g-PIP_25.

CHAPTER VI

DIIMIDE HYDROGENATION OF NANOSIZED POLYISOPRENE LATEX IN THE PRESENCE OF CUPIC ION

6.1 Introduction

Hydrogenation of unsaturated polymers is a type of chemical modification of unsaturated polymers that has been an attractive process. Hydrogenation of diene rubbers helps to improve the thermal and oxidative stability of these rubbers when the radical-susceptible C=C are replaced by saturated hydrocarbon bonds. As a potential alternative to conventional hydrogenation technology, the diimide hydrogenation is a method, in which gaseous hydrogen, organic solvents and precious transition-metal catalysts are not necessary. From the reviews in Chapter 1, the diimide hydrogenation process which is the reaction between hydrogen peroxide and hydrazine can be employed to hydrogenate rubber in latex form. Different catalysts, different procedures of reactant addition and different additives are used to achieve the efficient hydrogenation. Cupric ion has been found to be an effective catalyst [106].

For diimide hydrogenation of natural rubber latex (NRL) using copper sulfate as catalyst, it was found that 67.8% hydrogenation was achieved within 6 h at 55 °C and a low rubber concentration and a high hydrazine concentration provided the optimum condition [73]. Moreover, the diimide hydrogenation of NR latex provided a method to improve the thermal stability of natural rubber. However, the hydrogenation level of natural rubber was low due to the large NR latex particle size (1–2 μm). However, when skim natural rubber latex (SNR) of small particles (0.2-1 μm) with 3–10% dry rubber content produced as a by-product from the production of concentrated NRL, was hydrogenated by diimide reduction the hydrogenation efficiency was expected to be increased [107]. The optimum hydrogenation condition was achieved at a hydrazine: hydrogen peroxide ratio of 1.6:1 and a low copper

sulfate concentration of 49.5 μM. Moreover, the increase in the decomposition temperature of hydrogenated SNR indicated that the diimide hydrogenation increased the thermal stability of SNR. However, the hydrogenation level of NRL and SNR were lower than that of synthetic rubber due to the large particle size compared with synthetic latex. To increase hydrogenation efficiency, thus, it is necessary to reduce particle size of the rubber latex.

In this study, the diimide hydrogenation of nanosized polyisoprene (nanosized PIP) latex was accomplished by using hydrazine hydrate/hydrogen peroxide and Cu^{2+} as catalyst. The effect of process parameters on the degree of hydrogenation and the properties of hydrogenated nanosized PIP were investigated. Nanosized PIP latex was prepared by differential microemulsion polymerization using 2,2'-Azoisobutyronitrile as an initiator. The optimum conditions of PIP synthesis gave the highest monomer conversion of 90% and an average particle size of PIP of 27 nm. The structure of the hydrogenatedpolymer product is similar to an alternating ethylene–propylene copolymer (EPDM). Thus, the nanosized hydrogenated PIP latex is also expected to be a replacement for the use of EPDM in rubber blend compounds.

6.2 Characterization of Hydrogenated Nanosized Polyisoprene

Figure 6.1(a) and 6.1(b) illustrate the ^{1}H-NMR spectra of nanosized PIP and 65.7% hydrogenated PIP, respectively. From the ^{1}H-NMR spectrum of nanosized PIP, the sharp chemical shift from the methyl protons of *cis*-1,4 (d) and *trans*-1,4 units (j) were observed at 1.58 and 1.68 ppm, respectively.

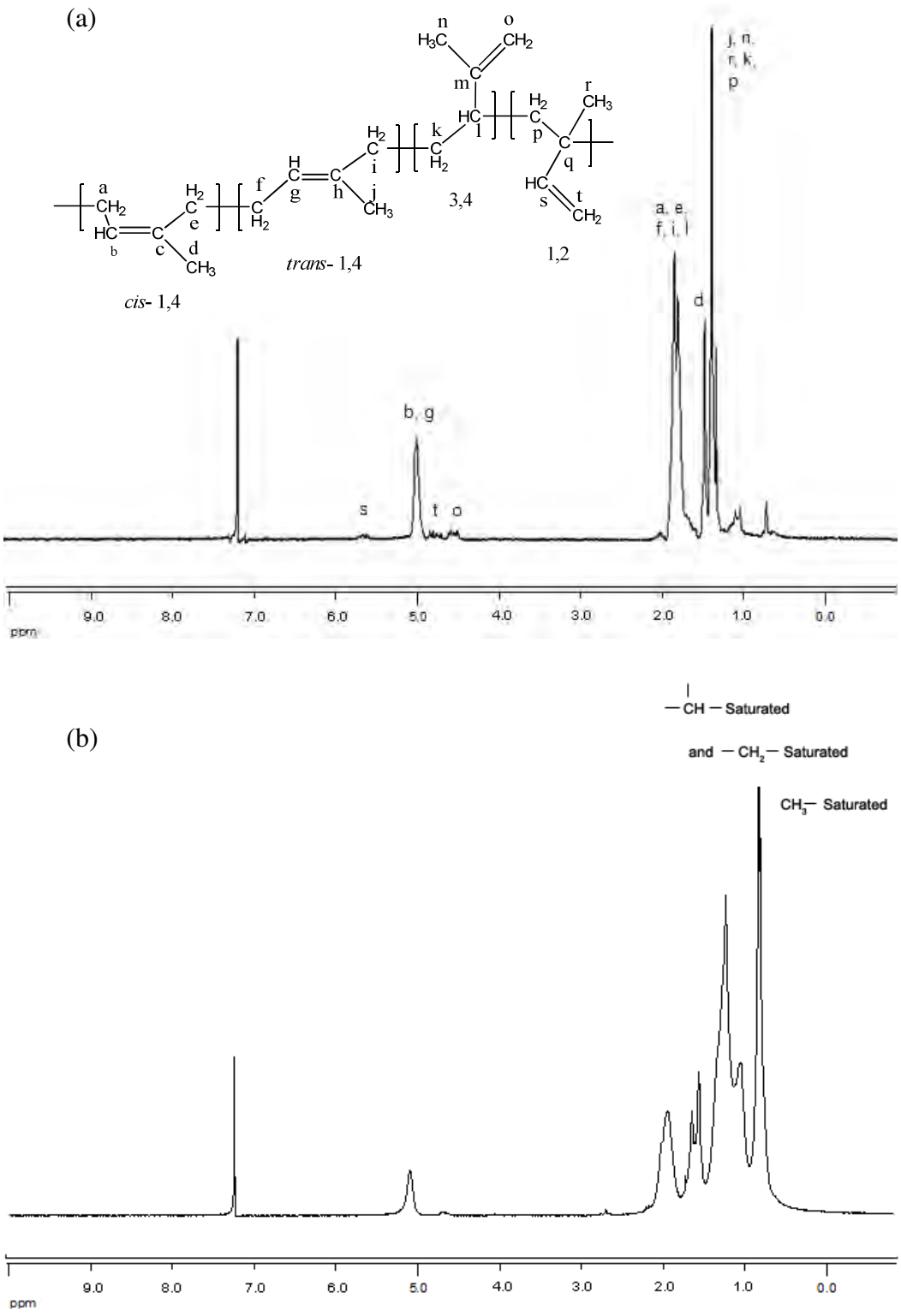

Figure 6.1 ^{1}H-NMR spectra: (a) nanosized polyisoprene and (b) hydrogenated nanosized PIP.

The major peaks were obtained in the aliphatic (1.68 and 2.2 ppm) regions. The olefinic protons signal of *cis*- and *trans*-1,4 was observed at 5.13 ppm. The signals at 4.60-4.78 ppm were attributed to olefinic protons of 3,4-addition. The peaks at 4.80-4.95 and 5.70-5.80 ppm indicated the olefinic protons of 1,2-addition. These peaks confirm the formation of 1,4-polyisoprene, 3,4-polyisoprene and 1,2-polyisoprene. After hydrogenation, the olefinic peak area decreased considerably and new peaks appeared at 0.8–1.2 ppm which were attributed to $–CH_3$ and saturated $–CH_2–$ units as shown in Figure 6.1(b). Integration of the spectra was used to determine the amount of characteristic protons of each structure in the polymer. The integration peak area for the saturated protons ($–CH_2–$ and $–CH_3$) in the range of 0.8–2.2 ppm and the unsaturated protons peak area at 5.13 ppm were measured in order to calculate the degree of hydrogenation.

6.3 Conversion Profile of Diimide Hydrogenation of Nanosized Polyisoprene

For hydrogenation of nanosized PIP, the conversion profile was studied at 80 °C in the presence of 3.53 M [H_2O_2], 2.20 M [N_2H_4], 0.98 M [C=C] and 49.4 μM [$CuSO_4$]. The reaction was performed over an interval of time from 0 to 9 h. From Figure 6.2(a), the degree of hydrogenation increased with an increase in reaction time. For hydrogenation of 30 nm PIP, maximum conversion of 59%, was achieved at 8 h. The degree of hydrogenation was increased with time and then leveled off. The reason for the increase in the hydrogenation degree was possibly the result due to the fact that the diimide was formed as an active species at the surface and then diffused into the outer layer of the latex particles. For longer reaction time above 8 h, the conversion remained quite stable due to a mass-transfer limitation of diimide diffusing into the C=C deep inside the rubber particle. In addition, the decomposition of diimide species may have occurred during the long reaction time. The conversion plots exhibited an apparent first-order dependence for hydrogenation on C=C concentration during first 9 h. Rate constant (k') has been calculated from the slope of the linear plot of $\ln(1 - x)$ versus time (Figure 6.2(b)).

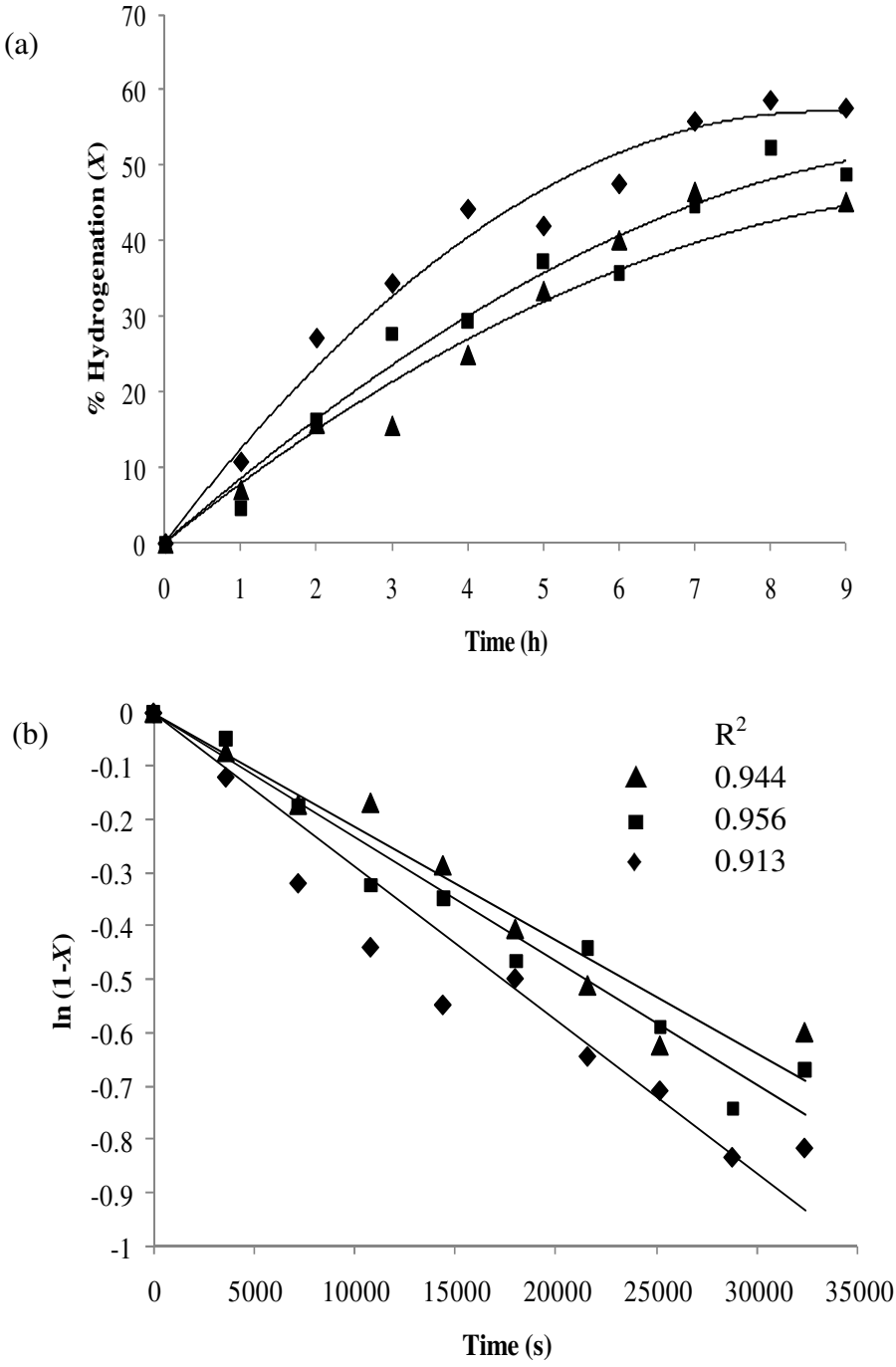

Figure 6.2 Hydrogenation profile of nanosized PIP: (a) conversion profile and (b) plot of ln(1-x) as a function of time. (♦) PIP_30, (■) PIP_40, (▲) PIP_50, $[H_2O_2]$ = 3.53 M, $[N_2H_4]$ = 2.20 M, [C=C] = 0.98 M, $[CuSO_4]$ = 49.4 μM, total volume = 150 mL, temperature = 80 °C.

From Figure 6.2 (b), the first-order rate equation expressed in terms of the conversion of unsaturated double bonds (the extent of hydrogenation, *x*), is shown as following equations (6.1 and 6.2) where *k'* is a pseudo first order rate constant.

$$-\frac{d[C=C]}{dt} = k'[C=C] \tag{6.1}$$

$$-\ln(1-x) = -k't \tag{6.2}$$

The rate constant (*k'*) of diimide hydrogenation of nanosized PIP at various particle sizes are presented in Table 6.1. From these results, the hydrogenation of nanosized PIP with small particle size gave higher rate constant (*k'*) than that of large particle size. The maximum rate constant (*k'*) was 2.88×10^{-5} $s^{-1}$for diimide hydrogenation of nanosized PIP_30.

Table 6.1 Rate constant for diimide hydrogenation of nanosized PIP.

Hydrogenation	Size (nm)		$k'\times10^5$ (s^{-1})	% Hydrogenation at 9 h.
	PIP	HPIP		
Nanosized PIP_30	28.4	32.7	2.88	55.5
Nanosized PIP_40	37.0	37.5	2.32	48.8
Nanosized PIP_50	48.7	58.6	2.13	45.1

Condition: $[H_2O_2]$ = 3.53 M, $[N_2H_4]$ = 2.20 M, [C=C] = 0.98 M, $[CuSO_4]$ = 49.4 μM, total volume = 150 mL, temperature = 80 °C.

6.4 Effect of Process Parameters

The diimide hydrogenation for nanosized PIP latex was accomplished by using hydrazine hydrate/hydrogen peroxide and Cu^{2+} as catalyst. The overall hydrogenation reaction of the unsaturated polymer latex with diimide can be expressed as follows:

$$N_2H_4 + H_2O_2 + \sim CH{=}CH\sim \rightarrow N_2 + \sim CH_2\text{-}CH_2\sim + 2H_2O \quad (6.3)$$

The diimide hydrogenation was achieved by two steps: (1) the reaction between hydrazine and hydrogen peroxide to produce the diimide and (2) the reaction between diimide and carbon–carbon double bonds to form the hydrogenated polymer, as given by the following equations:

$$N_2H_4 + H_2O_2 \rightarrow N_2H_2 + 2H_2O \quad (6.4)$$

$$N_2H_2 + \sim CH{=}CH\sim \rightarrow N_2 + \sim CH_2\text{-}CH_2\sim \quad (6.5)$$

However, according to the reactivity of diimide, two side reactions probably accompany the hydrogenation reaction. One is the further reaction of diimide with hydrogen peroxide to produce nitrogen and water, which most likely occurs at the interphase as the hydrogen peroxide resides in the water phase. Another reaction is the interaction between two diimide molecules to form one hydrazine molecule and release one nitrogen molecule, which most likely happens in the rubber phase [108].

$$N_2H_2 + H_2O_2 \rightarrow N_2 + 2H_2O \quad (6.6)$$

$$2N_2H_2 \rightarrow N_2H_4 + N_2 \quad (6.7)$$

The mechanism for hydrogenation of polyisoprene latex is shown in Figure 6.3.

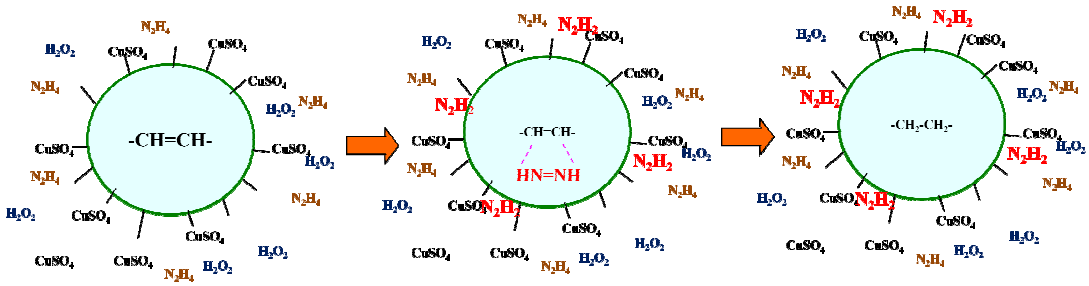

Figure 6.3 Mechanism for hydrogenation of polymer latex.

Based on the results of the kinetics of the hydrogenation, the effect of process parameters, the amount of nanosized PIP, hydrazine concentration, hydrogen peroxide concentration and PIP nanoparticle size, on hydrogenation were investigated and the mechanism was postulated. All the results will be subsequently discussed.

6.4.1 Effect of Polyisoprene Nanoparticle Size

The effect of PIP nanoparticle size (30-50 nm) on diimide hydrogenation was investigated. The hydrogenation reaction was carried out by using $[H_2O_2]$ = 3.53 M, $[N_2H_4]$ = 2.20 M, [C=C] = 0.98 M and $[CuSO_4]$ = 49.4 μM at temperature of 80 °C and 10 h reaction time. From Figure 6.4, the average particle size of the hydrogenated nanosized PIP remained quite constant and did not change with time. This can be explained by a shrinking core model, in which the PIP diameter remained constant but the core of C=C bond decreased with time (see Figure 6.4). While the degree of hydrogenation increased with time (Figure 6.2(a)). The smaller PIP nanoparticles had a higher hydrogenation degree than those of larger particle size. The nanopolymer with small particle size and high surface area could be hydrogenated completely. Thus, the high degree of hydrogenation could be achieved for very small particles. This behavior confirmed that the reaction rate of a small particle system was higher than that of a larger particle system. For the physical appearance of nanosized hydrogenated PIP at various particle sizes, the hydrogenated PIP latex was transparent as shown in Figure 6.5. The transparency decreased with increasing particle size of PIP.

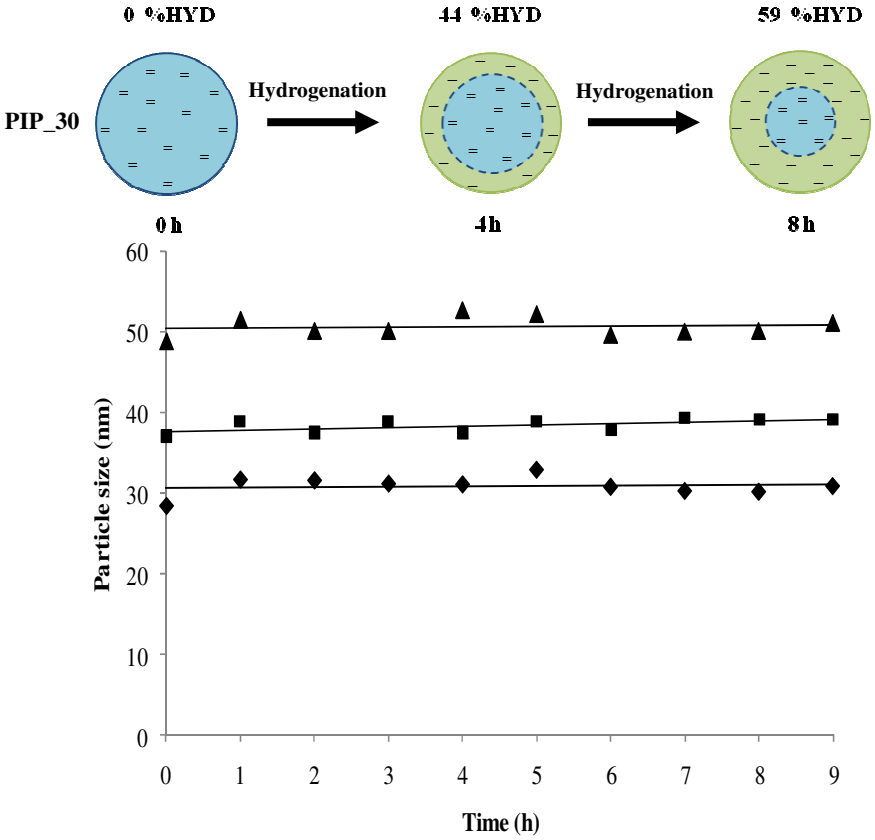

Figure 6.4 Effect of PIP nanoparticle size on nanosized PIP hydrogenation (♦) 30 nm PIP, (■) 40 nm PIP, (▲) 50 nm PIP, [H_2O_2] = 3.53 M, [N_2H_4] = 2.20 M, [C=C] = 0.98 M, [$CuSO_4$] = 49.4 μM, total volume = 150 mL, temperature = 80 °C, time = 10 h.

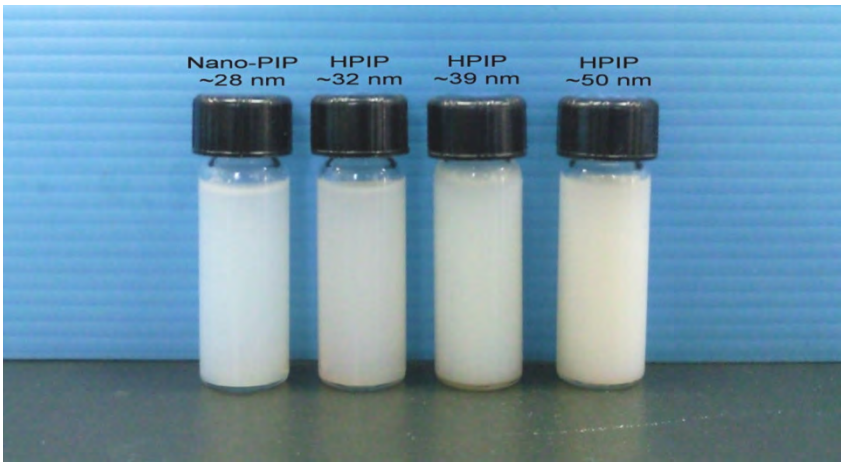

Figure 6.5 Appearance of nanosized PIP latex and hydrogenated PIP latex at different particle size.

6.4.2 Effect of Hydrazine Concentration

The effect of hydrazine concentration on diimide hydrogenation of nanosized PIP was investigated over the range of 0.60-3.57 M. The hydrogenation reaction was carried out at 60 °C, [H_2O_2] = 3.53 M, [$CuSO_4$] = 49.4 μM and [C=C] = 0.55 M. From Figure 6.6, the degree of hydrogenation increased with increasing [N_2H_4]. From the equations (6.3)-(6.7), it could be expected that the amount of diimide and the active species for the hydrogenation process was increased when the [N_2H_4] was in excess. High amount of diimide was expected to enhance the rate of C=C reduction resulting in an increase in the hydrogenation degree. However, the degree of hydrogenation began to slowly decrease when [N_2H_4] was higher than 2.68 M. This phenomenon could be explained by equations (6.6) and (6.7) in that the diimide species could self-react at high diimide concentration to cause a decrease in hydrogenation efficiency. Another possible explanation for the lower hydrogenation efficiency was that the excess diimide in this system might diffuse into the aqueous phase [109]. This behavior was also observed for diimide hydrogenation of NR, SNR and NBR latex using Cu^{2+} as catalyst [73, 107, 109].

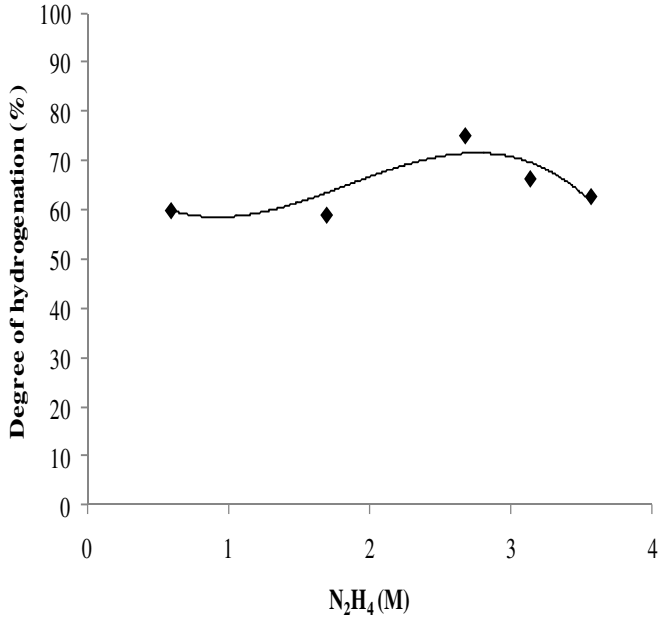

Figure 6.6 Effect of hydrazine concentration on nanosized PIP hydrogenation. [H_2O_2] = 3.53 M, [C=C] = 0.55 M, [$CuSO_4$] = 49.4 μM, total volume 150 mL, temperature = 60 °C, time = 6 h.

6.4.3 Effect of Hydrogen Peroxide Concentration

For the effect of hydrogen peroxide, the hydrogenation reaction was carried out by varying hydrogen peroxide concentration over the range of 1.23-5.08 M at 60 °C, $[N_2H_4]$ = 2.20 M, $[CuSO_4]$ = 49.4 μM and [C=C] = 0.55 M. The results presented in Figure 6.7 indicated that the hydrogenation conversion increased with increasing $[H_2O_2]$. The maximum degree of hydrogenation was around 75% at 5.08 M $[H_2O_2]$. This occurrence can be explained by a surface-controlled process where the nanosized PIP seed has large reaction surface as active sites for diimide reduction. It was probable that the reaction between diimide and carbon-carbon double bonds (equation (6.5)) was higher than the competitive reaction between hydrazine and hydrogen peroxide (equation (6.6)). This observation was opposite to that of the diimide hydrogenation of NBR, SBR, NR and SNR latex [71, 73, 106, 107, 109] in which the degree of hydrogenation of the large rubber particle size was decreased with increasing hydrogen peroxide concentration. This can be explained in that the large rubber particle resulted in possible crosslinking, which reduced the number of free carbon-carbon double bonds available for diimide reduction [72]. Thus, the side reaction which in hydrazine was consumed (according to equation (6.6)) might occur easier than the reaction between diimide and the rubber double bonds resulting in a decrease in the degree of hydrogenation.

The optimum ratio of $[N_2H_4]$:$[H_2O_2]$ in this experiment was between 1:1.32 (2.68 M:3.53 M) and 1:2.31 (2.02 M:5.08 M). Although, the suitable ratio for generation of the diimide species should be 1:1 of $[N_2H_4]$:$[H_2O_2]$ which is based on the reaction stoichiometry according to equation (6.3). This suitable $[N_2H_4]$:$[H_2O_2]$ ratio for hydrogenation of nanosized PIP latex were higher than that of other rubbers investigated earlier. The optimum ratio of diimide species for the hydrogenation of NBR, SBR and XSBR (carboxylated styrene butadiene rubber) latex was 1:2 [71, 72, 106]. The optimum ratio of $[N_2H_4]$:$[H_2O_2]$ for NR hydrogenation was between 1:0.97 and 1:1.29 [73]. It could be implied that the diimide in nanosized PIP hydrogenation had more chance to diffuse into the rubber phase and higher hydrogenation efficiency was achieved even at high hydrogen peroxide concentration.

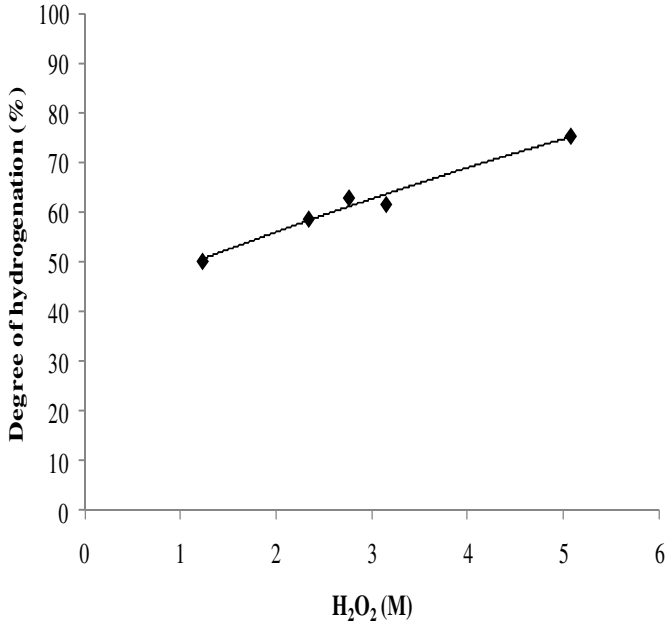

Figure 6.7 Effect of hydrogen peroxide concentration on nanosized PIP hydrogenation. [N_2H_4] = 2.20 M, [C=C] = 0.55 M, [$CuSO_4$] = 49.4 μM, total volume 150 mL, temperature = 60 °C, time = 6 h.

6.4.4 Effect of Rubber Concentration

For the effect of rubber concentration on hydrogenation as presented in terms of carbon-carbon double bonds concentration, the hydrogenation reaction was carried out by varying [C=C] over the range of 0.49-0.63 M at 60 °C, [H_2O_2] = 3.53 M, [N_2H_4] = 2.20 M, and [$CuSO_4$] = 49.4 μM. From Figure 6.8, the degree of hydrogenation slightly changes with increasing rubber concentration and then decreased at a rubber concentration above 0.58 M which affected the efficiency of diimide species in this system. At high rubber concentration, the diimide species might self-decompose prior to the hydrogenation process resulting in a lower degree of hydrogenation. Over an optimum rubber concentration range, the diimide hydrogenation reaction occurred in the rubber phase. Therefore, the optimum rubber concentration for nanosized PIP hydrogenation was in the range of [C=C] of 0.49 and 0.58 M.

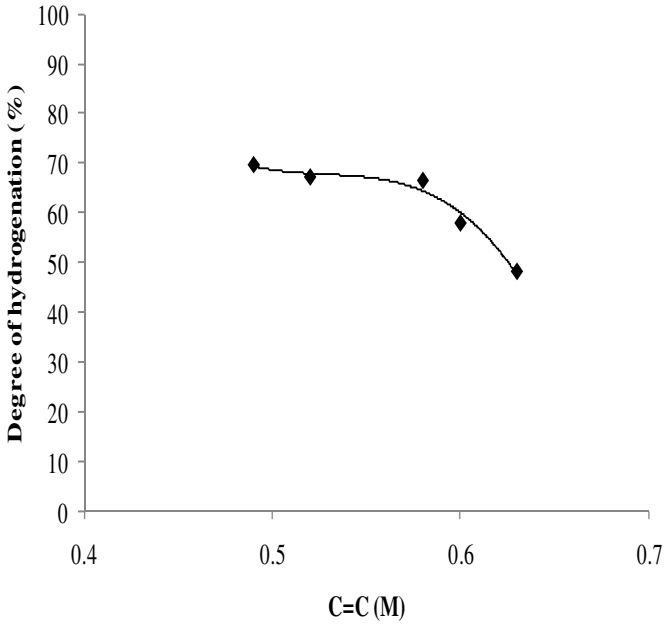

Figure 6.8 Effect of rubber concentration on nanosized PIP hydrogenation. [H_2O_2] = 3.53 M, [N_2H_4] = 2.20 M, [$CuSO_4$] = 49.4 μM, total volume 150 mL, temperature = 60 °C for 6 h.

6.5 Thermal Properties of Hydrogenated Nanosized Polyisoprene

Thermal analysis was used to investigate some physical properties of the hydrogenated nanosized PIP. Thermal gravimetric analysis (TGA) was used to determine the initial decomposition temperature (T_{id}) and the maximum decomposition temperature (T_{max}). TGA of nanosized PIP (D_n = 27.7 nm, M_w = 2.37×10^6) and nanosized hydrogenated PIP samples at various % hydrogenation were conducted under a nitrogen atmosphere. T_{id} was determined from the intersection of two tangents at the onset of the decomposition temperature. T_{max} was obtained from the peak maximum of the derivative of the TG curves. Table 6.2 summarizes the degradation temperature and maximum temperature (T_{id} and T_{max}) of all rubber samples. The results show that the degradation temperatures of hydrogenated nanosized PIP samples increased with an increase in the reduction of carbon-carbon double bonds in nanosized PIP. Therefore, hydrogenation could improve the thermal

stability of nanosized PIP by converting the weak π bond within nanosized PIP to the stronger C-H σ bond. From Table 6.2, it is seen that the PIP nanoparticle size had no significant affect on T_{id} and T_{max} of the hydrogenated nanosized PIP sample.

Differential scanning calorimetry (DSC) was used to determine the glass transition temperature (T_g) which is one of the most important parameters for characterization of the polymer structure. T_g is the transition related to the motion in the amorphous section of the polymer. It is determined from the midpoint of the baseline shift of the DSC thermogram. The DSC thermogram of hydrogenated nanosized PIP sample indicated only one step base-line shift. These observations were different from those of diimide hydrogenated NR and SNR which had two step base-line shifts [73, 107]. This could imply that hydrogenated nanosized PIP had a single glass transition temperature (T_g) and this behavior had similar trend with the complete HNR produced from hydrogenation of NR in the presence of $OsHCl(CO)(O_2)(PCy_3)_2$. All DSC thermograms of 99% HNR samples indicated the one step base-line shift at -61.8 °C [62] and -59.6 °C [61]. From Table 6.2, T_g of nanosized hydrogenated PIP was increased with increasing degree of hydrogenation.

Table 6.2 Glass transition temperature and decomposition temperature of rubber samples

Rubber sample	Hydrogenation (%)	Size (nm)		T_g (°C)	T_{id} (°C)	T_{max} (°C)
		PIP	HPIP			
Nanosized PIP	-	27.7	-	-61.9	358.8	393.2
HPIP_20	48.1	27.2	30.2	-49.5	365.0	427.7
HPIP_30	58.8	28.4	32.7	-42.3	387.0	436.9
HPIP_40	49.4	37.0	37.5	-41.4	379.0	430.2
HPIP_50	49.1	48.7	58.6	-41.0	365.5	431.6

6.6 Morphology of Nanosized Hydrogenated Polyisoprene

The morphologies of nanosized PIP and hydrogenated PIP examined by TEM micrographs are shown in Figure 6.9. Since OsO_4 staining agent can only stain the carbon–carbon double bonds, the lightly colored domain indicates the region of lower carbon–carbon double bond concentration. Form Figure 6.9, the non-hydrogenated nanosized PIP showed relatively sharp particle edges because of the high OsO_4 concentration inside the particle. The 50% hydrogenated HPIP_50 (50 nm) showed the contrast between the core and the shell of hydrogenated rubber particle. The PIP nanoparticle seemed to be hydrogenated from the outer layer to the center of rubber particle according to the layer model. This behavior was also observed in hydrogenated SBR, NR and SNR latex [71, 73, 107] For 61% hydrogenated HPIP_30 (28 nm), much lighter color was observed due to the small amount of carbon–carbon double bonds and some PIP nanoparticles were completely hydrogenated all over. This evidence could be implied that the nanoseed polymer particles could be completely hydrogenated and the high degree of hydrogenation could be achieved at the optimum hydrogenation condition.

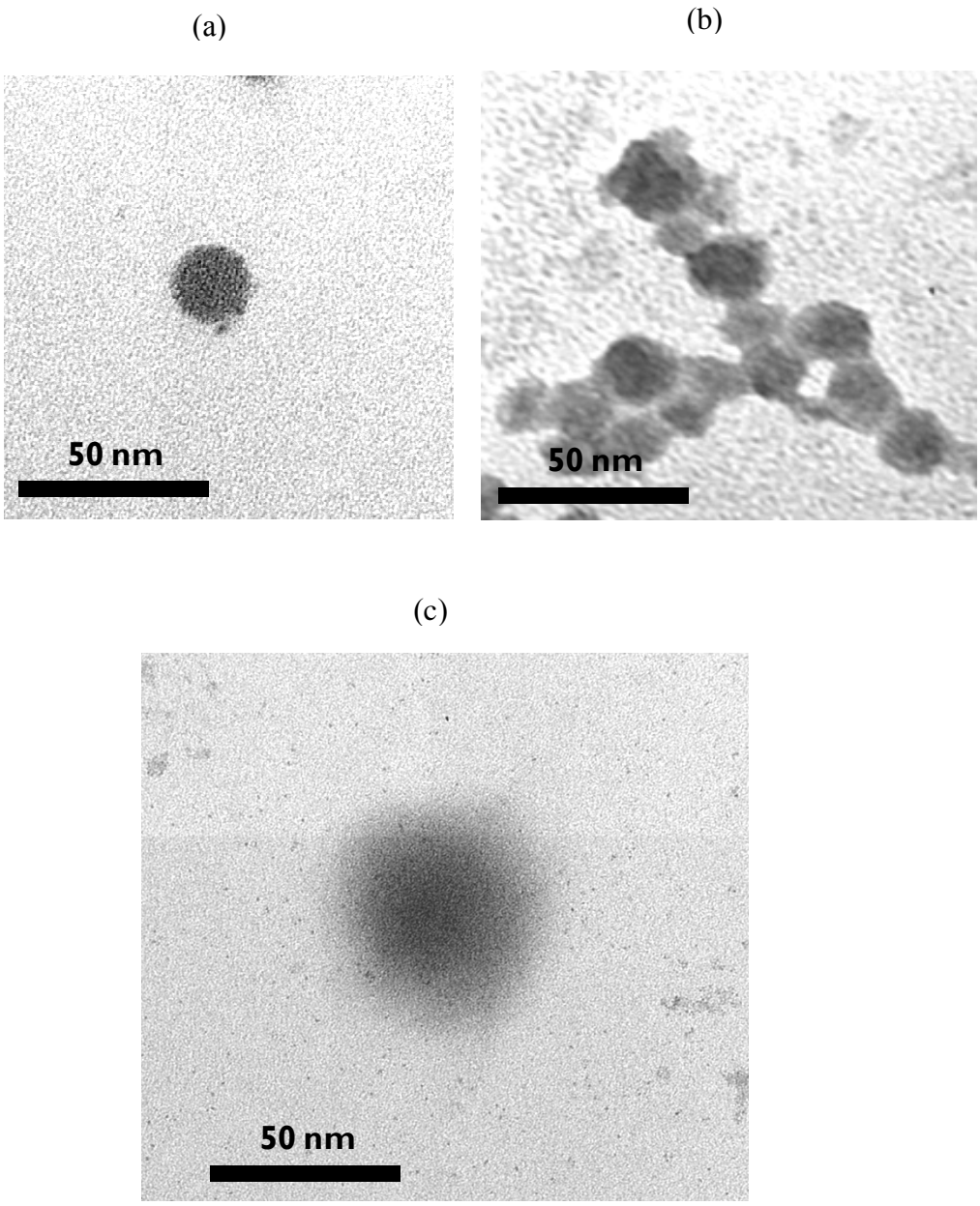

Figure 6.9 Transmission electron micrographs (×50,000) of (a) nanosized PIP latex, (b) 61% hydrogenated HPIP_30 and (c) 50% hydrogenated HPIP_50.

CHAPTER VII

MECHANICAL PROPERTIES OF NR/NANOSIZED PIP AND NR/MODIFIED NANOSIZED PIP BLENDS

7.1 Introduction

In Chapters 3-6, the synthesis of nanosized polyisoprene (PIP) and their chemical modifications were reported. It was found that the chemical modification of C=C unsaturated polymers via graft copolymerization and hydrogenation techniques could change the physical properties and thermal properties such as thermal stability which are the inherent properties of each elastomer. For graft copolymerization, the rigid chains of poly(methyl methacrylate) or polystyrene could be graft onto the flexible chains of the rubber and this characteristic molecular geometry could give graft rubber having high resistance to the outdoor environment but poor film-forming properties. Although the natural rubber latex (NRL) possesses excellent film-forming properties and has been widely used in the manufacture of dipping products such as gloves and condoms, the hardness of this film is low, and the tear strength of this film is comparatively poor [110].

Lu et al. studied blends of NRL and methyl methacrylate-graft rubber latex (MMA-g-NR) and their pre-vulcanization and the modulus, anti-aging properties, and tear strength of the blending films increased with increasing the content of MMA-g-NR [111]. Arayapranee and Rempel investigated the morphology and mechanical properties of natural rubber and styrene-graft natural rubber latex (ST-g-NR) compounds pre-vulcanization [110]. The tensile and tear strength were decreased, whereas Young's modulus and hardness were increased at high content of ST-g-NR. Addition of ST-g-NR improved the resistance of the compounds to heat and weather ageing.

There is no earlier work on the preparation of nanosized rubber and its blends as film. This is the first investigation which, reports on the preparation of the

pre-vulcanized blend of NRL and nanosized PIP, MMA-g-PIP or ST-g-PIP and these blends are expected to possess excellent film-forming properties. The mechanical properties and dynamic mechanical analysis (DMA) were evaluated. The heat ageing and morphology of NR/PIP and NR/ST-g-PIP films were also studied.

7.2 Physical properties of pre-vulcanized latex compound

The latex compounds of NRL and nanosized PIP, graft PIP or hydrogenated PIP were prepared prior to vulcanization. The physical appearance of NRL, nanosized PIP, MMA graft PIP and ST graft PIP emulsion before vulcanization is shown in Figures 7.1(a) – 7.1(d). The nanosized PIP latex was more transparent than NRL. While the MMA graft PIP and ST graft PIP latex were lightly yellow. However, the color of NR/ graft PIP (85/15) emulsion was white prior to vulcanization as shown in Figures 7.1(e) and 7.1(f).

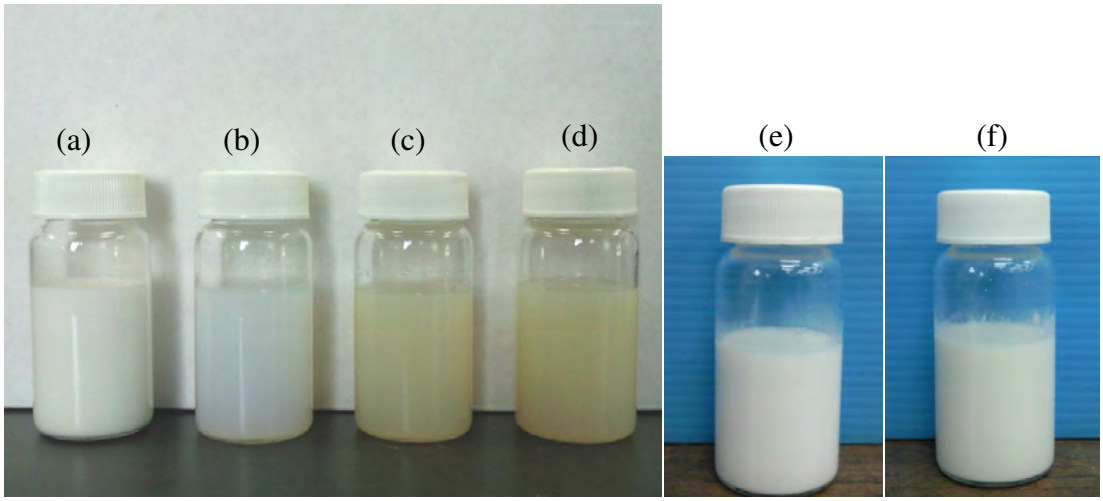

Figure 7.1 Appearance of rubber latex samples: (a) natural rubber latex, (b) emulsion of nanosized polyisoprene (20 nm), (c) 100MMA-g-PIP_25, (d) 100ST-g-PIP_25, (e) NR/100MMA-g-PIP_25 (85/15) and (f) NR/100ST-g-PIP_25 (85/15).

The NR has the excellent film forming properties while the nanosized PIP has lower film forming properties than NR. The film casted from NRL and nanosized PIP emulsion were tacky and soft. The ST graft PIP, MMA graft PIP and hydrogenated PIP were poor in film forming properties. For NR/ST graft PIP or NR/MMA graft PIP blend, a combination of elastic properties of NR and hardness of ST graft PIP or MMA graft PIP could be achieved. However, the film forming properties of the compound film of NR/ST graft PIP or NR/MMA graft PIP at high percentage graft PIP were stiffer and less tacky than NR film. The physical appearance of dipping pre-vulcanization film is shown in Figure 7.3. The appearance of dipping vulcanized latex compound films (Figure 7.2 (b)-(e)) were more transparent than dipping vulcanized NR film (Figure 7.2(a)). From Figure 7.2(b) and 7.2(c), the transparency increased with increasing nanosized PIP content in the latex compound.

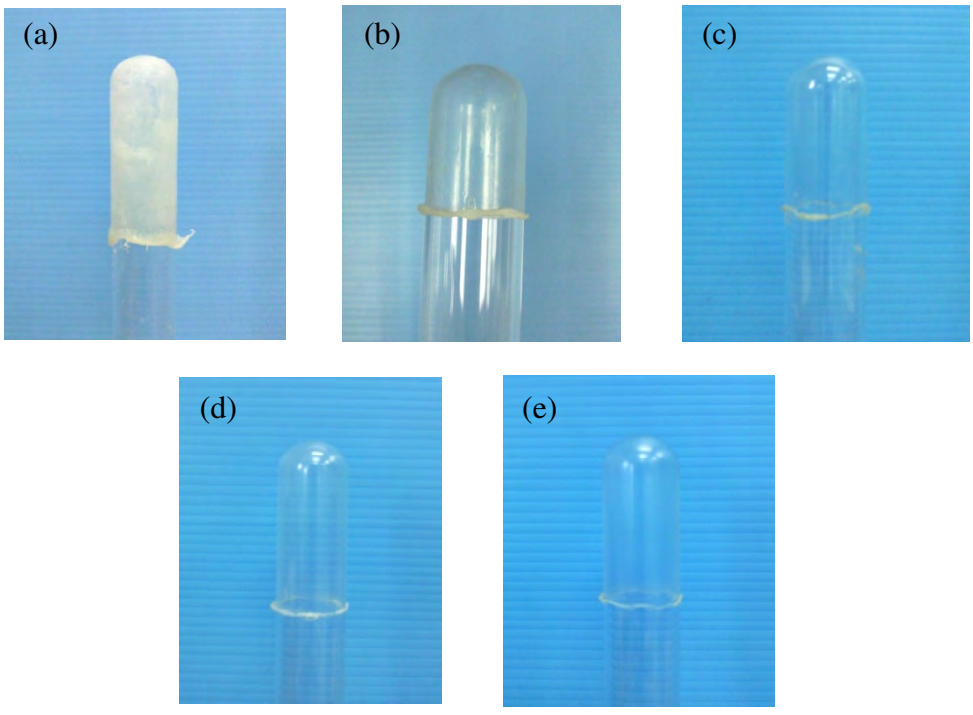

Figure 7.2 Appearance of dipping pre-vulcanized rubber film samples: (a) NR latex, (b) NR/PIP (85/15), (c) NR/PIP (70/30), (d) NR/100ST-g-PIP_25 and (e) NR/HPIP.

For the physical properties such as equilibrium swelling, crosslink density and chloroform number of pre-vulcanized latex and compound film, the physical properties are provided in Table 7.1.

7.2.1 Crosslink Density and Swelling Index

The degree of crosslinking density of latex compounds, NR/nanosized PIP, NR/graft PIP or NR/hydrogenated PIP are summarized in Table 7.1. The results show that the crosslink densities of NR and NR/PIP films were quite similar (~0.085-0.089). While the crosslink density of NR/graft PIP or NR/hydrogenated PIP were lower (decrease to 0.0422 or 0.0008 mmol/cm^3). This can be explained in that the carbon double bond at the outer layer of the PIP particle was reduced due to the chemical modification of nanosized PIP by graft copolymerization or hydrogenation and the nanoparticles of modified PIP latex was homogeneously dispersed in the system. The modification may cause the obstruction of the crosslink chain due to the C=C bond reduction. Thus, the low crosslink density was observed for NR/ST graft PIP, NR/MMA graft PIP or NR/hydrogenated PIP film.

Table 7.1 Physical properties of pre-vulcanized latex and compounds film.

Rubber	Crosslink density (mmol/cm^3)	Swelling Index (Q)	Chloroform number
NR	0.0888	4.25	2
NR/PIP (85/15)	0.0891	4.74	2.5
NR/PIP (70/30)	0.0830	4.96	2.5-3
NR/ST-g-PIP	0.0557	5.96	3-3.5
NR/MMA-g-PIP	0.0422	6.56	3-3.5
NR/HPIP	0.0008	13.67	2

Condition: 50% ZDEC dispersion = 1 phr, 50% sulfur dispersion = 1.5 phr, 50% ZnO = 2 phr, temperature = 60 °C and pre-vulcanization time = 2 h.

Equilibrium swelling or swelling index also indicates the extent of vulcanization in vulcanized rubber. Table 7.1 presents the swelling index of pre-vulcanized rubber. The results show that the swelling indexes of NR and NR/PIP films were quite the same (~0.5-0.7). While the swelling indexes of NR/graft PIP were higher (increase to ~1.7-2.3). For NR/hydrogenated PIP, the swelling index increased around 9.4. These results show the relation between swelling index and crosslink density. Swelling index increased with decreasing the crosslink density

7.2.2 Chloroform Number

Chloroform number was also used to indicate the extent of crosslinking in rubber blends. The chloroform number could be assigned from the appearance of pre-vulcanized coagulum. The results are presented in Table 7.1. For short vulcanization at 60 °C and 2 h, the chloroform number of NR/PIP and NR/graft PIP reached a level of 3.5 indicating the moderately vulcanized compound latex. While the chloroform number of NR pre-vulcanized was only at a level of 2 in which the NR latex was lightly vulcanized. This is one advantage of nanosized latex compounding resulting in an increase in colloidal stability of pre-vulcanized latex (see Figure 7.3). Nanosized PIP and graft PIP particles were supposed to have high dispersion and compatibility with pre-vulcanized NR latex. Thus, the improved dispersion of curing agent also causes an increase in the active surface. Moreover, the colloidal stability of prevulcanized NR latex depended on two opposing factors which were the amount of vulcanizing agent and the impurities in NR latex, proteins and phospholipids [77]. The presence of residual vulcanizing ingredients such as zinc oxide could reduce the stability of the latex because of zinc oxide thickening. At the same time, the addition of synthesized nanosized PIP or graft PIP containing surfactant could increase the stability by increasing the negative charge on the surface of the particles and by increasing surface adsorption. Thus, the colloidal stability of pre-vulcanized latex increased when nanosized PIP or nanosized ST or MMA graft PIP was blended with NR latex. Figure 7.4 shows the appearance of pre-vulcanized coagulum rubber samples. Coagulum of vulcanized NR contained small tender lumps as shown in Figure 7.4(a). For coagulum of compound NR/PIP or NR/graft PIP, the coagula were non-tacky crumbs as shown in Figure 7.4(b) and 7.4(c). While coagulum of

vulcanized NR/hydrogenated PIP (Figure 7.4(d)) showed the tender lumps similar to vulcanized NR.

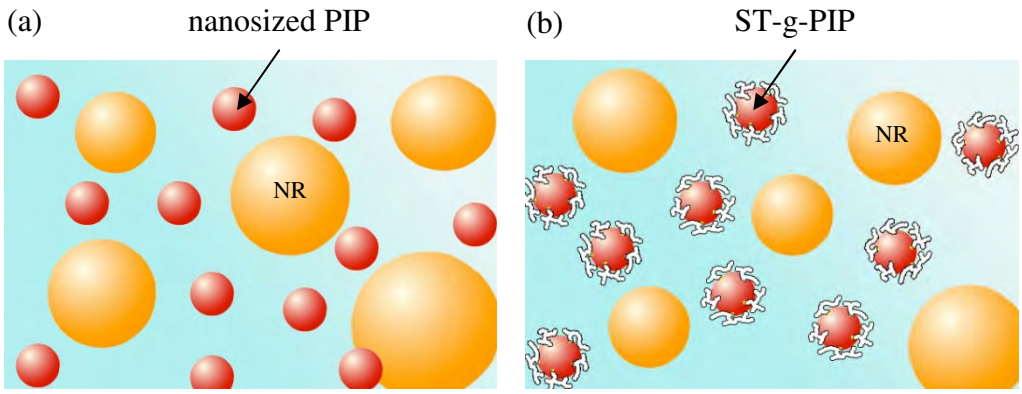

Figure 7.3 Appearance of pre-vulcanized latex compounds: (a) NR/PIP blend and (b) NR/ST-g-PIP (85:15) blend.

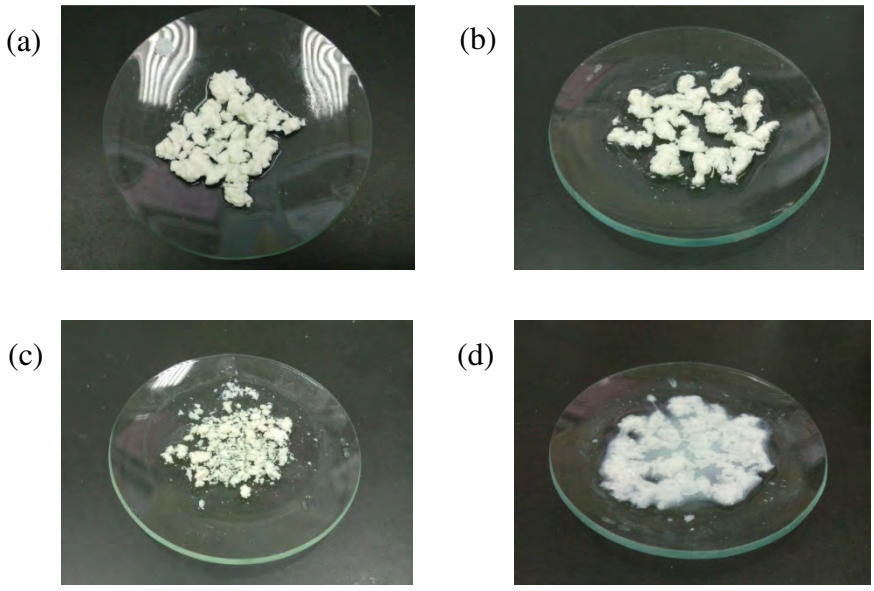

Figure 7.4 Appearance of pre-vulcanized coagulum rubber samples: (a) NR, (b) NR/PIP (85/15), (c) NR/ST-g-PIP (85/15) and (d) NR/HPIP (85/15).

7.3 Mechanical properties of vulcanized rubber

Mechanical properties of pre-vulcanized rubber films, NR, NR/PIP and NR/ST graft PIP were measured in term of tensile strength, Young's modulus at 100% elongation, elongation at break and hardness according to ASTM methods. The results of mechanical properties are summarized in Table 7.2 and Figure 7.5.

Comparison between un-aged vulcanized films, NR, NR/PIP at 85/15 and 70/30 revealed that the mechanical properties of pre-vulcanized films decreased with increasing nanosized PIP content. The NR rich compounds possessed the highest tensile strength and elongation at break due to the NR crystallization exhibited upon stretching. While the nanosized PIP with short rubber chains has lower crystallinity, tensile strength and elongation at break than NR. Thus, the mechanical properties of NR/PIP compounds were lower than that of NR film. However, the presence of increasing the amount of nanosized PIP in the film did not cause a significant change in the Young's modulus at 100% elongation. On the other hand, the mechanical properties of blend NR/PIP films were retained after heat aging. The percentage retention in tensile strength, elongation at break and hardness, increased with increasing amount of nanosized PIP. This indicated that NR/PIP film was more resistant to heat.

For comparison of un-aged vulcanized NR film and NR/ST-g-PIP film (85/15), the tensile strength, elongation at break and hardness of NR/ST-g-PIP film were lower than that of NR film. This can be explained in that the addition of ST-g-PIP (rigid chains) reduced the elasticity of the NR resulting in lower tensile strength and elongation at break of the compound. Similar results was also observed for NR/ST graft NR blend [110]. However, the hardness of NR /ST graft PIP compound was lower than that of NR film. It can be noted that the addition of ST graft PIP makes the final product soft due to a colloidal phenomena (Figure 7.3). For Young's modulus as the indication of the relative stiffness of material, the ST graft PIP content in NR did not cause a significant change in the Young's modulus at 100% elongation of film similar to NR/PIP compounds.

Table 7.2 Mechanical properties of pre-vulcanized compounds before and after aging.

Rubber	Tensile Strength		Modulus at 100% elongation		Elongation at Break (%)		Hardness	
	Before aging (MPa)	Retention (%)	Before aging (MPa)	Retention (%)	Before aging (%)	Retention (%)	Before aging (Shore A)	Retention (%)
NR	28.1	43.8	0.7	85.7	900	93.3	38	92.1
NR/PIP (85/15)	17.7	75.7	0.7	71.4	860	104.7	31	93.6
NR/PIP (70/30)	8.7	106.9	0.6	83.3	820	104.9	25	104.0
NR/STgPIP (85/15)	9.9	92.9	0.8	100.0	800	110.0	33	124.2

* Heat aging was done at 100 °C for 22 h.

** % Retention $= \frac{\text{Properties after aging}}{\text{Properties before aging}} \times 100$

For NR/ST-g-PIP compound after aging showed a little lower tensile strength but higher elongation at break and hardness than the compound before aging. Then, regardless of their composition and nature, the compounds exhibited a reduction in tensile strength, indicating a deterioration of their properties with accelerated aging [112]. The accelerated aging of rubbers that contain unsaturated bonds normally reduces their strength properties. However, the retention in tensile strength of the compound increased and was higher than that of the NR vulcanized film. In addition, the hardness of aged NR/ST-g-PIP vulcanized film was higher than that of the film before aging. These results might be related to a decrease in the unsaturated bonds in the compound by grafting ST onto PIP, resulting in an improvement of the resistance of the compounds to heat aging. This indicates that the presence of ST graft PIP in the compound provided the good heat resistant properties.

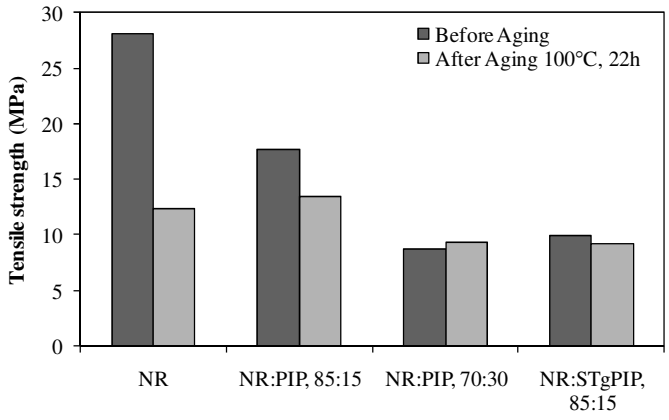

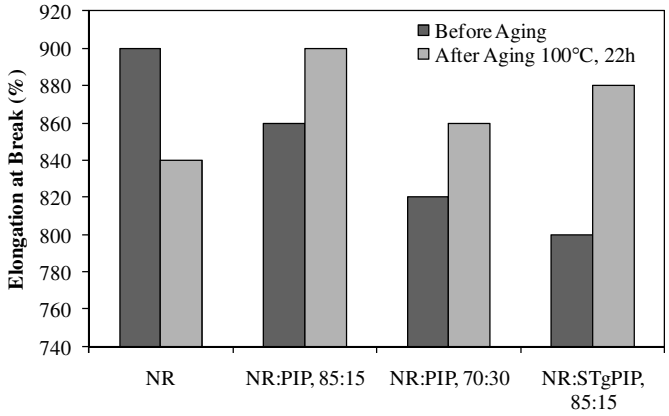

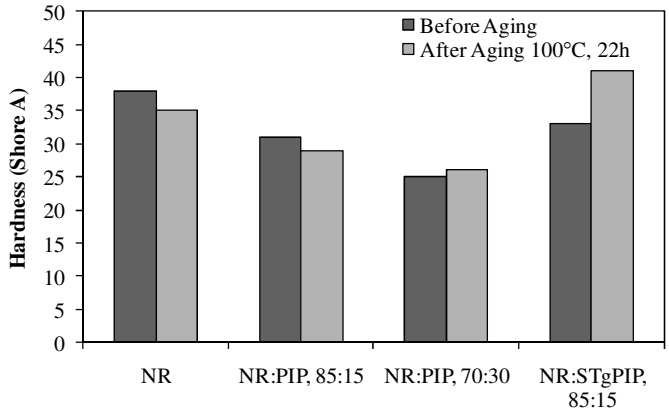

Figure 7.6 Mechanical properties before and after aging at 100 °C for 22 h of pre-vulcanized rubber compound films.

7.4 Dynamic mechanical properties of vulcanized rubber

The elastic modulus of a material and its mechanical damping or energy dissipation characteristics as a function of frequency and temperature can be measured by dynamic mechanical analysis. The storage modulus or elastic modulus (E'), dynamic loss or viscous modulus (E") and tan δ of pre-vulcanized rubber samples are shown in Figure 7.6. The quantity E' is measurement of the energy stored elastically and it also indicates the stiffness of the material, whereas E" is a measurement of energy dissipation as heat [82]. These indicate the impact strength or ability of the system to absorb energy. For another measurement, tan δ is called the loss tangent and determined from E"/E'.

From Figure 7.6(a), the storage modulus of all samples decreased with increasing temperature. Moreover, the storage modulus was sharply decreased around the transition region which was a state after the onset of a sharp reduction in storage modulus because the mobility of polymer chains increased with increasing temperature [113, 114]. Thus, this pointed out that the samples have some elastic properties near their glass transition temperature (T_g). Before the transition region, the E' of the pre-vulcanized nanosized rubber compound was lower than that of the pre-vulcanized NR. However, the E' of pre-vulcanized NR/MMA-g-PIP, NR/ST-g-PIP and NR/PIP (70/30) in the transition region were higher than that of pre-vulcanized NR. The higher storage modulus of pre-vulcanized hybrid nanoparticles in NR could be explained in that the free volume and the mobility of NR molecules were decreased by the addition of nanosized polymer.

The tan δ of pre-vulcanized rubber films is shown in Figure 7.6(b), where the T_g value of pre-vulcanized films can be determined from the peak temperature of tan δ curves. The T_g of NR/PIP, NR/ST-g-PIP and NR/MMA-g-PIP films were slightly higher than that of NR film. Moreover, the vulcanized NR/PIP, NR/MMA-g-PIP and NR/ST-g-PIP showed a lower internal fraction loss factor (tan δ) than vulcanized NR, and this indicated that the high NR-nanosized compound interactions existed in these blendings. This caused the low ΔE' (E'-E") values which meant low loss modulus of the NR compounds. This also indicated that the nanosized

PIP, MMA-g-PIP or ST-g-PIP was homogenously dispersed in the NR matrix. Similar results were also observed for nanosized silica filled in styrene–butadiene rubber (SBR) matrix [115].

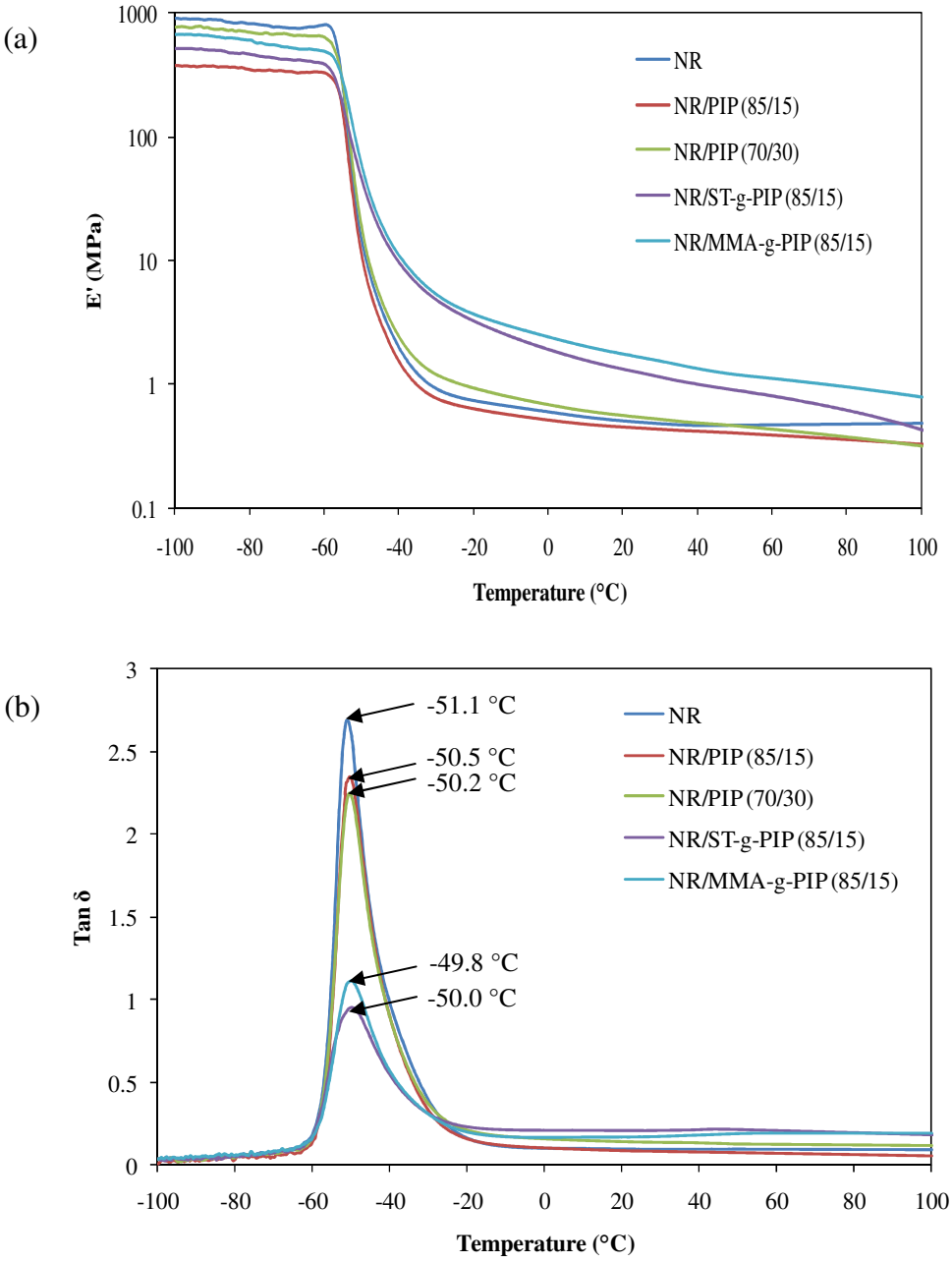

Figure 7.6 Temperature dependence of (a) the storage modulus (E') and (b) the loss tangent (tan δ) for pre-vulcanized rubber compound film compared with natural rubber pre-vulcanized film.

7.5 Morphology

The morphology of pre-vulcanized NR latex compound with nanosized PIP or ST graft PIP films after tensile fracture is shown in Figure 7.7. Figure 7.7(a) shows the vulcanized NR morphology. Then, the roughness of the tensile fracture surface of NR is a typical feature of ductile failure indicating the high tensile strength of vulcanized NR film. For incorporation of nanosized PIP into the NR compounds, Figure 7.7(c) and 7.7(e) show that higher content of nanosized PIP in NR compounds caused a scaly surface due to the short polyisoprene chains in NR compounds resulting in the low tensile strength. While the addition of nanosized ST-g-PIP in NR compounds is shown in Figure 7.7(g), the surface morphology was brittle and scaly surface presenting the microcharacteristics of a rigid and glassy type structure as evidenced by the absence of fibrils on fracture surface. Therefore, the tensile strength of vulcanized NR compounds was lower than that of vulcanized NR film (presented in section 7.3).

Figure 7.7(b), 7.7(d), 7.7(f) and 7.7(h) show the morphology of aged vulcanized NR compounds film after tensile fracture. The fracture surfaces after aging were smooth compared with those before aging which show the evidences of matrix tearing indicated by their rough appearance. This implies that brittle failure has occurred in the aged samples. From Figure 7.7(b) shows the extreme change in the tensile fracture surface of vulcanized NR. While Figure 7.7(d), 7.7(f) and 7.7(h) show a little change in the tensile fracture surface of vulcanized NR/PIP or NR/ST-g-PIP. Thus it could be implied that the vulcanized NR film had lower heat resistance than the NR/PIP and NR/ST-g-PIP.

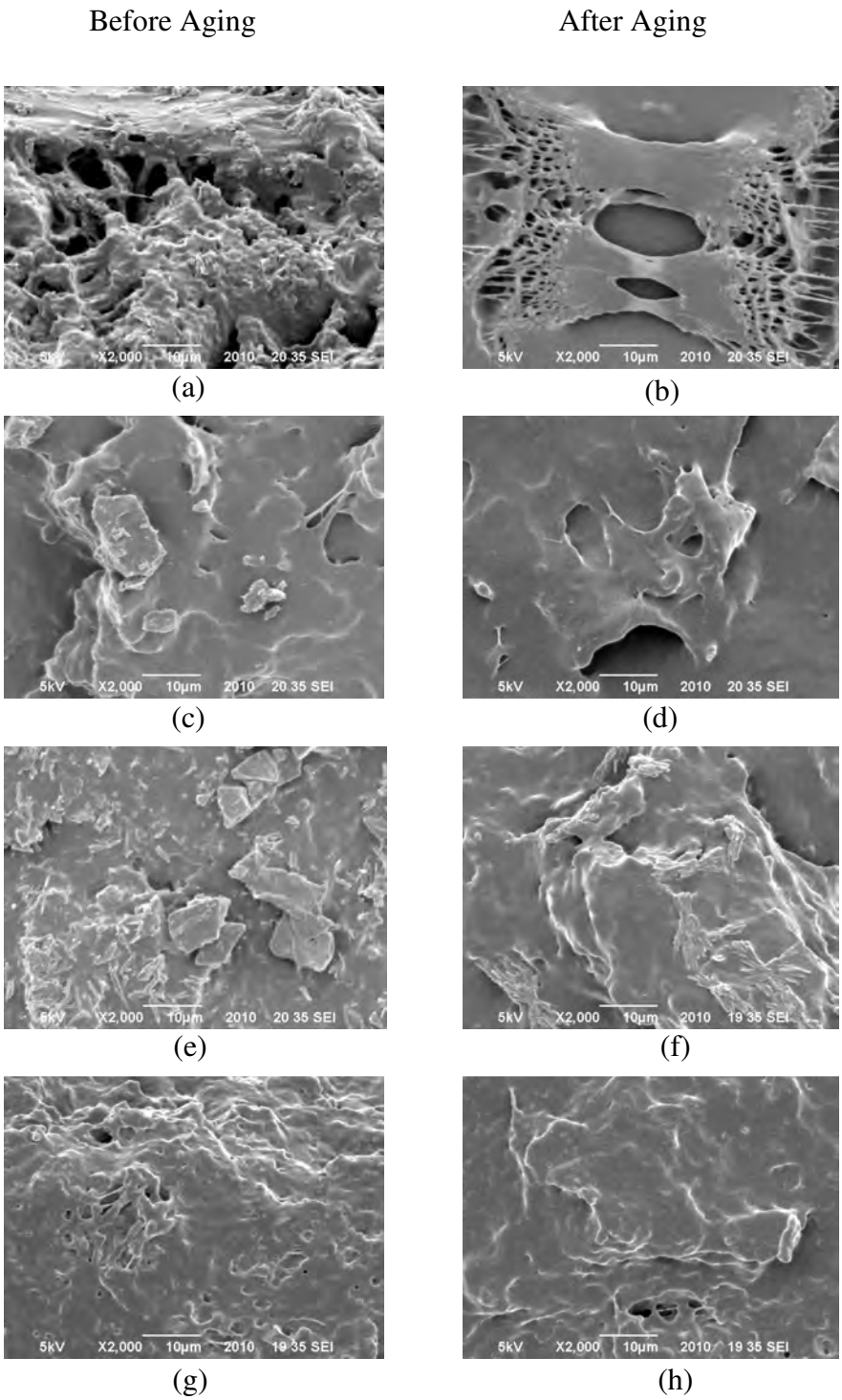

Figure 7.7 SEM micrographs of before and after aging of tensile fracture surfaces (×2000): (a) NR**,** (b) aged NR, (c) NR/PIP (85/15), (d) aged NR/PIP (85/15), (e) NR/PIP (70/30), (f) aged NR/PIP (70/30), (g) NR/ST-g-PIP (85/15) and (h) aged NR/ST-g-PIP (85/15).

CHAPTER VIII

CONCLUSION AND RECOMMENDATIONS

8.1 Conclusion

8.1.1 Synthesis Nanosized Polyisoprene via Differential Microemulsion Polymerization

Using differential microemulsion polymerization, nanosized polyisoprene particles can be controllably synthesized. To synthesize nanosized polyisoprene, polymerization using AIBN as an initiator is the most appropriate system due to a high monomer conversion of the synthesized rubber with low gel content and high molecular weight with a low polydispersity index. A fractional factorial experimental design was applied to study the main effects on the nanosized polyisoprene synthesis. From this design, the amount of initiator, reaction temperature and stirring speed over the range of the investigation were all found to have significant effects on polyisoprene particle size. The significant effects on monomer conversion were reaction temperature, stirring speed and interaction between reaction temperature and stirring speed over the range of this investigation. Moreover, the polyisoprene nanoparticle size could be controlled by the surfactant concentration and isoprene monomer/water ratio.

8.1.2 Graft Copolymerization of Methyl Methacrylate onto Nanosized Polyisoprene Using Redox initiator System

The graft copolymerization of MMA monomer onto nanosized PIP was carried out by CHPO/TEPA as redox initiators. A 2^3 factorial experimental design showed that the monomer concentration, the reaction temperature and interaction between initiator concentration and reaction temperature significantly affected the percentage graft onto PIP. The optimal relation was observed denoting that low CHPO initiator concentration level; low reaction temperature level but high MMA

concentration level yielded a high percentage of graft PIP. For the effect of PIP nanoparticle size, the high conversion and high degree of grafting could be achieved when very small particles were used as core polymer. The morphology of the graft copolymers from TEM photographs indicated that the grafting of the MMA monomer onto nanosized PIP exhibited the core–shell structure, with nanosized PIP as the core and PMMA as the shell. The micrograph inferred that the nanosized PIP seed particle had a complete closed shell with ca. 2-10 nm in thickness. The degradation temperatures of MMA graft PIP were quite the same with nanosized PIP and the nanoparticle size of initial PIP did not have an appreciable effect on the glass transition temperature of MMA graft polymer.

8.1.3 Graft Copolymerization of Styrene onto Nanosized Polyisoprene Using Redox Intitiator System

The graft copolymerization of ST monomer onto nanosized PIP was carried out using CHPO/TEPA as redox initiators. The effect of PIP nanoparticle size showed that the high conversion and high degree of grafting could be achieved when a small particle was used as the core polymer. The grafting efficiency and monomer conversion increased with increasing reaction temperature. As the amount of ST monomer increased, the grafting efficiency and monomer conversion increased and reached a maximum at a ST monomer concentration of 100 phr. The morphology of the graft copolymers from TEM photographs indicated that the small PIP nanoparticle was completely coated with PST by grafting which shows the core shell morphology of nanosized graft PIP. While the larger PIP nanoparticles might not be completely coated with PST but the PST might be distributed like raspberry morphology in some portion of the particle. The thickness of ST shell was estimated to be around 10 nm depending on the grafting efficiency level.

8.1.4 Diimide Hydrogenation of Nanosized Polyisoprene Latex in The Presence of Cupric Ion

Diimide hydrogenation is an alternative route for hydrogenation of nanosized PIP latex in which molecular hydrogen is not required. The diimide

reduction technique of nanosized PIP latex was accomplished by using hydrazine hydrate/hydrogen peroxide and Cu^{2+} as catalyst. The hydrogenated products were characterized by NMR spectroscopy. The degree of hydrogenation increased with increasing in reaction time and then leveled off after 8 h. The conversion profile was shown to be first order with respect to C=C concentration. Low rubber concentration and high hydrazine concentration provided the most favorable conditions. For the rate constant (*k'*) of diimide hydrogenation, the nanosized PIP with smaller particle size gave higher rate constant than that of large particle size. The optimum ratio of $[N_2H_4]$:$[H_2O_2]$ in this experiment was 1:1.32 at the [C=C] of 0.55 and the 75 % hydrogenation was achieved. The diimide hydrogenation of nanosized PIP latex provides a method to improve the thermal stability of nanosized PIP. The morphology of the hydrogenated nanosized PIP from Transmission Electron Micrographs indicated a non-hydrogenated nanosized PIP core and a hydrogenated outer layer.

8.1.5 Mechanical Properties of Vulcanized NR/Nanosized PIP and NR/Modified Nanosized PIP

Nanosized PIP and nanosized graft PIP such as ST-g-PIP could be used as compatibilizers for vulcanized rubber latex. From the physical properties of pre-vulcanized compounds, NR/ST-g-PIP, NR/MMA-g-PIP and NR/HPIP blends had low crosslink density and increased swelling index compared with NR film. The addition of nanosized PIP and ST-g-PIP strongly influenced the mechanical properties of the NR-based compound. Tensile strength, elongation at break and hardness of NR/PIP, NR/ST-g-PIP blends were decreased whereas the Young modulus was essentially the same. Aging test results showed that the tensile strength of NR compounds decreased but elongation increased with accelerated aging. Incorporation of nanosized PIP and ST-g-PIP resulted in an improvement of the resistance of the compounds to heat aging. Morphology studies of the compounds indicate that the addition of nanosized PIP and ST-g-PIP has changed the fracture surface behavior from ductile behavior to brittle type.

8.2 Recommendations

A further study of the chemical modification of nanosized PIP should be concerned with the following aspects:

1. Improvement of diimide hydrogenation process

Due to the incomplete hydrogenation, about 75% conversion, the second treatment of hydrogenated PIP may be used to increase the degree of hydrogenation. For further research work, the treatment effect on the hydrogenation level after each treatment should be investigated. The product from the previous hydrogenation treatment (75% hydrogenation) should be used as the starting material for the next hydrogenation treatment at the same reaction condition. Moreover, effect of reaction temperature and their kinetic should be studied.

2. Applications of nanosized PIP and modified nanosized PIP latex

The compound film of NR filled with nanosized PIP and NR filled with modified nanosized PIP exhibited good resistance to thermal degradation. However, the mechanical properties need to be improved. The optimum pre-vulcanization condition of nanosized compounds should be explored.

REFERENCES

[1] Liu, Y., Fan, Z., Ma, H., Tan, Y., and Qiao, J. Application of nano powdered rubber in friction materials. Wear. 2006. 261(2): 225-229.

[2] Navrotsky, A. Nanomaterials in the environment, agriculture, and technology (neat). Journal of Nanoparticle Research. 2000. 2(3): 321-323.

[3] Birnbaum, D. T., Kosmala, J. D., and Brannon-Peppas, L. Optimization of preparation techniques for poly(lactic acid-*co*-glycolic acid) nanoparticles. Journal of Nanoparticle Research. 2000. 2(2): 173-181.

[4] Hillaireau, H. and Couvreur, P. Polymeric nanoparticles as drug carriers. In: Polymers in drug delivery., Uchegbu, I., Schaetzlein, AG., Editor. 2006, CRC Press Boca Raton, FL, USA. p. 101-110.

[5] Antonietti, M. and Landfester, K. Miniemulsions for nanoparticle synthesis, in Colloid chemistry II. 2003, Springer Berlin / Heidelberg. p. 75-123.

[6] Okubo, M., et al. Miniemulsion polymerization, in Polymer particles. 2005, Springer Berlin / Heidelberg. p. 129-255.

[7] Chern, C.-S. and Tang, H.-J. Microemulsion polymerization kinetics and mechanisms. Journal of Applied Polymer Science. 2005. 97(5): 2005-2013.

[8] Xu, X.-J. and Gan, L. M. Recent advances in the synthesis of nanoparticles of polymer latexes with high polymer-to-surfactant ratios by microemulsion polymerization. Current Opinion in Colloid & Interface Science. 2005. 10(5-6): 239-244.

[9] Odian, G. Other emulsion polymerization systems, in Principles of polymerization. 2004, John Wiley & Sons: New Jersey, US. p. 367-368.

[10] Atik, S. S. and Thomas, J. K. Polymerized microemulsions. Journal of the American Chemical Society. 1981. 103(14): 4279-4280.

[11] Stoffer, J. O. and Bone, T. Polymerization in water-in-oil microemulsion systems. I. Journal of Polymer Science: Polymer Chemistry Edition. 1980. 18(8): 2641-2648.

[12] O'Donnell, J. and Kaler, E. W. Microstructure, kinetics, and transport in oil-in-water microemulsion polymerizations. Macromolecular Rapid Communications. 2007. 28(14): 1445-1454.

[13] Yildiz, U. and Capek, I. Microemulsion polymerization of styrene in the presence of macroinimer. Polymer. 2003. 44(8): 2193-2200.

[14] Zhang, Q., Bao, X., Lin, M., and Hourston, D. J. Preparation of nanometer-sized poly(methacrylic acid) particles in water-in-oil microemulsions. Journal of Applied Polymer Science. 2006. 100(3): 2497-2503.

[15] Capek, I. and Chudej, J. On the fine emulsion polymerization of styrene with non-ionic emulsifier. Polymer Bulletin. 1999. 43(4): 417-424.

[16] Gan, L. M., Lian, N., Chew, C. H., and Li, G. Z. Polymerization of styrene in a Winsor I-like system. Langmuir. 1994. 10(7): 2197-2201.

[17] Loh, S. E., Gan, L. M., Chew, C. H., and Ng, S. C. Polymerization of methyl methacrylate in Winsor I-like system. Journal of Macromolecular Science, Part A: Pure and Applied Chemistry. 1996. 33(3): 371 - 384.

[18] Antonietti, M., Basten, R., and Lohmann, S. Polymerization in microemulsions — a new approach to ultrafine, highly functionalized polymer dispersions. Macromolecular Chemistry and Physics. 1995. 196(2): 441-466.

[19] Antonietti, M., et al. Synthesis and size control of polystyrene latices via polymerization in microemulsion. Macromolecules. 1991. 24(25): 6636-6643.

[20] Ming, W., Jones, F. N., and Fu, S. High solids-content nanosize polymer latexes made by microemulsion polymerization. Macromolecular Chemistry and Physics. 1998. 199(6): 1075-1079.

[21] Ming, W., Zhao, J., Lu, X., Wang, C., and Fu, S. Novel characteristics of polystyrene microspheres prepared by microemulsion polymerization. Macromolecules. 1996. 29(24): 7678-7682.

[22] Rabelero, M., Zacarias, M., Mendizabal, E., Puig, J., Dominguez, J., and Katime, I. High-content polystyrene latex by microemulsion polymerization. Polymer Bulletin. 1997. 38(6): 695-700.

[23] Roy, S. and Devi, S. High solids content semicontinuous microemulsion copolymerization of methylmethacrylate and butylacrylate. Polymer. 1997. 38(13): 3325-3331.

[24] Dan, Y., Yang, Y., and Chen, S. Synthesis and structure of the poly(methyl methacrylate) microlatex. Journal of Applied Polymer Science. 2002. 85(14): 2839-2844.

[25] He, G. Synthesis and characterization of nano-sized polymer particles using differential microemulsion polymerization. Doctoral dissertation, Chemical Engineering, University of Waterloo, 2006

[26] He, G., Pan, Q., and Rempel, G. L. Synthesis of poly(methyl methacrylate) nanosize particles by differential microemulsion polymerization. Macromolecular Rapid Communications. 2003. 24(9): 585-588.

[27] Norakankorn, C., Pan, Q., Rempel, G. L., and Kiatkamjornwong, S. Synthesis of poly(methyl methacrylate) nanoparticles initiated by 2,2′-azoisobutyronitrile via differential microemulsion polymerization. Macromolecular Rapid Communications. 2007. 28(9): 1029-1033.

[28] Norakankorn, C., Pan, Q., Rempel, G. L., and Kiatkamjornwong, S. Synthesis of poly(methyl methacrylate) nanoparticles initiated by azobisisobutyronitrile using a differential microemulsion polymerization technique. Journal of Applied Polymer Science. 2009. 113(1): 375-382.

[29] Bayer, A. G. Ullman's encyclopedia of industrial chemistry. Vol. A23. New York, USA: VCH Publisher, 1992.

[30] Bhowmick, A. K. and Stephens, H. L., eds. Handbook of elastomers. New York and Basel: Marcel Dekker, 1988.

[31] Duck, E. W. and Deniels, D. J. Plastics and rubber. Norwich, UK: Page Bros, 1971.

[32] McManus, N. T. and Rempel, G. L. Chemical modification of polymers: Catalytic hydrogenation and related reactions. 1995. 35(2): 239 - 285.

[33] Schulz, D. N., Turner, S. R., and Golub, M. A. Recent advances in the chemical modification of unsaturated polymers Rubber Chemistry and Technology. 1982. 55(3): 809-859.

[34] Odian, G. Graft copolymers, in Principles of polymerization. 2004, John Wiley & Sons: New Jersey, US. p. 752-756.

[35] Schildknecht, C. E. Polymerization processes. New York: Wiley-Interscience, 1977.

[36] Huang, N.-J. and Sundberg, D. C. Fundamental studies of grafting reactions in free radical copolymerization. I. A detailed kinetic model for solution polymerization. Journal of Polymer Science Part A: Polymer Chemistry. 1995. 33(15): 2533-2549.

[37] Oommen, Z. and Thomas, S. Mechanical properties and failure mode of thermoplastic elastomers from natural rubber/poly(methyl methacrylate)/natural rubber-g-poly(methyl methacrylate) blends. Journal of Applied Polymer Science. 1997. 65(7): 1245-1255.

[38] Schneider, M., Pith, T., and Lambla, M. Preparation and morphological characterization of two- and three-component natural rubber-based latex particles. Journal of Applied Polymer Science. 1996. 62(2): 273-290.

[39] Asaletha, R., Groeninckx, G., Kumaran, M. G., and Thomas, S. Melt rheology and morphology of physically compatibilized natural rubber–polystyrene blends by the addition of natural rubber-g-polystyrene. Journal of Applied Polymer Science. 1998. 69(13): 2673-2690.

[40] Aerdts, A. M., de Krey, J. E. D., Kurja, J., and German, A. L. Emulsifier free grafting of styrene and methyl methacrylate concurrently onto polybutadiene and determination of the copolymer microstructure. Polymer. 1994. 35(8): 1636-1647.

[41] Aerdts, A. M., Theelen, S. J. C., Smit, T. M. C., and German, A. L. Grafting of styrene and methyl methacrylate concurrently onto polybutadiene in semi-continuous emulsion processes and determination of copolymer microstructure. Polymer. 1994. 35(8): 1648-1653.

[42] Arayapranee, W., Prasassarakich, P., and Rempel, G. L. Process variables and their effects on grafting reactions of styrene and methyl methacrylate onto natural rubber. Journal of Applied Polymer Science. 2003. 89(1): 63-74.

[43] Arayapranee, W., Prasassarakich, P., and Rempel, G. L. Blends of poly(vinyl chloride) (PVC)/natural rubber-g-(styrene-*co*-methyl methacrylate) for improved impact resistance of PVC. Journal of Applied Polymer Science. 2004. 93(4): 1666-1672.

[44] Braun, D., Schmiedel, B., Hellmann, G. P., Lambla, M., and Schneider, M. Structured latex particles based on natural rubber for high-impact polymer blends. Die Angewandte Makromolekulare Chemie. 1998. 254(1): 79-84.

[45] Schneider, M., Pith, T., and Lambla, M. Structured latex particles as impact modifiers for poly(styrene–*co*-acrylonitrile) blends. Polymers for Advanced Technologies. 1996. 7(7): 577-588.

[46] de Oliveira, P. C., et al. Modification of natural rubber: A study by 1H-NMR to assess the degree of graftization of polydmaema or polymma onto rubber particles under latex form in the presence of a redox couple initiator. European Polymer Journal. 2005. 41(8): 1883-1892.

[47] Ghosh, P. and Sengupta, P. K. Graft copolymerization of methyl methacrylate and natural rubber. Journal of Applied Polymer Science. 1967. 11(8): 1603-1611.

[48] Thiraphattaraphun, L., Kiatkamjornwong, S., Prasassarakich, P., and Damronglerd, S. Natural rubber-g-methyl methacrylate/poly(methyl methacrylate) blends. Journal of Applied Polymer Science. 2001. 81(2): 428-439.

[49] Mishra, S. N., Lenka, S., and Nayak, P. L. Graft copolymerization onto natural rubber--XI. Graft copolymerization of methyl methacrylate onto rubber using the hydrogen peroxide-sodium thiosulphate redox system. European Polymer Journal. 1991. 27(12): 1319-1322.

[50] Oliveira, P. C., et al. Poly(dimethylaminoethyl methacrylate) grafted natural rubber from seeded emulsion polymerization. Polymer. 2005. 46(4): 1105-1111.

[51] Kangwansupamonkon, W., Gilbert, R. G., and Kiatkamjornwong, S. Modification of natural rubber by grafting with hydrophilic vinyl monomers. Macromolecular Chemistry and Physics. 2005. 206(24): 2450-2460.

[52] Kochthongrasamee, T., Prasassarakich, P., and Kiatkamjornwong, S. Effects of redox initiator on graft copolymerization of methyl methacrylate onto natural rubber. Journal of Applied Polymer Science. 2006. 101(4): 2587-2601.

[53] George, B., Maiti, S. N., and Varma, I. K. Graft copolymerization of methyl methacrylate on to natural rubber: Effect of polymerization conditions on particle morphology. Journal of Elastomers and Plastics. 2006. 38(4): 319-331.

[54] Manaresi, P., Passalacqua, V., and Pilati, F. Kinetics of graft polymerization of styrene on *cis*-1,4-polybutadiene. Polymer. 1975. 16(7): 520-526.

[55] Sundberg, D. C., Arndt, J., and Tang, M.-Y. Grafting of styrene onto polybutadiene latices in batch and semi-continuous reactors. Journal of Dispersion Science and Technology. 1984. 5(3): 433 - 445.

[56] Xu, Y. S., Yuan, C. D., Wang, Y. J., Cao, T. Y., and Cao, P. Mechanism and grafting reactions in seeded emulsion polymerization with emulsified monomer feeding. Journal of Applied Polymer Science. 1999. 72(11): 1495-1499.

[57] Gasperowicz, A., Kolendowicz, M., and Skowronski, T. Grafting of styrene onto poly(butyl acrylate) in emulsion. Polymer. 1982. 23(6): 839-842.

[58] Mohammadi, N. A. and Rempel, G. L. Homogeneous selective catalytic hydrogenation of C=C in acrylonitrile-butadiene copolymer. Macromolecules. 1987. 20(10): 2362-2368.

[59] Guo, X.-Y. and Rempel, G. L. Catalytic hydrogenation of nitrile–butadiene copolymer emulsion. Journal of Applied Polymer Science. 1997. 65(4): 667-675.

[60] Murrer, B. A. and Jenkin, J. W. Method for the hydrogenation of emulsified unsaturated organic compound. U.S. Patent 4,469,849 (1984).

[61] Hinchiranan, N., Prasassarakich, P., and Rempel, G. L. Hydrogenation of natural rubber in the presence of $OsHCL(CO)(O_2)(PCy_3)_2$: Kinetics and mechanism. Journal of Applied Polymer Science. 2006. 100(6): 4499-4514.

[62] Mahittikul, A., Prasassarakich, P., and Rempel, G. L. Hydrogenation of natural rubber latex in the presence of oshcl(co)(o2)(pcy3)2. Journal of Applied Polymer Science. 2006. 100(1): 640-655.

[63] Wideman, L. G. and Lawson, G. Process for hydrogenation of carbon-carbon double bonds in an unsaturated polymer in latex form. U.S. Patent 4,452,950 (1984).

[64] Parker, D. K., Roberts, R. F., and Schiessl, H. W. A new process for the preparation of highly saturated nitrile rubber in latex form. Rubber Chemistry and Technology. 1992. 65: 245-257.

[65] Parker, D. K. and Ruthenburg, D. M. Process for the preparation of hydrogenated rubber. U.S. Patent 5,424,356 (1995).

[66] Xie, H.-Q., Li, X.-D., and Guo, J.-S. Hydrogenation of nitrile–butadiene rubber latex to form thermoplastic elastomer with excellent thermooxidation resistance. Journal of Applied Polymer Science. 2003. 90(4): 1026-1031.

[67] Zhou, S., Bai, H., and Wang, J. Hydrogenation of acrylonitrile–butadiene rubber latexes. Journal of Applied Polymer Science. 2004. 91(4): 2072-2078.

[68] Lin, X., Pan, Q., and Rempel, G. L. Hydrogenation of nitrile-butadiene rubber latex with diimide. Applied Catalysis A: General. 2004. 276(1-2): 123-128.

[69] Lin, X., Pan, Q., and Rempel, G. L. Gel formation in diimide-hydrogenated polymers. Journal of Applied Polymer Science. 2005. 96(4): 1122-1125.

[70] Lin, X., Pan, Q., and Rempel, G. L. Modeling and simulation of diimide hydrogenation of nitrile butadiene rubber latex. Industrial & Engineering Chemistry Research. 2006. 45(4): 1300-1306.

[71] He, Y., Daniels, E. S., Klein, A., and El-Aasser, M. S. Hydrogenation of styrene-butadiene rubber (sbr) latexes. Journal of Applied Polymer Science. 1997. 64(10): 2047-2056.

[72] De Sarkar, M., De, P. P., and Bhowmick, A. K. Thermoplastic elastomeric hydrogenated styrene-butadiene elastomer: Optimization of reaction conditions, thermodynamics, and kinetics. Journal of Applied Polymer Science. 1997. 66(6): 1151-1162.

[73] Mahittikul, A., Prasassarakich, P., and Rempel, G. L. Diimide hydrogenation of natural rubber latex. Journal of Applied Polymer Science. 2007. 105(3): 1188-1199.

[74] Mark, J. E., Erman, B., and Eirich, F. R. The science and technology of rubber. 3rd ed., USA: Elsevier Academic Press, 2005.

[75] Claramma, N. M. and Mathew, N. M. Effect of temperature on sulfur prevulcanization of natural rubber latex. Journal of Applied Polymer Science. 1997. 65(10): 1913-1920.

[76] Ho, C. C. and Khew, M. C. Surface morphology of prevulcanized natural rubber latex films by atomic force microscopy: new insight into the prevulcanization mechanism. Langmuir. 1999. 15(19): 6208-6219.

[77] Sasidharan, K. K., Joseph, R., Palaty, S., Gopalakrishnan, K. S., Rajammal, G., and Pillai, P. V. Effect of the vulcanization time and storage on the stability and physical properties of sulfur-prevulcanized natural rubber latex. Journal of Applied Polymer Science. 2005. 97(5): 1804-1811.

[78] Sasidharan, K. K., Palaty, S., Gopalakrishnan, K. S., George, K. E., and Joseph, R. Room temperature prevulcanization of natural rubber latex using xanthate. Journal of Applied Polymer Science. 2004. 94(3): 1164-1174.

[79] Arayapranee, W., Prasassarakich, P., and Rempel, G. L. Synthesis of graft copolymers from natural rubber using cumene hydroperoxide redox initiator. Journal of Applied Polymer Science. 2002. 83(14): 2993-3001.

[80] Arayapranee, W. and Rempel, G. L. Preparation of a natural rubber core/polymer shell in a nanomatrix by graft copolymerization. Journal of Applied Polymer Science. 2008. 110(4): 2475-2482.

[81] Zhou, M. H. and Cho, W.-J. Synthesis and properties of high oil-absorbent 4-tert-butylstyrene-EPDM-divinylbenzene graft terpolymer. Journal of Applied Polymer Science. 2002. 85(10): 2119-2129.

[82] Sperling, L. H. Introduction to physical polymer science. 4th Edition ed., New York: John Wiley and Son Inc., 2006.

[83] Flory, P. J. and Rehner, J. J. Statistical mechanics of cross-linked polymer networks II. Swelling. The Journal of Chemical Physics. 1943. 11(11): 521-526.

[84] Hinchiranan, N., Lertweerasirikun, W., Poonsawad, W., Rempel, G. L., and Prasassarakich, P. Hydrogenated natural rubber blends: Aspect on thermal stability and oxidative behavior. Journal of Applied Polymer Science. 2009. 113(3): 1566-1575.

[85] Lamb, D., Anstey, J. F., Lee, D.-Y., Fellows, C. M., Monteiro, M. J., and Gilbert, R. G. Rational design of polymer colloids. Macromolecular Symposia. 2001. 174(1): 13-28.

[86] Cheong, I. W., Fellows, C. M., and Gilbert, R. G. Synthesis and cross-linking of polyisoprene latexes. Polymer. 2004. 45(3): 769-781.

[87] Kangwansupamonkon, W., Fellows, C. M., Lamb, D. J., Gilbert, R. G., and Kiatkamjornwong, S. Kinetics of surface grafting on polyisoprene latexes by reaction calorimetry. Polymer. 2004. 45(17): 5775-5784.

[88] Kamenka, N., Burgaud, I., Zana, R., and Lindman, B. Electrical conductivity, self-diffusion, and fluorescence probe investigations of the interaction between sodium dodecyl sulfate and ethyl(hydroxyethyl)cellulose. The Journal of Physical Chemistry. 1994. 98(27): 6785-6789.

[89] Capek, I. and Potisk, P. Microemulsion and emulsion polymerization of butyl acrylate--I. Effect of the initiator type and temperature. European Polymer Journal. 1995. 31(12): 1269-1277.

[90] Shao, H., Huang, B., Yao, W., and Li, H. Synthesis and characterization of low relative molecular weight *trans*-1,4-poly(isoprene). Journal of Applied Polymer Science. 2008. 107(6): 3734-3738.

[91] Tangpakdee, J., Tanaka, Y. Characterization of sol and gel in hevea natural rubber. Rubber Chemistry and Technology. 1997. 70(5): 707-713.

[92] Imroz Ali, A. M., Tauer, K., and Sedlak, M. Comparing emulsion polymerization of methacrylate-monomers with different hydrophilicity. Polymer. 2005. 46(4): 1017-1023.

[93] Guowen, H., Shen, H., Fu, H., and Chen, H. Influence of initiator on synthesis and properties of polyurethane-acrylate hybrid emulsion. Journal of Wuhan University of Technology--Materials Science Edition. 2008. 23(1): 41-45.

[94] Bhawal, S., Devi, S., and Dhoble, D. Initiator artifacts in the emulsion and microemulsion copolymerization of partially water-soluble monomers. International Journal of Polymeric Materials. 2005. 55(4): 255 - 281.

[95] Gomez-Cisneros, M., et al. Surfactant concentration effects on the microemulsion polymerization of vinyl acetate. Polymer. 2005. 46(9): 2900-2907.

[96] Martinez, A., Gonzalez, C., Porras, M., and Gutierrez, J. M. Nano-sized latex particles obtained by emulsion polymerization using an amphiphilic block copolymer as surfactant. Colloids and Surfaces A: Physicochemical and Engineering Aspects. 2005. 270-271: 67-71.

[97] Capek, I., Lin, S.-Y., Hsu, T.-J., and Chern, C.-S. Effect of temperature on styrene emulsion polymerization in the presence of sodium dodecyl sulfate. II. Journal of Polymer Science Part A: Polymer Chemistry. 2000. 38(9): 1477-1486.

[98] Hinchiranan, N., Suppaibulsuk, B., Promprayoon, S., and Prasassarakich, P. Improving properties of modified acrylic sheet via addition of graft natural rubber. Materials Letters. 2007. 61(18): 3951-3955.

[99] Fukushima, Y., Kawahara, S., and Tanaka, Y. Synthesis of graft copolymers from highly deproteinised natural rubber. Journal of Rubber Research. 1998. 1(3): 154-166.

[100] Pukkate, N., et al. Nano-matrix structure formed by graft-copolymerization of styrene onto natural rubber. European Polymer Journal. 2007. 43(8): 3208-3214.

[101] Peng, Z., et al. Thermogravimetric analysis of methyl methacrylate-graft-natural rubber. Journal of Applied Polymer Science. 2002. 85(14): 2952-2955.

[102] Kongparakul, S. Modified natural rubber latex by graft copolymerization with methyl methacrylate and hydrogenation using $OsHCL(CO)(O_2)(PCy_3)$ as a catalyst. Doctoral dissertation, Department of Chemical Technology, Faculty of Science, Chulalongkorn University, 2007

[103] Lenka, S., Nayak, P. L., and Das, A. P. Graft copolymerization onto rubber. Vii. Graft copolymerization of methyl methacrylate onto rubber using potassium peroxydisulfate catalyzed by silver ion. Journal of Applied Polymer Science. 1985. 30(7): 2753-2759.

[104] Arayapranee, W., Prasassarakich, P., and Rempel, G. L. Factorial experimental design for graft copolymerization of styrene and methyl methacrylate onto styrene–butadiene rubber. Journal of Applied Polymer Science. 2006. 100(4): 2867-2874.

[105] Pukkate, N., Yamamoto, Y., and Kawahara, S. Mechanism of graft copolymerization of styrene onto deproteinized natural rubber. Colloid Polymer Science. 2008. 286(4): 411-416.

[106] Parker, D. K. and Purdon Jr., J. R. Ozonolysis of hydrogenated latices. U.S. Patent 5,039,737 (1991).

[107] Simma, K., Rempel, G. L., and Prasassarakich, P. Improving thermal and ozone stability of skim natural rubber by diimide reduction. Polymer Degradation and Stability. 2009. 94(11): 1914-1923.

[108] Lin, X., Pan, Q., and Rempel, G. L. Cupric ion catalyzed diimide production from the reaction between hydrazine and hydrogen peroxide. Applied Catalysis A: General. 2004. 263(1): 27-32.

[109] Xie, H.-Q., Li, X.-D., Liu, X.-Y., and Guo, J.-S. Hydrogenation and neutralization of carboxylic styrene–butadiene latex to form

thermoplastic elastomer with excellent thermooxidation resistance. Journal of Applied Polymer Science. 2002. 83(6): 1375-1384.

[110] Arayapranee, W. and Rempel, G. L. Morphology and mechanical properties of natural rubber and styrene-grafted natural rubber latex compounds. Journal of Applied Polymer Science. 2008. 109(3): 1395-1402.

[111] Lu, G., Li, Z.-F., Li, S.-D., and Xie, J. Blends of natural rubber latex and methyl methacrylate-grafted rubber latex. Journal of Applied Polymer Science. 2002. 85(8): 1736-1741.

[112] Botros, S. H. Preparation and characteristics of nr/epdm rubber blends. Polymer-Plastics Technology and Engineering. 2002. 41(2): 341 - 359.

[113] Hinchiranan, N. Hydrogenation of natural rubber catalyzed by $OsHCL(CO)(O_2)(PCy_3)_2$ and $[Ir(COD)(PCy_3)(Py)]PF_6$. Doctoral dissertation, Department of Chemical Technology, Faculty of Science, Chulalongkorn University, 2004

[114] Chuayjuljit, S. and Boonmahitthisud, A. Natural rubber nanocomposites using polystyrene-encapsulated nanosilica prepared by differential microemulsion polymerization. Applied Surface Science. 2010. 256(23): 7211-7216.

[115] Liu, X. and Zhao, S. Measurement of the condensation temperature of nanosilica powder organically modified by a silane coupling agent and its effect evaluation. Journal of Applied Polymer Science. 2008. 108(5): 3038-3045.

APPENDICES

Appendix A

The Overall Compositions of Rubbers

Table A-1 Properties of natural rubber latex

Properties	Test Results
Total solid Content, %	61.79
Dry rubber Content, %	60.12
Non Rybber Solid, %	1.67
Ammonia Content (on Total Weight). %	0.69
Ammonia Content (on Water Phase). %	1.81
pH Value	10.32
KOH Number	0.6020
Volatile Fatty Acid Number (VFA)	0.0288
Mechanical Stability Time at 55% TS.,Sec	900
Spacific Gravity at 25 °C	0.9461
Magnesium Content (ppm)	33.75
Viscosity (60% TS.Spindle no 1.60 rpm.) cps.	76
Coagulum content (80 mesh), ppm	28

All test are performed according to relevant ISO 2004-1997(E) specification

Appendix B

Calculations of graft copolymerization

1. Conversion of graft copolymerization

The graft copolymers are characterized according to the following equation:

$$\text{Total Conversion } (\%) = \frac{\text{Weight of monomer consumed}}{\text{Weight of monomer charged}} \times 100 \qquad \text{(B-1)}$$

2. Grafting efficiency

$$\text{Grafting efficiency (GE) } (\%) = \frac{\text{Weight of monomer grafted}}{\text{Total weight of monomer polymerized}} \times 100 \qquad \text{(B-2)}$$

$$\text{Graft PIP } (\%) = \frac{\text{Weight of graft copolymer}}{\text{Weight of gross polymer}} \times 100 \qquad \text{(B-3)}$$

$$\text{Homopolymer } (\%) = \frac{\text{Weight of free homopolymer}}{\text{Weight of gross polymer}} \times 100 \qquad \text{(B-4)}$$

Appendix C

Raw Data of Graft Copolymerization

Table C-1 Raw data of factorial design of MMA graft on nanosized polyisoprene. (Section 4.2)

Exp.	W. of DRC (g)	W. of MMA (g)	Sample (g)	W. A* (g)	W. B** (g)	% Graft PIP	% Ungraft PIP	% Free PMMA	$\overline{D_n}$ MMA-g-PIP (nm)
MMAgPIP1	18.65	11.19	2.06	1.73	1.39	67.5	16.0	16.5	31.8
	19.95	11.70	2.04	1.71	1.38	67.5	16.0	16.5	-
MMAgPIP2	16.53	6.61	2.19	1.77	1.34	61.2	19.2	19.6	35.3
	20.41	8.16	2.00	1.62	1.22	61.2	19.2	19.6	-
MMAgPIP3	20.39	8.16	2.00	1.49	1.24	62.0	25.5	12.5	30.4
	19.35	7.74	2.04	1.52	1.28	62.8	25.5	11.8	-
MMAgPIP4	20.21	8.08	2.20	1.60	1.17	53.2	27.3	19.6	32.0
	20.20	8.08	2.01	1.46	1.07	53.2	27.3	19.5	-

* W. A = Graft product was extracted by light petroleum ether for 24 h.
** W. B = Graft product was extracted by light petroleum ether for 24 h and then extracted by acetone for 24 h.

Table C-1 (Continue)

Exp.	W. of DRC (g)	W. of MMA (g)	Sample (g)	W. A* (g)	W. B** (g)	% Graft PIP	% Ungraft PIP	% Free PMMA	$\overline{D_n}$ MMA-g-PIP (nm)
MMAgPIP5	19.16	7.66	2.02	1.57	1.24	61.4	22.3	16.3	28.1
	21.20	8.48	2.01	1.56	1.23	61.3	22.2	16.5	-
MMAgPIP6	18.89	11.40	2.03	1.76	1.47	72.4	13.3	14.3	31.0
	18.89	11.33	2.06	1.79	1.49	72.1	13.2	14.7	-
MMAgPIP7	18.55	11.40	2.10	1.66	1.23	58.6	21.0	20.5	30.9
	19.89	11.93	2.02	1.59	1.18	58.5	21.1	20.4	-
MMAgPIP8	19.00	11.40	2.06	1.73	1.39	67.5	16.0	16.5	29.9
	17.13	10.28	2.03	1.70	1.37	67.4	16.0	16.6	-

* W. A = Graft product was extracted by light petroleum ether for 24 h.
** W. B = Graft product was extracted by light petroleum ether for 24 h and then extracted by acetone for 24 h.

Table C-2 Raw data of effect of monomer concentration and polyisoprene particle size on MMA graft nanosized polyisoprene. (Sections 4.3)

Exp.	$\overline{D_n}$ PIP (nm)	$\overline{D_n}$ MMA-g-PIP (nm)	W. of DRC (g)	W. of MMA (g)	Sample (g)	W. A* (g)	W. B** (g)	% Conv.	% Graft PIP	% Ungraft PIP	% Free PMMA	% GE
40MMA-g-PIP_25	25.0	28.1	19.16	7.66	2.02	1.57	1.24	66.4	61.4	22.3	16.3	14.7
			21.20	8.48	2.01	1.56	1.23	66.1	61.3	22.2	16.5	13.9
60MMA-g-PIP_25	25.1	31.0	18.89	11.40	2.03	1.76	1.47	73.8	72.4	13.3	14.3	39.6
			18.89	11.33	2.06	1.61	1.44	71.8	60.3	28.9	10.9	36.7
100MMA-g-PIP_25	24.9	38.0	21.08	21.00	1.50	1.30	1.11	96.0	74.2	13.2	12.6	71.3
			18.84	18.80	1.61	1.33	1.01	95.2	62.7	17.4	19.9	56.4
100MMA-g-PIP_25	24.9	37.9	19.53	19.53	1.01	0.85	0.67	97.1	66.6	15.3	18.1	61.4
			19.53	19.53	1.01	0.84	0.64	97.0	63.4	16.4	20.2	57.2
100MMA-g-PIP_40	44.0	49.0	20.18	20.18	1.03	0.96	0.85	98.4	81.9	7.2	10.9	76.8
			20.18	20.18	1.04	0.96	0.85	98.5	82.2	7.1	10.7	77.2
100MMA-g-PIP_60	62.3	78.8	19.42	19.42	1.01	0.94	0.78	99.4	77.2	6.9	15.9	67.8
			19.42	19.42	1.01	0.95	0.79	99.4	78.1	6.4	15.5	68.6

* W. A = Graft product was extracted by light petroleum ether for 24 h.
** W. B = Graft product was extracted by light petroleum ether for 24 h and then extracted by acetone for 24 h.

Table C-3 Raw data of conversion and grafting efficiency profile of MMA graft nanosized polyisoprene. (Sections 4.4)

Exp.	Time (h)	W. of DRC (g)	W. of MMA (g)	Sample (g)	W. A* (g)	W. B** (g)	% Conv.	% Graft PIP	% Ungraft PIP	% Free PMMA	% GE
100MMA-g-PIP_25	2	20.18	20.00	1.60	1.27	1.07	87.9%	66.9	20.6	12.5	64.2
100MMA-g-PIP_25	4	20.74	20.50	1.58	1.18	0.87	94.4%	55.1	25.3	19.6	56.0
100MMA-g-PIP_25	6	19.45	19.45	1.59	1.01	0.74	96.3%	56.5	26.5	17.0	63.0
100MMA-g-PIP_25	8	21.08	21.00	1.50	1.06	0.85	96.0%	56.7	29.3	14.0	68.5

* W. A = Graft product was extracted by light petroleum ether for 24 h.

** W. B = Graft product was extracted by light petroleum ether for 24 h and then extracted by acetone for 24 h.

Table C-4 Raw data of effect of polyisoprene particle size and reaction temperature on ST graft nanosized polyisoprene. (Sections 5.2 and 5.3)

Exp.	$\overline{D_n}$ PIP (nm)	$\overline{D_n}$ ST-g-PIP (nm)	W. of DRC (g)	W. of ST (g)	Sample (g)	W. A* (g)	W. B** (g)	% Conv.	% Graft PIP	% Ungraft PIP	% Free PST	% GE
100ST-g-PIP_25	24.4	27.6	19.32	19.32	1.02	0.90	0.70	89.1	69.0	12.1	19.0	53.3
(ST-g-PIP_T50)			19.32	19.32	1.01	0.90	0.68	89.1	67.4	11.3	21.3	48.8
100ST-g-PIP_40	38.5	41.5	20.59	20.59	1.01	0.92	0.85	90.0	84.0	8.4	7.7	75.5
			20.59	20.59	1.01	0.92	0.85	90.0	84.7	8.2	7.2	76.4
100ST-g-PIP_60	51.1	60.2	19.42	19.42	1.02	0.91	0.68	93.6	67.3	11.0	21.7	51.5
			19.42	19.42	1.01	0.89	0.67	93.6	66.5	11.6	21.9	51.1
ST-g-PIP_T40	20.2	25.4	18.19	18.19	1.02	0.88	0.67	84.9	65.2	13.9	20.9	46.3
			18.19	18.19	1.03	0.88	0.67	84.9	65.3	14.7	20.0	47.9
ST-g-PIP_T60	22.9	28.2	19.18	19.18	1.03	0.93	0.72	93.7	69.3	9.9	20.8	53.4
			19.18	19.18	1.03	0.92	0.71	93.7	69.3	10.4	20.3	54.4
ST-g-PIP_T70	24.5	27.5	19.21	19.21	1.01	0.88	0.70	92.7	69.5	13.0	17.5	59.1
			19.21	19.21	1.01	0.87	0.70	92.7	69.0	13.7	17.3	59.4

* W. A = Graft product was extracted by light petroleum ether for 24 h.
** W. B = Graft product was extracted by light petroleum ether for 24 h and then extracted by methyl ethyl ketone for 24 h.

Table C-5 Raw data of effect of monomer concentration on ST graft nanosized polyisoprene. (Sections 5.4)

Exp.	Time (h)	$\overline{D_n}$ ST-g-PIP (nm)	W. of DRC (g)	W. of ST (g)	Sample (g)	W. A* (g)	W. B** (g)	% Conv.	% Graft PIP	% Ungraft PIP	% Free PST	% GE
60ST-g-PIP_25	2	27.28	1.83	1.10	1.00	0.79	0.68	71.4	67.8	21.2	11.0	45.2
			1.83	1.10	1.00	0.79	0.68	71.4	67.4	21.2	11.5	44.0
60ST-g-PIP_25	6	30.3	1.77	1.06	1.00	0.78	0.55	72.1	54.3	21.9	23.8	15.3
			1.77	1.06	1.00	0.79	0.65	72.1	64.3	21.4	14.2	38.1
60ST-g-PIP_25	8	27.59	16.24	9.75	1.00	0.79	0.68	75.8	67.6	21.2	11.3	48.4
			16.24	9.75	1.00	0.77	0.67	75.8	66.3	22.9	10.8	49.7
100ST-g-PIP_25	2	33.2	1.67	1.67	1.00	0.82	0.59	80.9	59.2	18.5	22.2	40.7
			1.67	1.67	1.01	0.82	0.61	80.9	60.3	18.3	21.5	42.1
100ST-g-PIP_25	6	32.8	1.72	1.72	1.01	0.82	0.62	81.3	61.8	18.7	19.5	45.8
			1.72	1.72	1.01	0.82	0.62	81.3	61.7	18.3	20.0	44.9
100ST-g-PIP_25	8	31.9	17.38	17.38	1.01	0.85	0.66	92.2	65.2	16.6	18.2	57.1
			17.38	17.38	1.00	0.84	0.66	92.2	65.7	16.6	17.8	58.1

* W. A = Graft product was extracted by light petroleum ether for 24 h.

** W. B = Graft product was extracted by light petroleum ether for 24 h and then extracted by methyl ethyl ketone for 24 h.

Table C-5 (Continue)

Exp.	Time (h)	$\overline{D_n}$ ST-g-PIP (nm)	W. of DRC (g)	W. of ST (g)	Sample (g)	W. A* (g)	W. B** (g)	% Conv.	% Graft PIP	% Ungraft PIP	% Free PST	% GE
150ST-g-PIP_25	2	29.49	1.46	2.19	1.01	0.82	0.51	61.6	51.0	18.8	30.3	22.8
			1.46	2.19	1.00	0.81	0.49	61.6	48.7	19.5	31.8	20.8
150ST-g-PIP_25	6	31.1	1.50	2.24	1.00	0.76	0.44	61.7	43.8	24.6	31.6	21.2
			1.50	2.24	1.01	0.76	0.44	61.7	44.0	24.1	31.9	20.8
150ST-g-PIP_25	8	32.6	16.46	24.70	1.01	0.78	0.50	64.3	49.4	23.1	27.5	28.3
			16.46	24.70	1.02	0.80	0.53	64.3	52.2	22.2	25.6	30.8

* W. A = Graft product was extracted by light petroleum ether for 24 h.

** W. B = Graft product was extracted by light petroleum ether for 24 h and then extracted by methyl ethyl ketone for 24 h.

Appendix D

Calculations of % Hydrogenation

Species 1

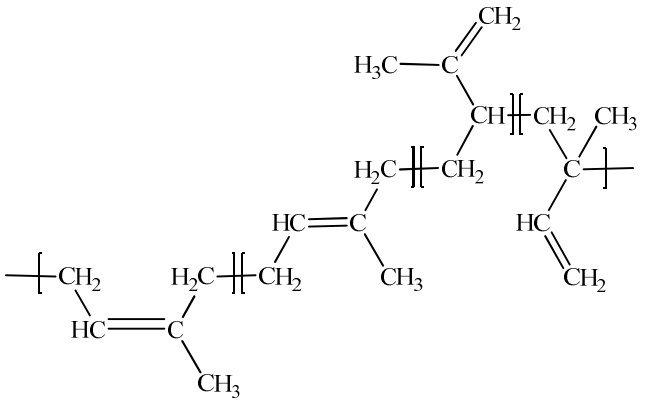

cis- 1,4 *trans*- 1,4 3,4 1,2

Hydrogenation

Species 2

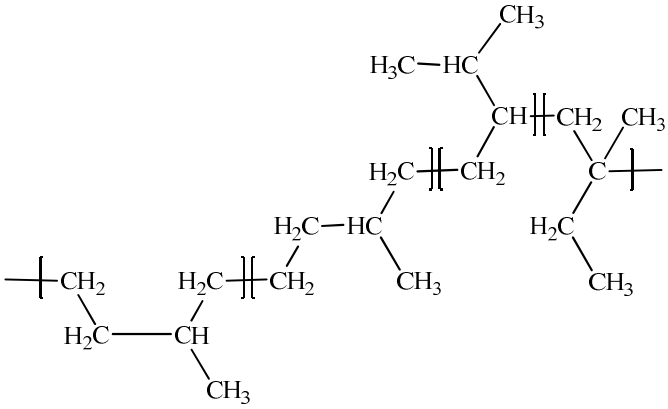

Proton of repeating unit except =CH in Species 1 = 7 protons

Proton of repeating unit in Species 2 = 10 protons

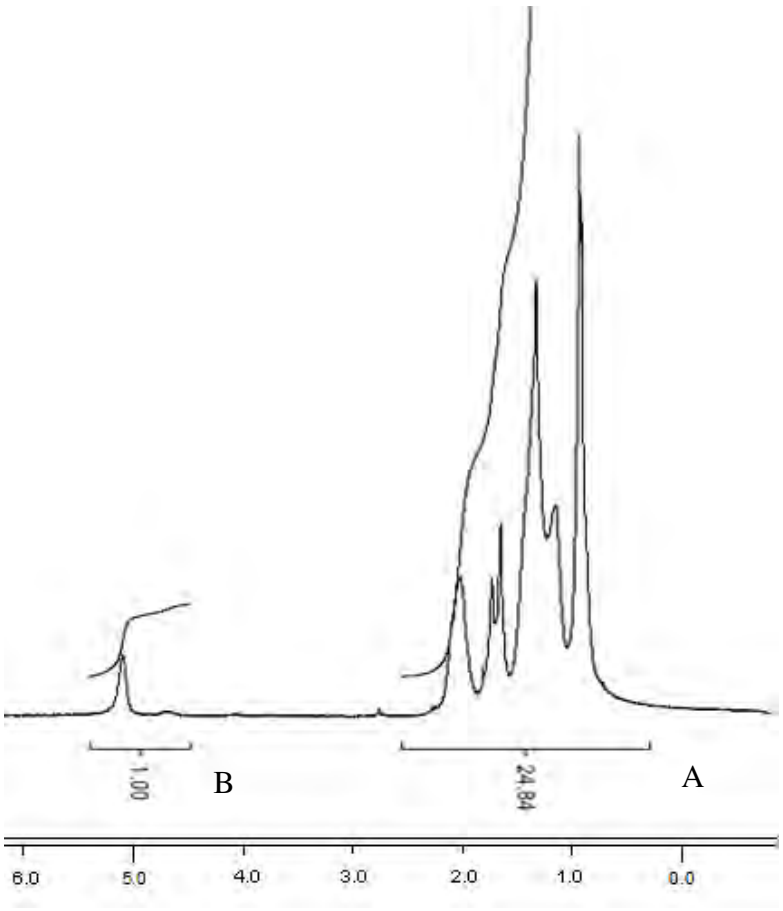

A = Peak area except at 5.2 ppm

B = Peak area at 5.2 ppm

C = Peak area of saturated $–CH_2-$ and $-CH_3$

$$A = 10C + 7B$$

$$C = \frac{A - 7B}{10}$$

Total peak area = Peak area of saturated $–CH_2–$ and $–CH_3$ + Peak area at 5.2 ppm

$$= \frac{A - 7B}{10} + B$$

$$= \frac{A - 3B}{10}$$

%Hydrogenation = [(Peak area of saturated $-CH_2$ and $-CH_3$)/(Total peak area)] $\times 100$

$$= \frac{(A - 7B)/10}{(A + 3B)/10} \times 100$$

$$= \frac{A - 7B}{A + 3B} \times 100$$

For example: A = 24.84 and B = 1.00

$$\%\text{Hydrogenation} = \frac{24.84 - 7(1.00)}{24.84 + 3(1.00)} \times 100$$

$$= 64.1\%$$

Appendix E

Results of Diimide Hydrogenation of Nanosized Polyisoprene

Table E-1 Results of Nanosized Polyisoprene Hydrogenation Profile by Diimide Hydrogenation in the Presence of Cupric ion (Section 6.3 and 6.4.1)

Exp. No.	Time (s)	Particle size (nm)	Average %Hydrogenation
HPIP_30	0	28.36	0.0
	3600	31.6	11.4
	7200	31.5	27.3
	10800	31.1	35.5
	14400	31	42.1
	18000	32.8	39.2
	21600	30.7	47.5
	25200	30.2	50.7
	28800	30.1	56.5
	32400	30.8	55.8
	36000	32.7	53.8
HPIP_40	0	37	0.0
	3600	38.9	4.6
	7200	37.5	16.1
	10800	38.9	27.7
	14400	37.5	29.3
	18000	38.9	37.2
	21600	37.8	35.7
	25200	39.3	44.5
	28800	39.1	52.4
	32400	39.1	48.8
	36000	37.5	49.4
HPIP_50	0	47.4	0.0
	3600	49.7	7.1
	7200	49.7	15.8
	10800	50.1	15.5
	14400	49.9	24.9
	18000	51.4	33.4
	21600	51.1	40.1
	25200	52.1	46.5
	28800	50.4	35.3
	32400	50.9	45.1
	36000	50.3	49.1

Table E-2 Results of Nanosized Polyisoprene Hydrogenation by Diimide Hydrogenation in the Presence of Cupric ion (Section 6.4.2-6.4.4)

Exp. No.	$CuSO_4$ (μM)	N_2H_4 (M)	H_2O_2 (M)	C=C (M)	Temp (^oC)	Total Volume (ml)	%Hydrogenation
1	49.4	0.6	3.53	0.55	60	150	56.2
2	49.4	1.7	3.53	0.55	60	150	77.0
3	49.4	2.68	3.53	0.55	60	150	72.2
4	49.4	3.14	3.53	0.55	60	150	70.9
5	49.4	3.57	3.53	0.55	60	150	68.5
6	49.4	2.2	1.23	0.55	60	150	41.5
7	49.4	2.2	2.34	0.55	60	150	67.0
8	49.4	2.2	2.76	0.55	60	150	69.3
9	49.4	2.2	3.15	0.55	60	150	62.2
10	49.4	2.2	5.08	0.55	60	150	77.2
11	49.4	2.2	3.53	0.49	60	150	75.4
12	49.4	2.2	3.53	0.52	60	150	70.3
13	49.4	2.2	3.53	0.58	60	150	69.5
14	49.4	2.2	3.53	0.6	60	150	64.1
15	49.4	2.2	3.53	0.63	60	150	67.6
16	49.4	0.6	3.53	0.55	60	150	63.4
17	49.4	1.7	3.53	0.55	60	150	40.8
18	49.4	2.68	3.53	0.55	60	150	78.0
19	49.4	3.14	3.53	0.55	60	150	61.8
20	49.4	3.57	3.53	0.55	60	150	57.0
21	49.4	2.2	1.23	0.55	60	150	58.8
22	49.4	2.2	2.34	0.55	60	150	50.5
23	49.4	2.2	2.76	0.55	60	150	56.5
24	49.4	2.2	3.15	0.55	60	150	61.0
25	49.4	2.2	5.08	0.55	60	150	73.3
26	49.4	2.2	3.53	0.49	60	150	64.1
27	49.4	2.2	3.53	0.52	60	150	64.1
28	49.4	2.2	3.53	0.58	60	150	63.6
29	49.4	2.2	3.53	0.6	60	150	51.7
30	49.4	2.2	3.53	0.63	60	150	28.5

Appendix F

Mechanical Properties of Vulcanizates

Table F-1 Mechanical properties of pre-vulcanized latex compounds.

Rubber	Tensile Strength (MPa)		Modulus at 100% elongation (MPa)		Modulus at 300% elongation (MPa)		Modulus at 500% elongation (MPa)		Elongation at Break (%)		Hardness (Shore A)	
	Un-aged	Aged	Un-aged	Aged	Un-aged	Aged	Un-aged	Aged	Un-aged	Aged	Un-aged	Aged
NR	28.1	12.3	0.7	0.6	1.3	1.1	2.7	1.7	900	840	38	35
NR:PIP (85:15)	17.7	13.4	0.7	0.5	1.1	0.9	1.7	1.3	860	900	31	29
NR:PIP (70:30)	8.7	9.3	0.6	0.5	0.9	0.9	1.3	1.3	820	860	25	26
NR:STgPIP (85:15)	9.9	9.2	0.8	0.8	1.2	1.4	2.5	2.2	800	880	33	41

*Heat aging was done at 100 ℃ for 22 h.

VITA

Miss Bunthita Suppaibulsuk was born on September 2, 1983 in Bangkok, Thailand. She received her B.Sc. (Second class honors) degree in Chemical Engineering, Chulalongkorn University. Bunthita joined the Department of Chemical Technology, Chulalongkorn University as doctoral student in 2006. She has received the Royal Golden Jubilee Scholarship from Thailand Research Fund for her Ph.D. study. Bunthita also served as a teaching assistant for undergraduate courses “Material and Energy Balances” and “Chemical Engineering Thermodynamics”. While in graduate school, Bunthita spent one year (2007) and almost six months (2009) doing research at “Advanced Rubber Technology and Applied Catalysis Laboratory” in Chemical Engineering, University of Waterloo, ON, Canada. Her first paper entitled “Factorial design of nanosized polyisoprene synthesis via differential microemulsion polymerization” has been accepted for publication in “Polymer Advance Technology”. She participated in the 8th World Congress of Chemical Engineering in Canada to present her work. Moreover, she also presented her work at 1 conference in Singapore and 2 conferences in Thailand.